DOT/FAA/AR-98/65

Office of Aviation Research
Washington, D.C. 20591

Statistical Loads Data for MD-82/83 Aircraft in Commercial Operations

February 1999

Final Report

U.S. Department of Transportation
Federal Aviation Administration

NOTICE

This document is disseminated under the sponsorship of the U.S. Department of Transportation in the interest of information exchange. The United States Government assumes no liability for the contents or use thereof. The United States Government does not endorse products or manufacturers. Trade or manufacturer's names appear herein solely because they are considered essential to the objective of this report.

This report is available at the Federal Aviation Administration William J. Hughes Technical Center's Full-Text Technical Reports page: www.tc.faa.gov/its/act141/reportpage.html in Adobe Acrobat portable document format (PDF).

Technical Report Documentation Page

1. Report No.	2. Government Accession No.	3. Recipient's Catalog No.
DOT/FAA/AR-98/65		

4. Title and Subtitle	5. Report Date
STATISTICAL LOADS DATA FOR MD-82/83 AIRCRAFT IN COMMERCIAL OPERATIONS	February 1999
	6. Performing Organization Code

7. Author(s)	8. Performing Organization Report No.
Donald Skinn, Daniel O. Tipps, and John Rustenburg	UDR-TR-98-00077

9. Performing Organization Name and Address	10. Work Unit No. (TRAIS)
University of Dayton Research Institute Structural Integrity Division 300 College Park Dayton, OH 45469-0120	RPD-510-1998-00032
	11. Contract or Grant No.
	FAA Grant No. 96-G-020

12. Sponsoring Agency Name and Address	13. Type of Report and Period Covered
U.S. Department of Transportation Federal Aviation Administration Office of Aviation Research Washington, DC 20591	Final Report
	14. Sponsoring Agency Code
	ANM-100

15. Supplementary Notes

The Federal Aviation Administration William J. Hughes Technical Center COTR is Thomas DeFiore.

16. Abstract

The University of Dayton is supporting Federal Aviation Administration (FAA) research on the structural integrity requirements for the US commercial transport aircraft fleet. The primary objective of this research is to support the FAA Airborne Data Monitoring Systems Research Program by developing new and improved methods and criteria for processing and presenting large commercial transport aircraft flight and ground loads usage data. The scope of activities performed involved (1) defining the service related factors which affect the operational life of commercial aircraft; (2) designing an efficient software system to reduce, store, and process large quantities of optical quick access recorder data; and (3) providing processed data in formats that will enable the FAA to reassess existing certification criteria. Equally important, these new data will also enable the FAA, the aircraft manufacturers, and the airlines to better understand and control those factors which influence the structural integrity of commercial transport aircraft. Presented herein are analyses and statistical summaries of data collected from 3987 flights representing 7120 flight hours of six typical MD-82/83 aircraft during operational usage recorded by a single airline. The data include statistical information on accelerations, speeds, altitudes, flight duration and distance, gross weights, speed brake/spoiler cycles, thrust reverser usage, and gust velocities encountered.

17. Key Words	18. Distribution Statement
Optical quick access recorder, Flight profiles, Gust loads, Accelerations, Statistical summaries	This document is available to the public through the National Technical Information Service (NTIS), Springfield, Virginia 22161.

19. Security Classif. (of this report)	20. Security Classif. (of this page)	21. No. of Pages	22. Price
Unclassified	Unclassified	79	N/A

PREFACE

The Flight Systems Integrity Group of the Structural Integrity Division of the University of Dayton Research Institute performed this work under Federal Aviation Administration (FAA) Grant No. 96-G-020 entitled "Aircraft Operational Usage for Service Life Management and Design Criteria Development." The Program Manager for the FAA was Mr. Thomas DeFiore of the FAA Technical Center at Atlantic City International Airport, New Jersey, and the Program Technical Advisor was Mr. Terence Barnes of the FAA Aircraft Certification Office. Mr. Daniel Tipps was the Principal Investigator for the University of Dayton and provided oversight direction for this effort. Mr. Donald Skinn developed the data reduction algorithms, established data reduction criteria, performed the data reduction, and created the graphical presentations. Mr. John Rustenburg performed the data analysis and prepared the report.

TABLE OF CONTENTS

LIST OF FIGURES

LIST OF TABLES

LIST OF SYMBOLS AND ABBREVIATIONS

$\overline{A}$	aircraft PSD gust response factor
a	speed of sound (ft/sec)
$\overline{c}$	wing mean geometric chord (ft)
$\overline{C}$	aircraft discrete gust response factor
C_{L_α}	aircraft lift curve slope per radian
$C_{L_{max}}$	maximum lift coefficient
CAS	calibrated airspeed
c.g.	center of gravity
EAS	equivalent airspeed
F(PSD)	continuous gust alleviation factor
g	gravity constant, 32.17 ft/sec^2
H_p	pressure altitude, (ft)
K_g	discrete gust alleviation factor, $0.88\ \mu/(5.3 + \mu)$
KCAS	knots calibrated airspeed
KEAS	knots equivalent airspeed
KIAS	knots indicated airspeed
kts	knots
L	turbulence scale length (ft)
n	load factor (g)
N	number of occurrences for U_σ (PSD gust procedure)
nm	nautical mile
n_x	longitudinal load factor (g)
n_y	lateral load factor (g)
n_z	normal load factor (g)
N_0	number of zero crossings per nautical mile (PSD gust procedure)
q	dynamic pressure (lbs/ft^2)
S	wing area (ft^2)
TAS	true airspeed
U_{de}	derived gust velocity (ft/sec)
U_σ	continuous turbulence gust intensity (ft/sec)

V_B	design speed for maximum gust
V_C	design cruise speed
V_D	design dive speed
V_e	equivalent airspeed
V_T	true airspeed
W	gross weight (lbs)
Δm	incremental acceleration due to a turning maneuver
Δn_z	incremental normal load factor, n_z - 1
$\Delta n_{z_{man}}$	incremental maneuver load factor
$\Delta n_{z_{gust}}$	incremental gust load factor
μ	airplane mass ratio, $\frac{2(W/S)}{\rho g \bar{c} C_{L_\alpha}}$
μ_p	statistical mean of p (parameter on plots)
ρ	air density, slugs/ft^3 (at altitude)
ρ_0	standard sea level air density, 0.0023769 slugs/ft^3
σ_p	standard deviation of p (parameter on plots)
φ	bank angle (degrees)

EXECUTIVE SUMMARY

The University of Dayton Research Institute (UDRI) is supporting Federal Aviation Administration (FAA) research on the structural integrity requirements for the US commercial transport aircraft fleet. The primary objective of this research is to support the FAA Airborne Data Monitoring Systems Research Program, RPD-510, by developing new and improved methods and criteria for processing and presenting large commercial transport aircraft flight and ground loads usage data. The scope of activities performed involved (1) defining the service related factors which affect the operational life of commercial aircraft; (2) designing an efficient software system to reduce, store, and process large quantities of optical quick access recorder data; and (3) providing processed data in formats that will enable the FAA to reassess existing certification criteria. Equally important, these new data will also enable the FAA, the aircraft manufacturers, and the airlines to better understand and control those factors which influence the structural integrity of commercial transport aircraft. Presented herein are analyses and statistical summaries of data collected from 3987 flights representing 7120 flight hours recorded on six MD-82/83 aircraft during typical operational usage. The data include statistical information on accelerations, speeds, altitudes, flight duration and distance, gross weights, speed brake/spoiler cycles, thrust reverser usage, and gust velocities encountered.

1. INTRODUCTION.

The Federal Aviation Administration (FAA) has initiated an Airborne Data Monitoring Systems Research Program to collect, process, and evaluate statistical flight loads data from transport aircraft used in normal commercial airline operations. The objectives of this program are to (1) acquire, evaluate, and compare typical operational in-service data with prior data used in the design and qualification testing of civil transport aircraft and (2) provide a basis to improve the structural criteria and methods of design, evaluation, and substantiation of future aircraft. Since the inception of the FAA's Airborne Data Monitoring Systems Research Program, the scope of the program has steadily increased to include data collection on additional aircraft, different aircraft models, and additional operators. UDRI has supported the FAA efforts in data analysis and processing tasks and report preparation. In consultation with aircraft manufacturers and operators, the University has enhanced and improved the data processing capabilities to allow reducing, analyzing, and reporting additional aircraft usage and statistical loads data from the digital flight loads recorders into a form that will fulfill the requests of the aircraft manufacturers, the airlines, and the FAA. The report presents data obtained from six MD-82/83 aircraft over 3987 flights and 7120 hours of airline operations for a single operator.

2. AIRCRAFT DESCRIPTION.

Table 1 presents certain operational characteristics of the six MD-82/83 aircraft equipped with optical quick access recorders. Figure 1 shows front, top, and side views of the aircraft and identifies its major physical dimensions.

TABLE 1. MD-82/83 AIRCRAFT CHARACTERISTICS

Maximum Taxi Weight	150,500/161,000 lb
Maximum Takeoff Weight	149,000/160,000 lb
Maximum Landing Weight	130,000/139,500 lb
Zero-Fuel Weight	122,000/122,000 lb
Fuel Capacity	5,840/7,000 U.S. gallons
2 P&W JT8D-217A/C/219 Engines	@ 20,000/21.000 lbs static thrust each
Wing Span	107.85 ft
Wing Reference Area	1,209.3 ft^2
Wing MAC	11.21 ft
Wing Sweep	24.5 degrees
Length	147.8 ft
Height	29.6 ft
Tread	16.7 ft
Wheel Base	72.4 ft

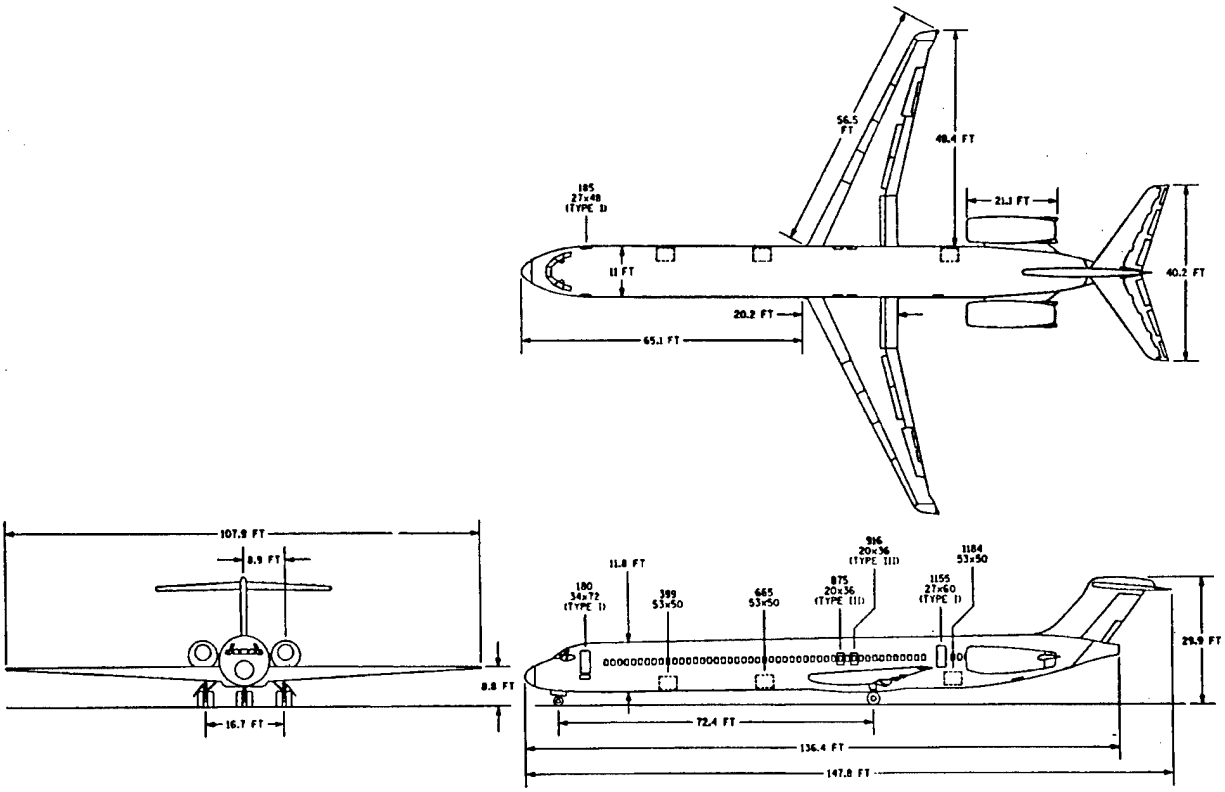

FIGURE 1. MD-82/83 THREE-VIEW DRAWING

3. AIRLINE DATA COLLECTION AND EDITING SYSTEMS.

The airline data collection and editing system consists of two major components: (1) the data collection system installed onboard the aircraft and (2) the ground data editing station. A schematic overview of the system is given in figure 2. The requirements for the data acquisition and processing are defined in reference 1. The collection and editing systems are discussed below.

3.1 DATA COLLECTION SYSTEM.

The onboard data collection system consists of a Digital Flight Data Acquisition Unit (DFDAU), a Digital Flight Data Recorder (DFDR), and an Optical Quick Access Recorder (OQAR). The DFDAU collects sensor signals and sends parallel data signals to both the DFDR and the OQAR. The OQAR is programmed to start recording once certain data signals are detected. The OQAR is equipped with an optical disk which can store up to 200 hours of flight data, whereas the DFDR uses a 25-hour looptape. The optical disk is periodically removed from the OQAR and forwarded to the ground processing station.

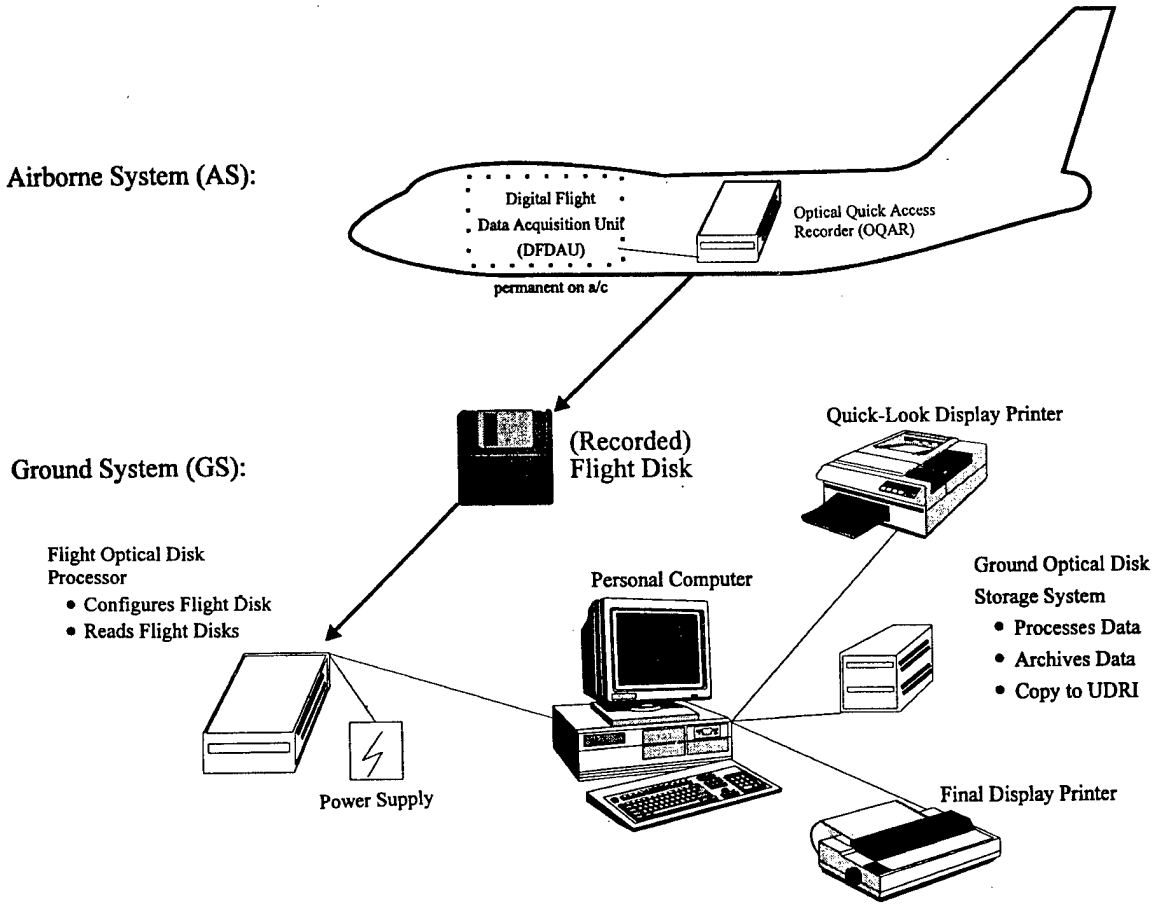

FIGURE 2. AIRLINE RECORDING AND EDITING SYSTEM

3.2 DATA EDITING SYSTEM.

The airline ground data editing station consists of a Pentium computer, a magneto-optical (MO) disk drive, and flight data editing software. The software performs a number of functions during the process of transferring the raw flight data into DOS file format onto hard disk. The most important of these functions includes a data integrity check and removal of flight sensitive information. Data considered sensitive are those which can be used to readily identify a specific flight. The desensitized data are forwarded to the University of Dayton Research Institute (UDRI) for flight loads processing and analysis. Table 2 presents the recorded data parameters provided by the airline to UDRI.

4. UNIVERSITY OF DAYTON RESEARCH INSTITUTE DATA PROCESSING.

The data parameters of table 2 are provided by the airline to UDRI for each recorded flight. The data are provided on magneto-optical disks containing binary files for multiple flights for different airplanes. These data are processed by UDRI to extract the parameters required for statistical flight loads presentation. This section describes the reduction of the data and the derivation of required parameters.

TABLE 2. RECORDED PARAMETERS PROVIDED TO UDRI

Parameter	Sample Rate
Normal Acceleration	8 per second
Lateral Acceleration	4 per second
Longitudinal Acceleration	4 per second
Aileron Position	1 per second
Elevator Position	1 per second
Rudder Position	2 per second
Pitch Trim Position	1 per second
Flap Position	1 per 2 seconds
Spoiler Deflection	2 per second
EPR #1	1 per second
EPR #2	1 per second
Thrust Reverser Status	1 per 2 seconds
Squat Switch (nose gear status)	1 per 2 seconds
Gear Status	1 per 2 seconds
Calibrated Airspeed	1 per second
Mach Number	1 per 2 seconds
Pressure Altitude	1 per second
Gross Weight	Adjusted for fuel burn rate
Bank Angle	2 per second
Pitch Angle	2 per second
Magnetic Heading	1 per second
Total Air Temperature	1 per 2 seconds
Radio Altitude (not available on all airplanes)	1 per second

4.1 DATA REDUCTION.

Each file provided by the airline contains multiple flights for each airplane. These files are first separated into individual flight files and subsequently into individual time history files for each flight. The time history files are compressed and stored on the same 230 MB magneto-optical disks for later recall by the flight loads processing software.

Data editing and verification are performed on the data as the time histories are being prepared. Messages alert the user when obviously erroneous data are removed and/or when questionable data are retained but need to be manually reviewed prior to their acceptance. Table 3 lists the limits against which the data are compared.

TABLE 3. PARAMETER EDITING VALUES

Item		Condition	Min	Max
1.	Gross Weight	At startup	75,000 lbs	160,000 lbs
2.	Pressure Altitude (Hp)	At all times	-2,000 ft	45,000 ft
3.	Calibrated Airspeed	At all times during flight operations	45 kts	420 kts
4.	Normal Acceleration	At startup and shutdown in flight	-2 g	+4 g
5.	Lateral Acceleration	At all times	±0.5 g	±0.5 g
6.	Longitudinal Acceleration	At all times	±1.0 g	±1.0 g
7.	Flap Handle Position	At all times	-1°	45°
8.	Elevator Position	At all times	±25°	±25°
9.	Aileron Position	At all times	±15°	±15°
10.	Rudder Position	At all times	±18°	±18°
11.	Trim Position	At all times	-15°	25°
12.	Spoiler Deflection	At all times	-1°	60°
13.	EPR 1 and 2	At all times	0.6°	2.5°
14.	Thrust Reverser Position	Stowed at startup and shutdown	0	1
15.	Autopilot Status	Off or on	0	1
16.	Landing Gear Position	Down at startup and shutdown Up within 10 seconds after takeoff Down within 10 minutes before landing	0	1
17.	Pitch Attitude	At all times	-20°	+30°
18.	Bank Attitude	At all times	±60°	±60°
19.	Mach Number	At all times	0	1

Important characteristics about each set of flights received from the airline are recorded in a relational database. Airline identifier, aircraft tail number, and disk identifier of the disk received from the airline are in the data. Each flight is assigned a unique flight sequence number. The flight sequence number assigned to the first flight of the set and the number of flights in the set are also entered. Also recorded is the disk identifier of the MO disk, which contains the compressed time history files of all flights in the set.

4.2 RECORDED PARAMETERS.

Not all parameters listed in table 2 are used for statistical analysis and data presentation. Table 4 lists the parameters used in the data reduction and for which time history files are created and compressed on the magneto-optical disk. These parameters are used by the summarization software for statistical analysis and data presentation.

TABLE 4. RECORDED PARAMETERS USED IN DATA REDUCTION

Flight Parameter	Sample Rate
Gross Weight	From flight log, and adjusted during flight for fuel burn
Fuel Quantity	From flight log, and adjusted during flight for fuel burn
Pressure Altitude	1 per second
Calibrated Airspeed	1 per second
Normal Acceleration (n_z)	8 per second
Lateral Acceleration (n_y)	4 per second
Longitudinal Acceleration (n_x)	4 per second
Flap Position	1 per 2 seconds
Spoiler Deflection	2 per second
Thrust Reverser Status	Discrete
Squat Switch (nose gear)	Discrete
Landing Gear Status	Discrete
Pitch Angle	2 per second
Bank Angle	2 per second
Mach Number	1 per 2 seconds
Magnetic Heading	1 per second

4.3 COMPUTED PARAMETERS.

Derived gust velocity, U_{de}, and continuous gust intensity, U_{σ}, are important statistical load parameters which are derived from measured normal accelerations. This derivation of gust velocity, U_{de}, and continuous gust intensity, U_{σ}, from measured normal accelerations requires knowledge of atmospheric density, equivalent airspeed, and dynamic pressure. These values are calculated using equations that express the rate of change of density as a function of altitude based on the International Standard Atmosphere.

4.3.1 Atmospheric Density.

For altitudes below 36,089 feet, the density ρ is expressed as a function of altitude by

$$\rho = \rho_o (1 - 6.876 \times 10^{-6} \times H_p)^{4.256} \quad (1)$$

where ρ_0 is air density at sea level (0.0023769 slugs/ft^3) and H_p is pressure altitude (ft). Pressure altitude is a recorded parameter.

4.3.2 Equivalent Airspeed.

Equivalent airspeed (V_e) is a function of true airspeed (V_T) and the square root of the ratio of air density at altitude (ρ) to air density at sea level (ρ_0)

$$V_e = V_T \sqrt{\frac{\rho}{\rho_0}} \tag{2}$$

True airspeed is derived from Mach number (M) and speed of sound (a) as

$$V_T = Ma \tag{3}$$

Mach number is a dimensionless, recorded parameter. The speed of sound (a) is a function of pressure altitude (H_p) and the speed of sound at sea level and is

$$a = a_0 \sqrt{(1 - 6.876 \times 10^{-6} \times H_p)} \tag{4}$$

Substituting equations 1 and 4 into equation 2 gives

$$V_e = M \times a_0 \times (1 - 6.876 \times 10^{-6} \times H_p)^{0.5} \times (1 - 6.876 \times 10^{-6} \times H_p)^{2.128} \tag{5}$$

and

$$V_e = M \times a_0 \times (1 - 6.876 \times 10^{-6} \times H_p)^{2.626} \tag{6}$$

where the speed of sound at sea level a_0 is 1116.4 fps or 661.5 knots.

4.3.3 Dynamic Pressure (q).

The dynamic pressure (q) is calculated from the air density and velocity

$$q = \frac{1}{2} \rho V^2 \tag{7}$$

where

ρ = air density at altitude (slugs/ft^3)
V = true airspeed (ft/sec)

4.3.4 Derived Gust Velocity (U_{de}).

The derived gust velocity, U_{de}, is computed from the peak values of gust incremental normal acceleration as

$$U_{de} = \frac{\Delta n_z}{\overline{C}} \tag{8}$$

where Δn_z is gust peak incremental normal acceleration and $\overline{C}$ is the aircraft response factor considering the plunge-only degree of freedom and is calculated from

$$\overline{C} = \frac{\rho_0 V_e C_{L_\alpha} S}{2W} K_g \tag{9}$$

where

ρ_0 = 0.002377 slug/ft^3, standard sea level air density
V_e = equivalent airspeed (ft/sec)
C_{L_α} = aircraft lift-curve slope per radian
S = wing reference area (ft^2)
W = gross weight (lbs)
K_g = $\frac{0.88\mu}{5.3+\mu}$ = gust alleviation factor

μ = $\frac{2W}{\rho g \bar{c} C_{L_\alpha} S}$

ρ = air density, slug/ft^3, at pressure altitude (Hp), from equation 1
g = 32.17 ft/sec^2
$\bar{c}$ = wing mean geometric chord (ft)

In this program, the lift-curve slope, C_{L_α}, is the untrimmed flexible lift-curve slope for the entire airplane. For the flaps retracted conditions, the lift-curve slope is given as a function of Mach number and altitude; for flaps extended, the lift-curve slope is a function of flap deflection and calibrated airspeed (CAS).

4.3.5 Continuous Gust Intensity (U_σ).

Power spectral density (PSD) functions provide a turbulence description in terms of the probability distribution of the root-mean-square (rms) gust velocities. The root-mean-square gust velocities, U_σ, are computed from the peak gust value of normal acceleration using the power spectral density technique as described in reference 2. The procedure is

$$U_\sigma = \frac{\Delta n_z}{\overline{A}} \tag{10}$$

where Δn_z = gust peak incremental normal acceleration

$$\overline{A} = \text{aircraft PSD gust response factor} = \frac{\rho_0 V_e C_{L\alpha} S}{2W} F(PSD)\ in\ \frac{1}{ft/sec} \tag{11}$$

ρ_0 = 0.002377 slug/ft^3, standard sea level air density
V_e = equivalent airspeed (ft/sec)
C_{L_α} = aircraft lift-curve slope per radian
S = wing reference area (ft^2)
W = gross weight (lbs)

$$F(PSD) = \frac{11.8}{\sqrt{\pi}}\left[\frac{\bar{c}}{2L}\right]^{\frac{1}{3}}\sqrt{\frac{\mu}{110+\mu}},\ dimensionless \tag{12}$$

$\bar{c}$ = wing mean geometric chord (ft)
L = turbulence scale length, 2500 ft

$$\mu = \frac{2W}{\rho g \bar{c} C_{L_\alpha} S},\ \text{dimensionless} \tag{13}$$

ρ = air density (slugs/ft^3)
g = 32.17 ft/sec^2

To determine the number of occurrences (N) for U_σ, calculate

$$N = \frac{N_0(o)_{ref}}{N_0(o)} = \frac{\pi\bar{c}}{203}\left[\frac{\rho}{\rho_0}\mu\right]^{0.46},\ \text{dimensionless} \tag{14}$$

where $\bar{c}$, ρ, ρ_0, and μ are defined above. Then each U_σ peak is counted as N counts at that U_σ value. This number of counts is used to determine the number of counts per nautical mile (nm)

or
$$\frac{\text{counts}}{nm} = \left(\frac{N}{\text{distance flown in counting interval}}\right) \tag{15}$$

Finally, the number of such counts is summed from the largest plus or minus value toward the smallest to produce the cumulative counts per nautical mile.

4.4 DATA REDUCTION CRITERIA.

To process the measured data into statistical flight loads format, specific data reduction criteria were established for each parameter. These criteria are discussed in this section.

4.4.1 Phases of Flight.

Each flight was divided into nine phases—four ground phases (taxi out, takeoff roll, landing roll with and without thrust reverser, and taxi in), and five airborne phases (departure, climb, cruise, descent, and approach). Figure 3 shows these nine phases of a typical flight. The phases of flight were not defined by the airline but had to be determined from the data. Table 5 lists the conditions for determining the starting times for each phase. It should be noted that an airborne phase can occur several times per flight because it is determined by the rate of climb and the position of the flaps. When this occurs, the flight loads data are combined and presented in a single flight phase. The UDRI software creates a file which chronologically lists the phases of flight and their corresponding starting times.

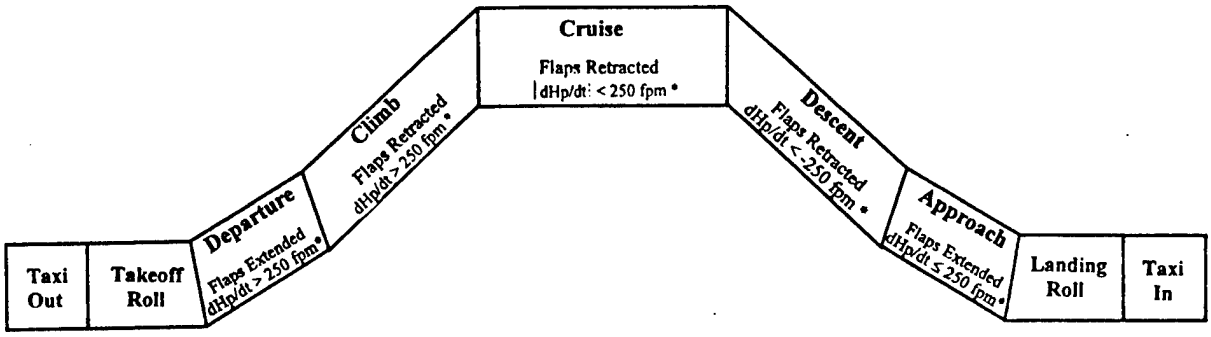

*Climb rate must be maintained for at least 1 minute before transition into another phase of flight takes place.

FIGURE 3. DESCRIPTION OF PHASES OF FLIGHT

TABLE 5. PHASE OF FLIGHT STARTING CRITERIA

Phase of Flight	Conditions at Start of Phase
Taxi Out	Initial condition
Takeoff Roll	Computed airspeed > 45 knots or n_x> 0.15 g
Departure	Time at liftoff; flaps extended
Climb	Flaps retracted; rate of climb ≥ 250 ft/min. for at least 1 minute
Cruise	Flaps retracted; rate of climb ≤ 250 ft/min. for at least 1 minute
Descent	Flaps retracted; rate of ≤ -250 ft/min. for at least 1minute
Approach	Flaps extended; rate of < 250 ft/min. for at least 1 minute
Landing Roll	Touchdown
Taxi In	Magnetic heading change greater than 13.5 degrees after touchdown

The criteria for the start of the takeoff roll is defined as the earlier of (1) the time that the computed speed exceeds 45 knots or (2) the time that the longitudinal acceleration exceeds 0.15 g prior to liftoff.

The criteria for the start of taxi in is defined as the time when the aircraft turns off the active runway. The method for detecting turnoff is to monitor the magnetic heading change for a change greater than 13.5 degrees from the landing magnetic heading. The time when the heading starts to change in the turnoff direction is then identified as the start of the turn or the beginning of the taxi in phase. This method can fail to detect a shallow turnoff onto a parallel taxiway. In this case an average landing roll of 32 seconds duration is assumed and the turnoff is marked as 32 seconds after touchdown.

The criteria for determining the pitch angle at takeoff has been defined as the angle occurring just prior to the airplane becoming airborne.

4.4.2 Flight Distance.

The flight distance can be obtained either by determining the stage length of the flight or by integrating the range with respect to changes in aircraft velocity as a function of time.

The stage length is defined as the distance from departure airport to destination airport and is determined as the great circle distance in nautical miles between the point of liftoff (departure) and the point of touchdown (destination). Appendix B describes the calculation of great circle distance. The time histories of longitude and latitude are matched against the UDRI generated phase of flight file to determine the geographical location of the aircraft at the point of liftoff and the point of touchdown.

The integrated flight distance D is obtained by the numerical integration from the time at liftoff (t_0) to the time of touchdown (t_n), and V is the average velocity during Δt.

$$D = \sum_{t_0}^{t_n} \Delta t \cdot V \tag{16}$$

4.4.3 Sign Convention.

Acceleration data are recorded in three directions: normal (z), lateral (y), and longitudinal (x). As shown in figure 4, the positive z direction is up; the positive y direction is airplane starboard; and the positive x direction is forward.

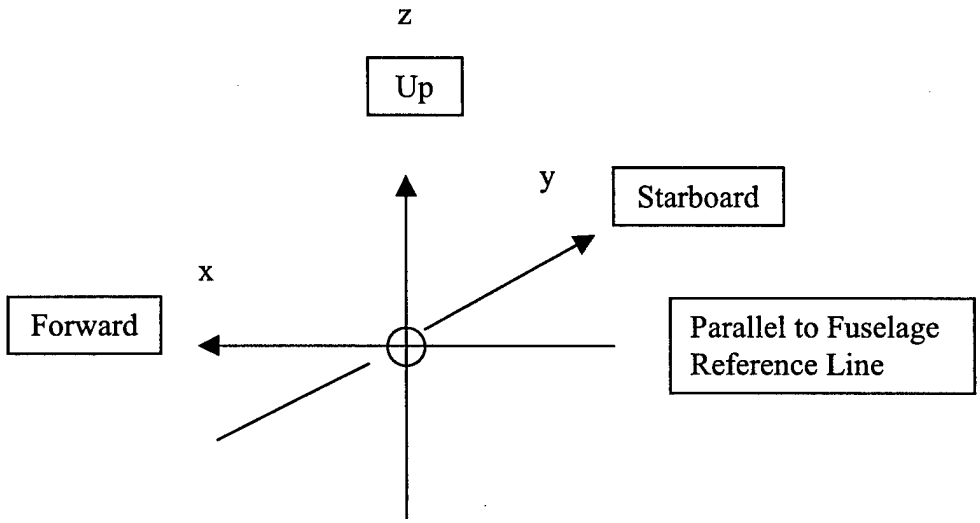

FIGURE 4. SIGN CONVENTION FOR AIRPLANE ACCELERATIONS

4.4.4 Peak-Valley Selection.

The peak-between-means method presented in reference 2 was used to select the peaks and valleys in the acceleration data. This method is consistent with past practices and pertains to all accelerations (n_x, n_y, Δn_z, $\Delta n_{z_{man}}$, $\Delta n_{z_{gust}}$). Figure 5 depicts an example of the peak-between-mean criteria. This method counts upward events as positive and downward events as negative. Only

one peak or one valley is counted between two successive crossings of the mean. A threshold zone is used in the data reduction to ignore irrelevant loads variations around the mean. For the normal accelerations Δn_z, $\Delta n_{z_{gust}}$, and $\Delta n_{z_{man}}$, the threshold zone is ±0.05 g; for lateral acceleration n_y, the threshold zone is ±0.005 g; and for longitudinal accelerations n_x, the threshold zone is ±0.0025 g.

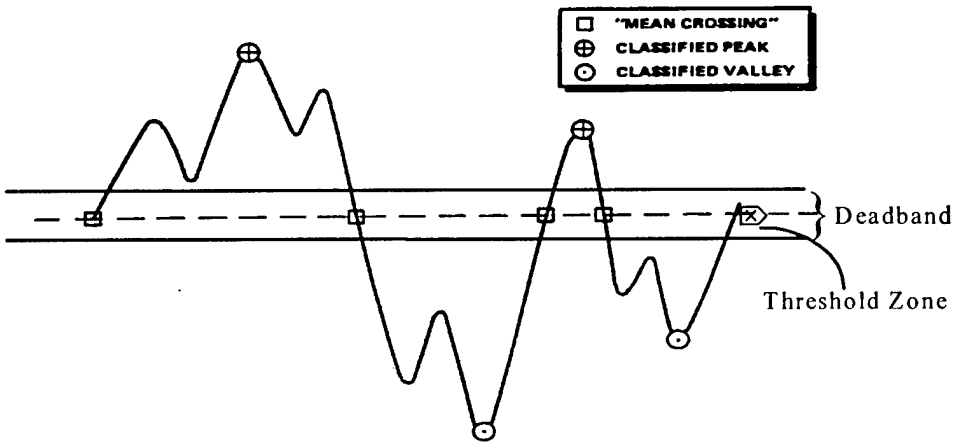

FIGURE 5. THE PEAK-BETWEEN-MEANS CLASSIFICATION CRITERIA

A peak is generated only when the acceleration data cross into or through the deadband. Two situations must be considered: the position of the current acceleration value relative to the deadband and the position of the previous acceleration value relative to the deadband. In the peak-between-means counting algorithm, the previous acceleration value is that value in a consecutive set of values all of which lie either above the deadband or below the deadband. The previous value is established as a peak when the current value has crossed into or through the deadband. Figures 6a and 6b demonstrate the concept of current and previous acceleration values. In figure 6a the current acceleration value passes into the deadband, whereas in figure 6b the current value passes through the deadband.

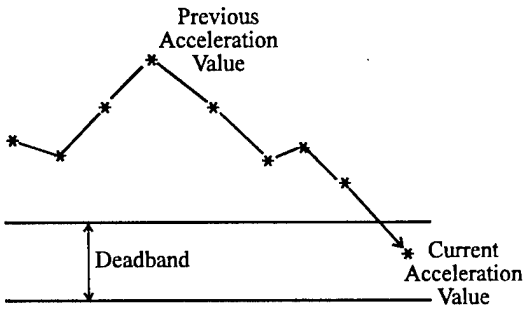

FIGURE 6a. CURRENT ACCELERATION VALUE PASSES INTO DEADBAND

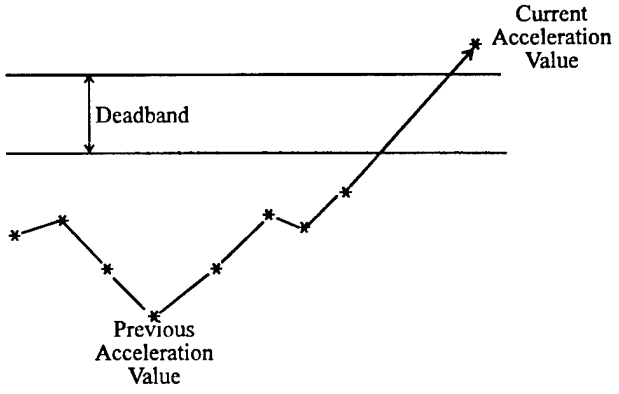

FIGURE 6b. CURRENT ACCELERATION VALUE PASSES THROUGH DEADBAND

Italicized text in table 6 summarizes the action(s) taken when the various possibilities occur. Note that when a previous acceleration value is retained as a potential peak, its coincident time is also retained.

TABLE 6. PEAK CLASSIFICATION CRITERIA

Previous Acceleration Value Relative to Deadband	Current Acceleration Value Relative to Deadband		
	Below	Within	Above
Above Previous value is potential positive peak	Current acceleration passes through deadband. *Previous value classified as a positive peak.* *Current value retained as a potential negative peak.*	Current acceleration passes into deadband. *Previous value classified as a positive peak.* *Acceleration value flagged as being in deadband.*	Current acceleration is on same side of deadband as previous. *If current > previous value, retain current value as potential positive peak and release previous.*
Within At start of processing, or a peak was established but current acceleration value has not since gone outside of deadband	Current acceleration passes downward out of deadband. *Current value is retained as a potential negative peak.*	*No Action Required*	Current acceleration passes upward out of deadband. *Current value retained as potential positive peak.*
Below Previous value is potential negative peak	Current acceleration is on same side of deadband as previous. *If current value < previous value, retain current value as potential negative peak and release previous value.*	Current acceleration passes into deadband. *Previous value is established as a negative peak.* *Acceleration value flagged as being in deadband.*	Current acceleration passes through deadband. *Previous value is classified as a negative peak.* *Current value retained as potential positive peak.*

4.4.5 Separation of Maneuver and Gust Load Factors.

The recorded normal acceleration (n_z) values included the 1 g flight condition. The 1 g condition was removed from each n_z reading which was then recorded as Δn_z. In order to avoid the inclusion of peaks and valleys associated with nonsignificant small load variations, a threshold zone of $\Delta n_z = \pm 0.05$ g was established. An algorithm was then developed to extract the acceleration peaks and valleys.

For each flight the maximum and minimum total accelerations were determined from just after liftoff to just before touchdown. For the five in-flight phases, the Δn_z cumulative occurrences were determined as cumulative counts per nautical mile and cumulative counts per 1000 hours using the peak-between-means counting method of reference 2 explained in section 4.4.4.

The incremental acceleration measured at the center of gravity (c.g.) of the aircraft may be the result of either maneuvers or gusts or a combination of both. In order to derive gust statistics, the maneuver induced acceleration is separated from the total acceleration history. Most maneuver induced loads are associated with turning maneuvers.

The increment due to a turning maneuver (Δm) is determined using the bank angle method discussed in reference 2 to calculate the maneuver acceleration $\Delta n_{z_{man}}$ as

$$\Delta n_{z_{man}} = (\sec \varphi - 1) \tag{17}$$

where φ is the bank angle. The remaining peaks and valleys are assumed to be gust induced, where gust normal acceleration ($\Delta n_{z_{gust}}$) is calculated as

$$\Delta n_{z_{gust}} = \Delta n_z - \Delta n_{z_{man}} \tag{18}$$

This approach does not separate the pitching maneuvers induced by pilot control inputs. In reference 2, J.B. de Jonge suggests that accelerations resulting from pitch maneuvers induced by pilot input to counteract turbulence can be considered as part of the aircraft system response to the turbulence. Accelerations that are induced by the pitch maneuver at the specific points of rotation and flare during takeoff and climb and approach and touchdown have not been removed during this initial data reduction effort. Since turbulence is a more dominant loading input on commercial aircraft than maneuvers, correcting for pitch maneuvers at a later time will not substantially alter the statistics presented herein.

Once calculated, the measurements of Δn_z, $\Delta n_{z_{gust}}$, and $\Delta n_{z_{man}}$ are maintained as three unique data streams. The $\Delta n_{z_{gust}}$ and $\Delta n_{z_{man}}$ data are plotted as cumulative occurrences of a given acceleration fraction per nautical mile and per 1000 flight hours. Separate plots are provided for each phase of flight and all phases combined. The Δn_z fraction is the recorded incremental normal load factor (airplane limit load factor minus 1.0 g). As a result of the threshold zone, only accelerations greater than ±0.05 g (measured from a 1.0 g base) are counted for data presentation.

4.4.6 Flap Detents.

When flaps are extended, the effective deflection is considered to be that of the applicable detent, as indicated in table 7. The flap deflection ranges and placard speeds reflect the flap design placards.

TABLE 7. FLAP DETENTS (MD-82/83)

Flap Detent	Minimum Flap Setting	Maximum Flap Setting	Design Placard Speed (KIAS)
1	> 0.1	≤1	280/280
13	>1	≤13	280/280
20	> 13	≤20	240/240
25	> 20	≤ 25	220/220
30	> 25	≤ 30	200/205
40	> 30	≤ 40	195/200

5. DATA PRESENTATION.

Table 8 lists the statistical data presentation formats for which data was processed and included in appendix A of this report.

Figures A-1 through A-78 present the processed data. It will be noted that the data presented in these figures are not always based on an identical number of flights. During data reduction it was found that the acceleration measurements in certain flights exhibited random errors and were unreliable. When this occurred, those flights were eliminated from the statistical data for any parameters associated, directly or indirectly, with the unreliable acceleration measurements. As a result, not all figures are based on data from identical numbers of flights, hours, or nautical miles.

5.1 AIRCRAFT OPERATIONAL USAGE DATA.

The aircraft usage data include flight profile statistics such as weights, altitudes, speeds, and flight distance information. This information is useful in the derivation of typical flight profiles and in defining ground-air-ground cycles for structural durability, damage tolerance analyses, future design criteria, and for use in the analysis of airline operating economics. Aircraft usage data are presented in figures A-1 through A-10.

5.1.1 Weight Data.

Statistical data on operational takeoff gross weights, landing gross weights, and fuel weights are presented in this section. These weights are also correlated to flight distance. The cumulative probabilities of takeoff gross weight, takeoff fuel weight, and landing weight are presented in figures A-1 through A-3 respectively. The correlation between fuel weight at takeoff and the flight distance is presented in figure A-4. A similar correlation for takeoff gross weight and flight distance is shown in figure A-5. The flight distances in figures A-4 and A-5 are based on the great circle distance between departure and arrival points. Figure A-6 provides the correlation between the takeoff gross weight and the landing gross weight. The correlation shows that for most flights with light takeoff weights (less than 110,000 pounds) the landing weight is within 10,000 pounds of the takeoff weight. For the medium takeoff weights from 100,000-130,000 pounds, the landing weights are from 10,000-20,000 pounds below takeoff weight. For the heavy weight takeoffs from 130,000-150,000 pounds, the landing weights are from 20,000-30,000 pounds below the takeoff weight.

5.1.2 Altitude Data.

Measured operational altitudes and their correlation to flight distance and maximum speed are presented. Figure A-7 shows the correlation between the maximum altitude attained in flight and the flight distance flown in percent of flights. The data show that over half of all flights are flown at a maximum altitude between 30,000 and 35,000 feet. Also, regardless of flight lengths most flights are flown in this same altitude band. For flight lengths greater than 250 miles over 70 percent of the flights are flown between 30,000 and 40,000 feet altitude. Less than 1 percent of flights are flown above 40,000 feet.

TABLE 8. STATISTICAL DATA FORMATS

Data Description	Figure
AIRCRAFT USAGE DATA	
WEIGHT DATA	
Cumulative Probability of Takeoff Gross Weight	A-1
Cumulative Probability of Takeoff Fuel Weight	A-2
Cumulative Probability of Landing Gross Weight	A-3
Correlation of Takeoff Fuel Weight and Flight Distance, Percent of Flights	A-4
Correlation of Takeoff Gross Weight and Flight Distance, Percent of Flights	A-5
Correlation of Gross Weight at Liftoff and Touchdown, Percent of Flights	A-6
ALTITUDE DATA	
Correlation of Maximum Altitude and Flight Distance, Percent of Flights	A-7
Percent of Total Distance in Altitude Bands	A-8
FLIGHT DISTANCES	
Cumulative Probability of Great Circle Flight Distance	A-9
Cumulative Probability of Integrated Flight Distance	A-10
GROUND LOADS DATA	
LATERAL LOAD FACTOR, n_y	
Cumulative Frequency of Maximum Side Load Factor During Ground Turns	A-11
LONGITUDINAL LOAD FACTOR, n_x	
Cumulative Frequency of Longitudinal Load Factor During Ground Taxi	A-12
Cumulative Frequency of Longitudinal Load Factor During Landing Roll	A-13
Cumulative Probability of Maximum Longitudinal Load Factor During Takeoff	A-14
Cumulative Probability of Minimum Longitudinal Load Factor During Landing	A-15
VERTICAL LOAD FACTOR, n_z	
Cumulative Frequency of Incremental Vertical Load Factor During Taxi Operations	A-16
Cumulative Frequency of Incremental Vertical Load Factor During Takeoff Roll	A-17
Cumulative Frequency of Incremental Vertical Load Factor During Landing Roll	A-18
Cumulative Probability of Minimum and Maximum Incremental Vertical Load Factor at Touchdown and Spoiler Deployment	A-19
Coincident Incremental Vertical Load Factor and Touchdown Gross Weight	A-20
AIRSPEED DATA	
Cumulative Probability of Airspeed at Liftoff	A-21
Cumulative Probability of Airspeed at Touchdown	A-22
FLARE DATA	
Cumulative Probability of Airspeed at Flare	A-23
PITCH/ROTATION DATA	
Cumulative Probability of Pitch Angle at Liftoff and Touchdown	A-24
Cumulative Probability of Maximum Pitch Rate at Liftoff and Nose Gear Touchdown	A-25
Cumulative Probability of Pitch Angle at Touchdown Peak Vertical Load Factor	A-26

TABLE 8. STATISTICAL DATA FORMATS (Continued)

Data Description	Figure
FLIGHT LOADS DATA	
GUST LOADS DATA	
Cumulative Occurrences of Vertical Gust Load Factor per 1000 Hours by Flight Phase	A-27
Cumulative Occurrences of Incremental Vertical Gust Load Factor per 1000 Hours, Combined Flight Phases	A-28
Cumulative Occurrences of Vertical Gust Load Factor per Nautical Mile by Flight Phase	A-29
Cumulative Occurrences of Incremental Vertical Gust Load Factor per Nautical Mile, Combined Flight Phases	A-30
Cumulative Occurrences of Derived Gust Velocityper Nautical Mile, < 500 Feet	A-31
Cumulative Occurrences of Derived Gust Velocityper Nautical Mile, 500-1,500 Feet	A-32
Cumulative Occurrences of Derived Gust Velocityper Nautical Mile, 1,500-4,500 Feet	A-33
Cumulative Occurrences of Derived Gust Velocityper Nautical Mile, 4,500-9,500 Feet	A-34
Cumulative Occurrences of Derived Gust Velocityper Nautical Mile, 9,500-19,500 Feet	A-35
Cumulative Occurrences of Derived Gust Velocityper Nautical Mile, 19,500-29,500 Feet	A-36
Cumulative Occurrences of Derived Gust Velocity per Nautical Mile, 29,500-39,500 Feet	A-37
Cumulative Occurrences of Derived Gust Velocity per Nautical Mile, Flaps Extended	A-38
Cumulative Occurrences of Derived Gust Velocity per Nautical Mile, Flaps Retracted	A-39
Cumulative Occurrences of Continuous Gust Intensity per Nautical Mile, Flaps Extended	A-40
Cumulative Occurrences of Continuous Gust Intensity per Nautical Mile, Flaps Retracted	A-41
MANEUVER LOADS DATA	
Cumulative Occurrences of Incremental Maneuver Load Factor per 1000 Hours During Departure by Altitude	A-42
Cumulative Occurrences of Incremental Maneuver Load Factor per 1000 Hours During Climb by Altitude	A-43
Cumulative Occurrences of Incremental Maneuver Load Factor per 1000 Hours During Cruise by Altitude	A-44
Cumulative Occurrences of Maneuver Load Factor per 1000 Hours During Descent by Altitude	A-45
Cumulative Occurrences of Maneuver Load Factor per 1000 Hours During Approach by Altitude	A-46
Cumulative Occurrences of Maneuver Load Factor per Nautical Mile During Departure by Altitude	A-47
Cumulative Occurrences of Maneuver Load Factor per Nautical Mile During Climb by Altitude	A-48
Cumulative Occurrences of Maneuver Load Factor per Nautical Mile During Cruise by Altitude	A-49
Cumulative Occurrences of Maneuver Load Factor per Nautical Mile During Descent by Altitude	A-50
Cumulative Occurrences of Maneuver Load Factor per Nautical Mile During Approach by Altitude	A-51
Cumulative Occurrences of Maneuver Load Factor per 1000 Hours by Flight Phase	A-52
Cumulative Occurrences of Maneuver Load Factor per 1000 Hours, Combined Flight Phases	A-53
Cumulative Occurrences of Maneuver Load Factor per Nautical Mile by Flight Phase	A-54
Cumulative Occurrences of Maneuver Load Factor per Nautical Mile, Combined Flight Phases	A-55
COMBINED MANEUVER AND GUST LOADS DATA	
Cumulative Occurrences of Combined Maneuver and Gust Vertical Load Factor per 1000 Hours by Flight Phase	A-56
Cumulative Occurrences of Vertical Load Factor per 1000 Hours, Combined Flight Phases	A-57
Cumulative Occurrences of Vertical Load Factor per Nautical Mile by Flight Phase	A-58
Cumulative Occurrences of Vertical Load Factor per Nautical Mile, Combined Flight Phases	A-59
Cumulative Occurrences of Lateral Load Factor per 1000 Hours, Combined Flight Phases	A-60
Coincident Maneuvers Load Factor and Speed Versus V-n Diagram for Flaps Retracted	A-61
Coincident Maneuvers Load Factor and Speed Versus V-n Diagram for Flaps Extended	A-62
Coincident Gust Load Factor and Speed Versus V-n Diagram for Flaps Retracted	A-63
Coincident Gust Load Factor and Speed Versus V-n Diagram for Flaps Extended	A-64

TABLE 8. STATISTICAL DATA FORMATS (Continued)

Data Description	Figure
MISCELLANEOUS OPERATIONAL DATA	
FLAP USAGE DATA	
Cumulative Probability of Maximum Airspeed in Flap Detent During Departure	A-65
Cumulative Probability of Maximum Airspeed in Flap Detent During Approach	A-66
Percent of Time in Flap Detent During Departure	A-67
Percent of Time in Flap Detent During Approach	A-68
Cumulative Probability of Maximum Dynamic Pressure in Flap Detent During Departure	A-69
Cumulative Probability of Maximum Dynamic Pressure in Flap Detent During Approach	A-70
SPEED BRAKE/FLIGHT SPOILER DATA	
Cumulative Probability of Maximum Speed During Speed Brake Deployment	A-71
Cumulative Frequency of Speed at Speed Brake Deployment	A-72
Cumulative Frequency of Altitude at Speed Brake Deployment	A-73
Cumulative Probability of Maximum Deployment Angle During Speed Brake Deployment, Flaps Retracted	A-74
THRUST REVERSER DATA	
Cumulative Probability of Time With Thrust Reversers Deployed	A-75
LANDING GEAR EXTENSION/RETRACTION DATA	
Cumulative Probability of Time With Landing Gear Extended After Liftoff	A-76
Cumulative Probability of Time With Landing Gear Extended Prior to Touchdown	A-77
Cumulative Probability of Maximum Airspeed With Gear Extended	A-78

Figure A-8 presents the percent of total flight distance spent in various altitude bands as a function of flight distance. The flight distances in figure A-7 reflect the stage lengths, whereas the flight distances in figure A-8 are based on the numerical integration approach mentioned in paragraph 4.4.2. The combined information in figures A-7 and A-8 provide a comprehensive picture of the flight profile distribution.

5.1.3 Flight Distance Data.

Flight distance statistics useful in the generation of flight profiles were derived and are presented here. The cumulative probability of flight distances flown is presented in figures A-9 and A-10. The great circle distance reflects the ground distance between two points as obtained from the great circle distance calculation but does not necessarily reflect the actual distance flown. Deviation from direct flight between departure and arrival points resulting from traffic control requirements will increase the actual distance flown by some unknown amount. To a much lesser extent, the climb and descent distances are slightly larger than the level flight distance. Head or tail winds also are unknown contributors. The integrated distance accounts for such variables. The figure provides a graphical presentation of the differences in flight distance obtained by the two approaches.

5.2 GROUND LOADS DATA.

The ground loads data include frequency and probability information on vertical, lateral, and longitudinal accelerations, speeds, and pitch rotation associated with takeoff, landing, and

ground operations. These data are of primary importance to landing gear and landing gear backup structure and to a lesser extent to the wing, fuselage, and empennage.

5.2.1 Lateral Load Factor Data.

Lateral load factor statistics resulting from ground turning during taxi were derived and are presented. Figure A-11 shows the cumulative frequency of maximum side load factor during ground turns. The information is presented for pre- and postflight taxi, as well as, left and right turns. The turning load factors during taxi in are shown to be more severe than those experienced during turning while taxiing out. This is likely the result of higher taxi in speeds. There is no significant difference between the number of left and right turns.

5.2.2 Longitudinal Load Factor Data.

Longitudinal load factor statistics were derived for all phases of ground operation, including pre- and postflight taxi, and takeoff and landing roll. Figures A-12 and A-13 present the cumulative frequency of longitudinal load factor during ground operations. Figure A-12 shows the data for pre- and postflight taxi. The higher number of occurrences of negative longitudinal load factor less than -0.15 g during the taxi in phase are possibly due to braking action occurring at the higher taxi in speeds. Figure A-13 shows the landing rollout with and without thrust reverser deployment. Figures A-14 and A-15 present the cumulative probability of the maximum longitudinal load factor measured during the takeoff and landing rolls respectively.

5.2.3 Vertical Load Factor Data.

Vertical load factor statistics during all phases of ground operation with and without thrust reverser were derived and are presented. Figure A-16 presents the cumulative frequency of incremental vertical load factor during pre- and postflight taxi. There is no significant difference between the occurrences for the taxi in and taxi out phases. Figure A-17 presents the cumulative frequency of incremental vertical load factor during the takeoff roll, while figure A-18 presents the cumulative frequency of incremental vertical load factor during the landing roll for operation with and without thrust reverser. As can be seen, there is little difference in the frequency of vertical load factor occurrences resulting from taxi, takeoff roll, and landing roll except for positive occurrences during landing without thrust reverser. It is noteworthy (see figure A-13) that while the longitudinal load factor activity during landing without thrust reversers is less than for operation with thrust reversers, the opposite is true for the vertical load factors. Figure A-19 presents the cumulative probability of the minimum and maximum incremental vertical load factors associated with touchdown and ground spoiler deployment. Figure A-20 shows the coincident incremental vertical load factor and gross weight at touchdown for all flights.

5.2.4 Airspeed Data.

Figures A-21 and A-22 show the cumulative probabilities of airspeed at liftoff and touchdown rotation respectively. The liftoff speeds are approximately 20 knots higher than the touchdown speeds.

5.2.5 Flare Data.

Figure A-23 presents the cumulative probability of airspeed at flare. Since the actual instant of flare is difficult to determine with any great accuracy, the start of flare was assumed to occur 3 seconds prior to main gear squat switch closure.

5.2.6 Pitch/Rotation Data.

The cumulative probability of maximum pitch angle at takeoff and landing is presented in figure A-24. Figure A-25 presents the cumulative probability of maximum takeoff pitch rate at takeoff rotation and at nose gear touchdown. For liftoff the pitch rate is for nose up rotation while for the nose gear touchdown condition the pitch rate is for a nose down rotation. Figure A-26 presents the cumulative probability of pitch angle that occurs at touchdown peak vertical load factor.

5.3 FLIGHT LOADS DATA.

The flight loads data include the statistical data that describe the gust and maneuver environment. The gust environment is presented in the form of cumulative occurrences of derived gust velocity, continuous gust intensity, and vertical load factor. The derived gust velocity and continuous gust intensity are computed values as described in section 4.3. Since the 1950's, it has been common practice to present flight loads data as cumulative occurrences. Data that were previously recorded on the B-737 are reported in references 4 and 5 as cumulative occurrences per 1000 hours. To compare to data from different references, the normal acceleration data are plotted two ways, as cumulative occurrences per 1000 hours and as cumulative occurrences per nautical mile.

5.3.1 Gust Loads Data.

The gust data are presented in the form of derived gust velocity, U_{de}, and continuous gust intensities, U_{σ}. The magnitudes of the derived gust velocities and the continuous gust intensities were derived from the measured gust accelerations in accordance with the procedures presented in paragraphs 4.3.4 and 4.3.5. Figure A-27 presents the cumulative occurrences of incremental vertical gust load factor per 1000 hours. The data are presented by phase of flight. Figure A-28 shows cumulative occurrences of incremental vertical gust load factor for the total combined airborne phases per 1000 hours. Figure A-29 presents the cumulative occurrences of incremental vertical gust load factor per nautical mile by phase of flight, and figure A-30 shows the cumulative occurrences of incremental vertical gust load factor for the total combined airborne phases per nautical mile. In figures A-31 through A-37 the derived gust velocity, U_{de}, is plotted as cumulative counts per nautical mile for altitudes from sea level to 39,500 feet. The figures also present the repeated gust velocities from reference 6. The gust velocity data from reference 6 are frequently used in establishing structural design criteria for commercial aircraft. As can be seen, the gust velocity data presented in this report exceeds the data from reference 6 at altitudes below 4500 feet. At higher altitudes the data from reference 6 becomes more severe than that obtained from the measurements presented in this report. Figures A-38 and A-39 present the derived gust velocity, U_{de}, as cumulative counts per nautical mile with flaps extended and

retracted respectively. Figures A-40 and A-41 present the cumulative occurrences of continuous gust intensity per nautical mile for flaps extended and flaps retracted conditions respectively.

5.3.2 Maneuver Loads Data.

The technique used to identify maneuvers assumes that maneuvers are associated primarily with turning conditions and that the impact of pitch maneuvers is insignificant and can be ignored. As a result, maneuvers resulting from push down or pull up maneuvers are ignored and only positive maneuver load factors resulting from banked turns are identified.

Figures A-42 through A-46 present the cumulative occurrences of maneuver load factor per 1000 hours by altitude for each of the airborne flight phases, i.e., departure, climb, cruise, descent, and approach. Figures A-47 through A-51 show the cumulative occurrences of maneuver load factor by altitude per nautical mile in the airborne phases of flight. Figure A-52 presents the total cumulative occurrences of incremental maneuver load factor per 1000 hours for each phase of flight, regardless of altitude. Figure A-53 shows the total cumulative occurrences of incremental maneuver load factor per 1000 hours for all flight phases combined. Figure A-54 shows the total cumulative occurrences of incremental maneuver load factor per nautical mile for each phase of flight regardless of altitude. Figure A-55 presents the total cumulative occurrences of incremental maneuver load factor per nautical mile for all flight phases combined.

5.3.3 Combined Maneuver and Gust Loads Data.

For the data presented in this section, the maneuver and gust load factors were not separated, but the total load factor occurrences regardless of the cause were used in the derivation of the figures. Figure A-56 shows the cumulative occurrences of total combined maneuver and gust normal load factor per 1000 hours by phases of flight, and figure A-57 shows the occurrences for all phases combined. Figures A-58 and A-59 show the data of figures A-56 and A-57 as occurrences per nautical mile. Figure A-60 presents the cumulative occurrences per 1000 hours of the lateral load factors measured during the flights. Assuming that normal banked turns are flown as coordinated maneuvers, the lateral load factors are the result of lateral turbulence inputs.

Federal Aviation Regulation (FAR) 25.333 requires that airplane structural operating limitations be established at each combination of airspeed and load factor on and within the boundaries of maneuvering and gust load envelopes (V-n diagrams). For purposes of displaying the coincident maneuver or gust accelerations, four representative V-n diagrams were developed from the FAR requirements.

The required limit load factors for maneuvers are specified in FAR 25.337. The positive limit maneuvering load factor (n) may not be less than 2.5, and the negative limit maneuvering load factor may not be less than -1.0 at speeds up to V_C, varying linearly with speeds to zero at V_D. FAR 25.345 specifies that the positive limit maneuver load factor is 2.0 g when the flaps are extended. The stall curve on the left side of the envelopes is determined by the maximum lift coefficient. The curve was estimated by using the 1 g stall speed to estimate $C_{L_{max}}$.

The required limit load factors for gusts result from gust velocities as specified in FAR 25.341. The FAR specifies positive (up) and negative (down) air gust design requirements for three different aircraft design speeds: maximum gust intensity (V_B), cruising speed (V_C), and dive speed (V_D). Between sea level and 20,000 feet, the gust requirement is constant, varying linearly to the value given for 50,000 feet. FAR 25.345 sets a requirement of positive, negative, and head-on for 25 fps gusts when flaps are extended. These gust design requirements are shown in table 9.

TABLE 9. FAR REQUIREMENTS FOR DERIVED DISCRETE GUST VELOCITIES

Aircraft Design Speed	Gust Velocity	
	0-20,000 Feet Altitude	50,000 Feet Altitude
V_B	66 fps	38 fps
V_C	50 fps	25 fps
V_D	25 fps	12.5 fps
Flaps Extended	25 fps	—

Sufficient data to generate V-n diagrams for all weight and altitude conditions were not available. Therefore, sea level data were used to develop the representative diagrams, and all of the recorded maneuvers and gusts were plotted on these. A weight of 115,000 lbs, the most frequent average landing weight, was used for the calculations required in developing these diagrams.

Figures A-61 through A-64 show the V-n diagrams for maneuver and for gust with flaps retracted and extended. Coincident acceleration and speed measurements are also plotted on the V-n diagrams. As can be seen in figure A-64, a large number of gust accelerations occurred outside the gust V-n diagram for the flaps extended case. This is consistent with the data of figures A-31 to A-33, which indicate larger and more frequent gust velocities at altitudes below 4500 feet.

5.4 MISCELLANEOUS OPERATIONAL DATA.

The miscellaneous operational data includes statistical usage information for flaps, speed brake/spoilers, thrust reversers, and landing gear operations. Although aileron and rudder deflection information was available, it was not processed because it was deemed that the slow sampling rates prevented the reduction of reliable statistical usage information for these components.

5.4.1 Flap Usage Data.

Flap usage statistics of value in the design of flap structure, backup structure, and other flap components were reduced from the measured data. Figure A-65 presents the cumulative probability of maximum airspeed encountered in various flap detents during the departure phase

of the flights. Detents 30 and 40 are not shown because only a single occurrence was identified during all the flights. The flap detents are defined in table 7. Figure A-66 presents similar data for the approach phase of the flights. Figures A-67 and A-68 present the percent of time spent in various flap detents during the departure and approach phases of flight, respectively. As shown in figure A-67, flap detent 13 was the detent used in almost all cases during departure. From figure A-68 it appears that very little time is spent in detent 25 during the approach phase of the flight. Figures A-69 and A-70 show the cumulative probability of maximum dynamic pressure encountered while in different flap detents for the departure and approach phases respectively.

5.4.2 Speed Brake/Spoiler Usage Data.

Information on speed brake operations during flight was determined to be of primary interest to various users of the data. Therefore, statistics on speed brake usage as a function of speed, altitude, and deflection angle were derived from the measured data. To be counted as a deployment cycle the speed brake had to deflect more than 7 degrees for a period of 3 seconds. Data on spoiler operations occurring during the landing roll are available but were not reduced into statistical format. Figure A-71 presents the cumulative occurrences of maximum speed encountered while the speed brakes were deployed, while figure A-72 shows the cumulative occurrences of speed at the moment of speed brake deployment. Figure A-73 presents the cumulative occurrences of altitude at the moment of speed brake deployment. Figure A-74 presents the cumulative probability of maximum deployment angle reached during the time that the speed brakes were deployed for the flaps retracted configuration. No speed brake cycles were counted for the conditions of flaps deflected in various detents.

5.4.3 Thrust Reverser Data.

Cumulative probabilities of duration and speed associated with thrust reverser operations were derived from the measured data. Figure A-75 presents the cumulative probability of total time that thrust reversers are deployed.

5.4.4 Landing Gear Extension and Retraction Data.

Landing gear operating statistics were reduced from the measured data. The information can be used to support design, evaluation, and monitoring of the landing gear and associated structure. Figure A-76 shows the cumulative probability of total time with the landing gear extended after liftoff. Figure A-77 shows the cumulative probability of time with the landing gear extended prior to touchdown. As is expected, the time with gear extended during approach is considerably longer than the time after liftoff when the pilot retracts the gear within seconds after liftoff. Figure A-78 presents the cumulative probability of the maximum airspeed during the time that the gear is extended for both the departure and approach phases of flight.

6. CONCLUSIONS.

Incorporation of the additional data formats in this report adds considerable value to the FAA Airborne Data Monitoring Systems Research Program. The data provides very useful statistical information to the aircraft manufacturers, airlines, and the FAA.

The data in this report is based on 7120 hours. For military aircraft a rule of thumb has been that a minimum of recorded flight hours equal to one design life is necessary to provide a reliable database. However, military aircraft generally fly a variety of different mission profiles. In contrast, the commercial aircraft is used in a fairly well defined mission, except for duration. Thus recorded flight hours equal to one design life may not be necessary. What this number should be is not quite clear at this time. At the same time the number of hours on which the data in reference 3 was based was found to be insufficient to provide meaningful results. It would seem prudent to continue the data gathering for some time until a stable database is obtained.

The data in figure A-66 shows that the measured gust load factors for the flaps extended configuration often occur outside the design V-n diagram. Identical data in reference 3, based on fewer flight hours, do not show such occurrences. However, data in reference 7 based on considerably more flights show similar exceedances of the V-n diagram. Again, this points to the need for data based on an adequate number of flight hours and the danger of drawing conclusions based on limited data samples. Furthermore, the data suggests that the present gust design requirements for the flaps extended configuration may need to be reviewed for adequacy. An assessment of the appropriateness of the continued use of U_{de} values specified in FAR 25.345 for high lift devices appears to be justified. Derived gust velocity, U_{de}, values obtained from this effort show deviation from the data presented in reference 6. In general, for altitudes below 1500 feet the MD-82/83 data show higher levels of occurrences for the upward gusts and fewer for the downward gusts than presented in reference 6. For altitudes from 1500-4500 feet the new data is slightly higher than that of reference 6 for both downward and upward gusts. For the altitudes above 4500 feet the MD-82/83 occurrences are below those predicted by reference 6. In as much as reference 6 represented a rather preliminary effort to define atmospheric turbulence in power spectral format, the MD-82/83 data should also be compared to other study results to provide a more complete assessment of the MD-82/83 data and its influence on future design requirements.

Furthermore, calculation of turbulence field parameters, P and b values based on the MD-82/83 data, is considered desirable and should be included in future data reduction efforts. The resulting values should be compared with turbulence field parameters specified in reference 6 and appendix G to Part 25 of the FAR.

The technique used in this report to separate gust and maneuver accelerations results in positive maneuver occurrences only. The most common method previously used to separate maneuver and gust accelerations has been the so-called 2 second rule. From reviews of measured data and studies of aircraft response to elevator motion, it was determined that for larger aircraft essentially all of the maneuver load factor peaks can be expected to be counted if a time between zero crossings greater than 2 seconds is used. Load factor peaks with zero crossings less than 2 seconds will mostly all be gusts. This approach resulted in the identification of both positive and negative maneuver occurrences. A cursory review of the acceleration data shows that pitching maneuvers resulting in both positive and negative accelerations do occur with some frequency and magnitude in the climb phase. Unfortunately these occurrences are counted as gusts. A study to evaluate the impact of different maneuver and gust separation criteria is very important and should be done before much is made of the differences in the gust frequencies noted and before turbulence field parameters are derived.

Statistical information on flight control surface activity is a valuable input to the design requirements for these surfaces and their associated components. Flight control surface deflections are recorded at two samples per second (2 sps) and can easily be reduced to provide the desired information. Unfortunately, there are doubts about the adequacy of the sampling rates to provide reliable results. For this reason the flight control surface deflection data were not processed. A study to determine the sampling rates as a function of control surface deflection rate necessary to provide acceptable statistical surface deflection information would be invaluable.

7. REFERENCES.

1. Crabill, Norman L., "FAA/NASA Prototype Flight Loads Program Systems Requirements, B737-400 Aircraft," Eagle Aerospace Inc., Contract NAS1-19659, unpublished report, November 1994.

2. de Jonge, B., "Reduction of Incremental Load Factor Acceleration Data to Gust Statistics," DOT/FAA/CT-94/57, August 1994.

3. "Flight Loads Data for a Boeing 737-400 in Commercial Operation," Department of Transportation Report DOT/FAA/AR-95/21, April 1996.

4. "Data From Unusual Events Recording System in a Commercial 737 Aircraft," Technology Incorporated Instruments and Controls Division, Dayton OH, Report No. FAA-RD-72-113, November 1972.

5. Clay, Larry E., DeLong, Robert C., and Rockafellow, Ronald I., "Airline Operational Data From Unusual Events Recording Systems in 707, 727, and 737 Aircraft," Report No. FAA-RD-71-69, September 1971.

6. Press, Harry and Steiner, Roy, "An Approach to the Problem of Estimating Severe and Repeated Gust Loads for Missile Operations," National Advisory Committee for Aeronautics Technical Note 4332, September 1958, Langley Aeronautical Laboratory, Langley Field, Va.

7. "Flight Loads Data for a Boeing 737-400 in Commercial Operation," Department of Transportation Report DOT/FAA/AR-98/28, August 1998.

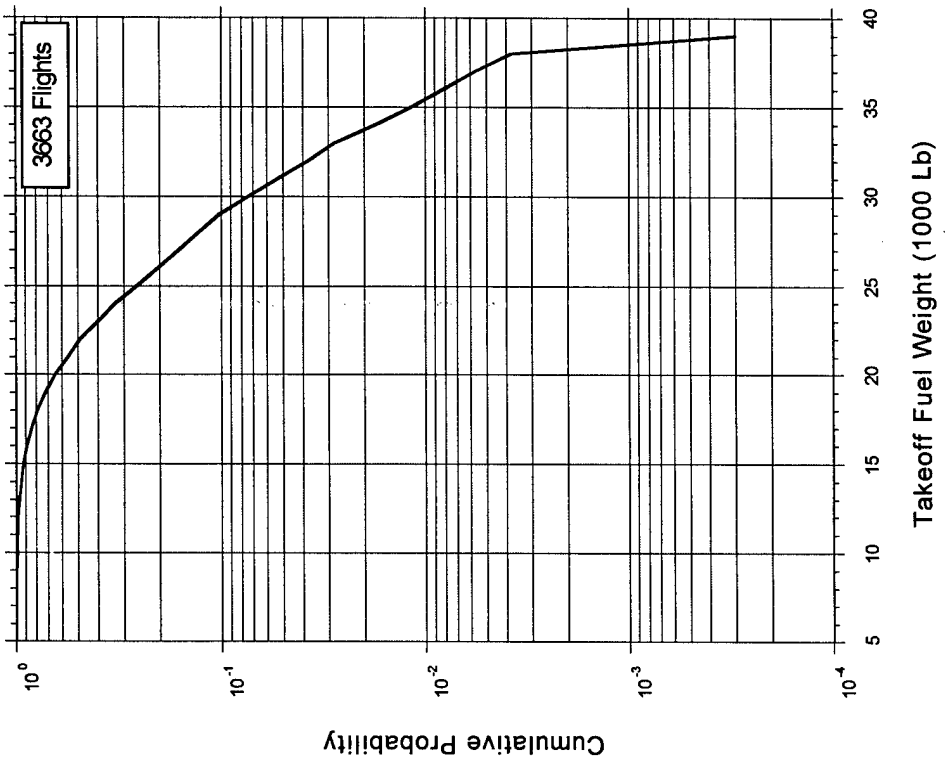

FIGURE A-2. CUMULATIVE PROBABILITY OF TAKEOFF FUEL WEIGHT

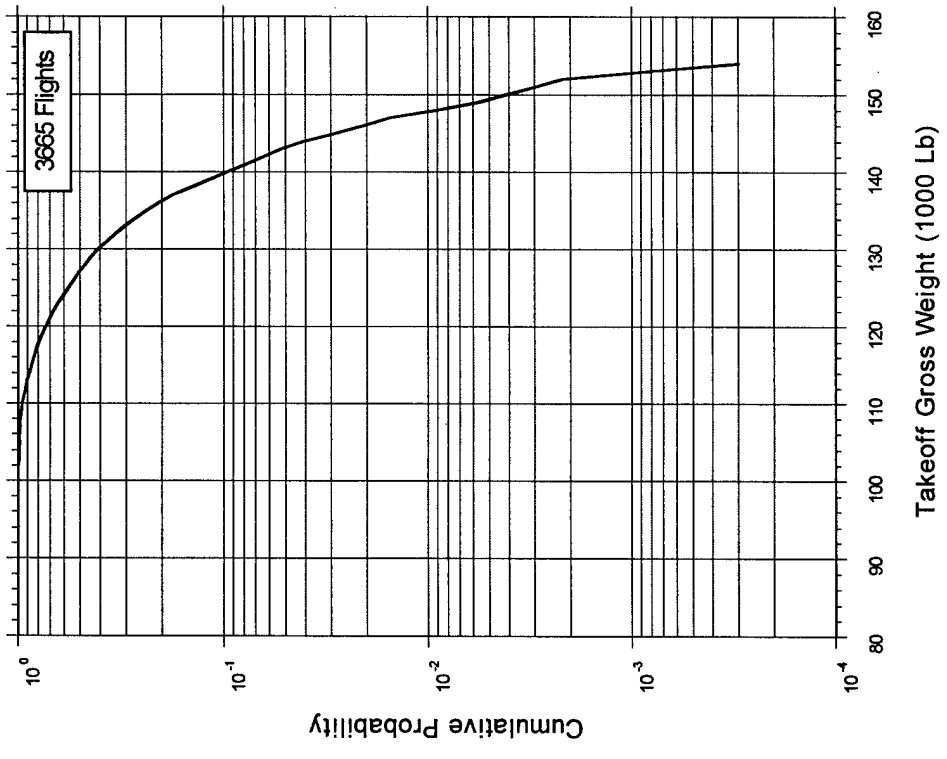

FIGURE A-1. CUMULATIVE PROBABILITY OF TAKEOFF GROSS WEIGHT

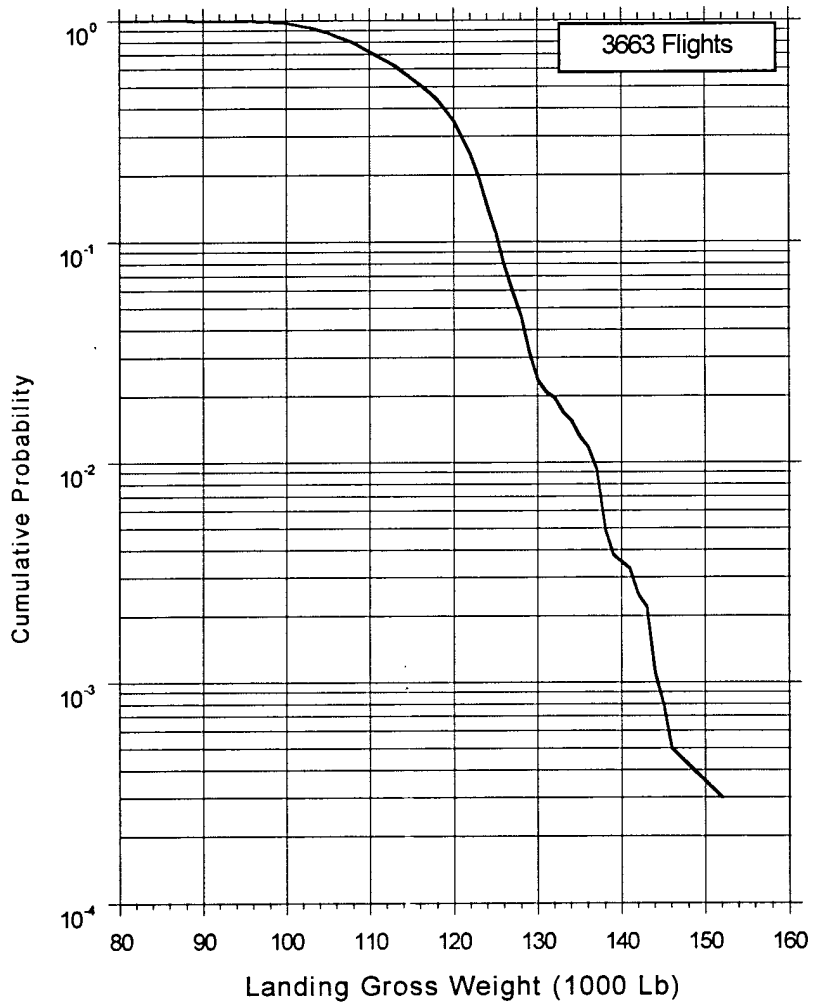

FIGURE A-3. CUMULATIVE PROBABILITY OF LANDING GROSS WEIGHT

Takeoff Fuel Weight (1000 Lb)

Flight Distance (nm)

3663 Flights	5-10	10-15	15-20	20-25	25-30	30-35	35-40	Total
0-250	0.137	5.815	6.197	4.313	1.256	0.218	0.027	17.963
250-500	0.055	0.983	10.538	2.812	1.256	0.137		15.779
500-750	0.109	0.055	10.511	12.968	2.839	0.137	0.055	26.672
750-1000	0.137	0.055	0.464	18.291	9.692	1.310	0.355	30.303
1000-1250	0.027			0.273	1.338	0.491		2.129
1250-1500	0.027	0.109		0.109	2.211	3.959	0.737	7.153
Total	0.491	7.016	27.710	38.766	18.591	6.252	1.174	100

FIGURE A-4. CORRELATION OF TAKEOFF FUEL WEIGHT AND FLIGHT DISTANCE, PERCENT OF FLIGHTS

Takeoff Gross Weight (1000 Lb)

Flight Distance (nm)

3665 Flights	80-90	90-100	100-110	110-120	120-130	130-140	140-150	150-160	Total
0-250	0.027	0.055	1.664	5.703	6.739	3.383	0.327	0.027	17.926
250-500			1.637	5.402	5.211	3.520			15.771
500-750			0.573	7.367	10.450	7.885	0.409		26.685
750-1000			0.300	3.138	8.513	13.888	4.447		30.286
1000-1250	0.027		0.027	0.273	0.628	0.546	0.655		2.156
1250-1500			0.055	0.218	1.173	2.074	3.274	0.382	7.176
Total	0.055	0.055	4.256	22.101	32.715	31.296	9.113	0.409	100

FIGURE A-5. CORRELATION OF TAKEOFF GROSS WEIGHT AND FLIGHT DISTANCE, PERCENT OF FLIGHTS

Gross Weight at Liftoff (1000 Lb)

Gross Weight at Touchdown (1000 Lb)

3665 Flights	80-90	90-100	100-110	110-120	120-130	130-140	140-150	150-160	Total
70-80	0.055								0.055
80-90			0.191						0.191
90-100		0.055	1.937	0.764					2.756
100-110			2.128	16.835	5.921	0.164			25.048
110-120				4.502	22.183	9.850	0.437		36.971
120-130					4.611	19.318	8.349	0.355	32.633
130-140						1.965	0.055		2.019
140-150							0.273	0.027	0.300
150-160								0.027	0.027
Total	0.055	0.055	4.256	22.101	32.715	31.296	9.113	0.409	100

FIGURE A-6. CORRELATION OF GROSS WEIGHT AT LIFTOFF AND TOUCHDOWN, PERCENT OF FLIGHTS

Maximum Altitude (1000 Feet)

Flight Distance (nm) 3987 Flights	0-5	5-10	10-15	15-20	20-25	25-30	30-35	35-40	40-45	Total
0-250	0.125	0.025	0.075	0.903	1.630	5.542	10.782	5.316	0.100	24.498
250-500				0.025	0.025	0.903	7.046	6.244	0.276	14.519
500-750					0.176	1.254	12.187	10.757	0.176	24.549
750-1000					0.050	1.028	17.528	9.027	0.226	27.859
1000-1250					0.050	0.075	1.053	0.777	0.025	1.981
1250-1500						0.100	4.388	2.081	0.025	6.595
Total	0.125	0.025	0.075	0.928	1.931	8.902	52.984	34.203	0.827	100

FIGURE A-7. CORRELATION OF MAXIMUM ALTITUDE AND FLIGHT DISTANCE, PERCENT OF FLIGHTS

Total Flight Distance (nm)

Altitude Band (Feet) 3987 Flights	0-250	250-500	500-750	750-1000	1000-1250	1250-1500	1500-1750
29500-39500	8.35	43.93	62.99	70.36	70.65	78.70	83.39
19500-29500	37.81	27.24	18.58	15.96	17.88	12.59	7.25
9500-19500	32.48	17.08	10.85	8.16	6.83	5.13	5.56
4500-9500	12.03	6.49	4.22	3.05	2.59	1.89	2.16
1500-4500	7.37	3.90	2.45	1.85	1.53	1.25	1.22
500-1500	1.40	0.88	0.60	0.43	0.37	0.32	0.29
0-500	0.55	0.47	0.32	0.19	0.16	0.12	0.14
Total	100	100	100	100	100	100	100

FIGURE A-8. PERCENT OF TOTAL DISTANCE IN ALTITUDE BANDS

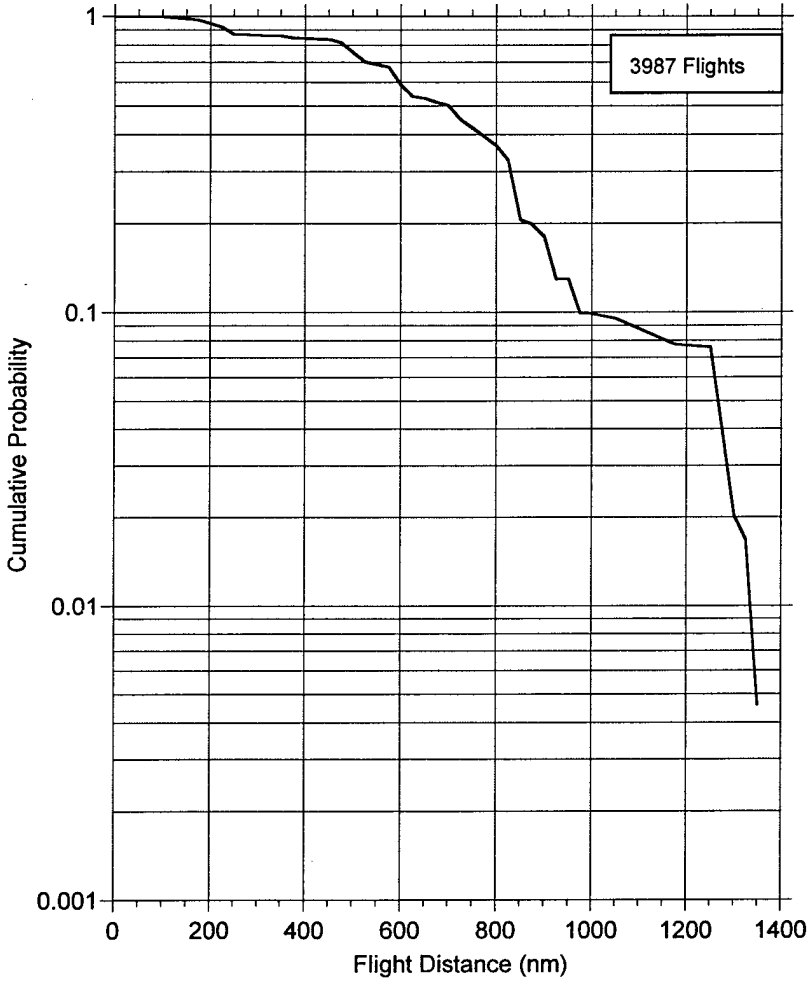

FIGURE A-9. CUMULATIVE PROBABILITY OF GREAT CIRCLE FLIGHT DISTANCE

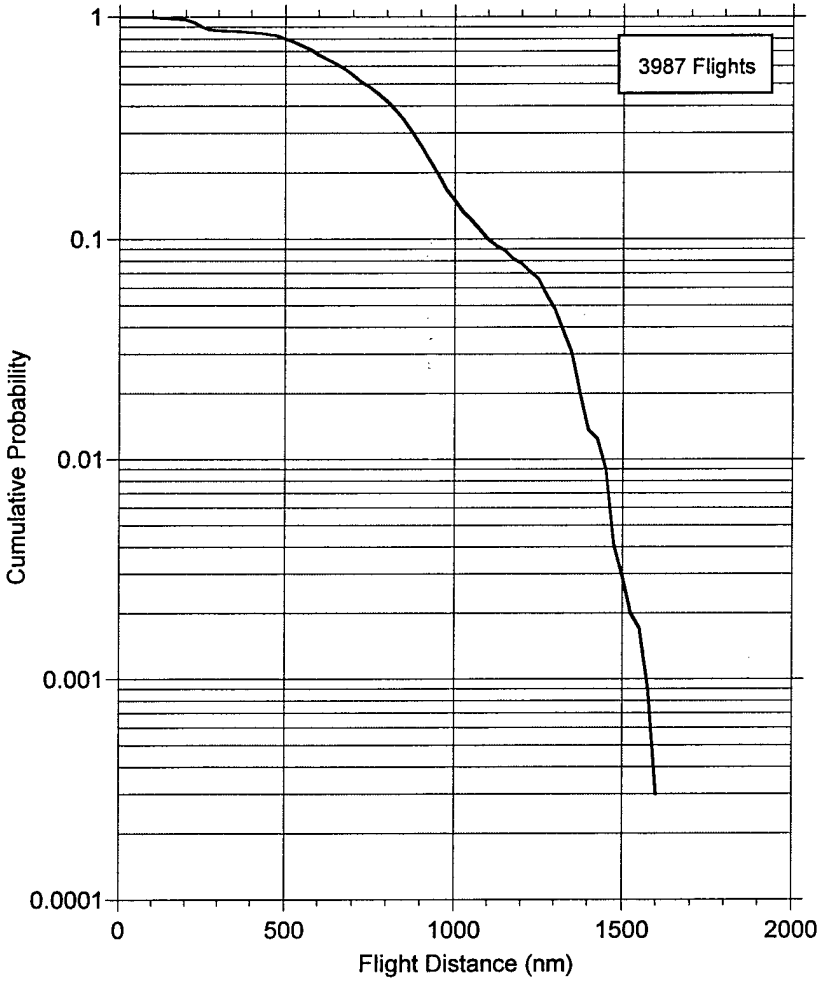

FIGURE A-10. CUMULATIVE PROBABILITY OF INTEGRATED FLIGHT DISTANCE

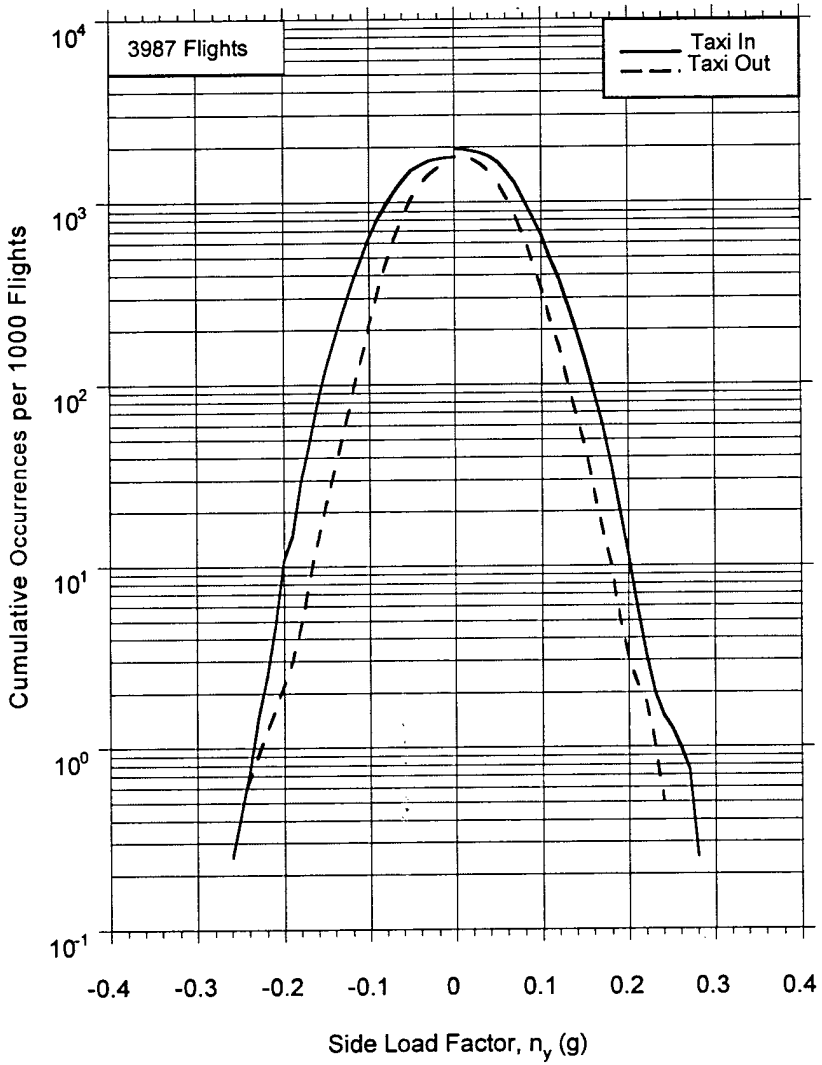

FIGURE A-11. CUMULATIVE FREQUENCY OF MAXIMUM SIDE LOAD FACTOR DURING GROUND TURNS

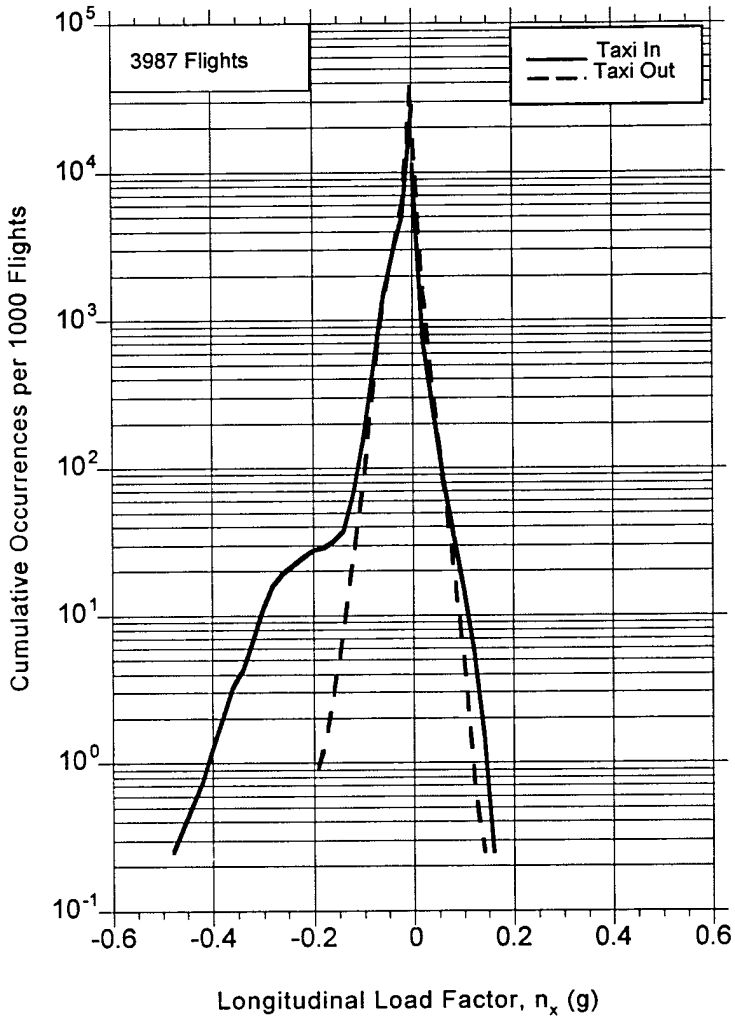

FIGURE A-12. CUMULATIVE FREQUENCY OF LONGITUDINAL LOAD FACTOR DURING GROUND TAXI

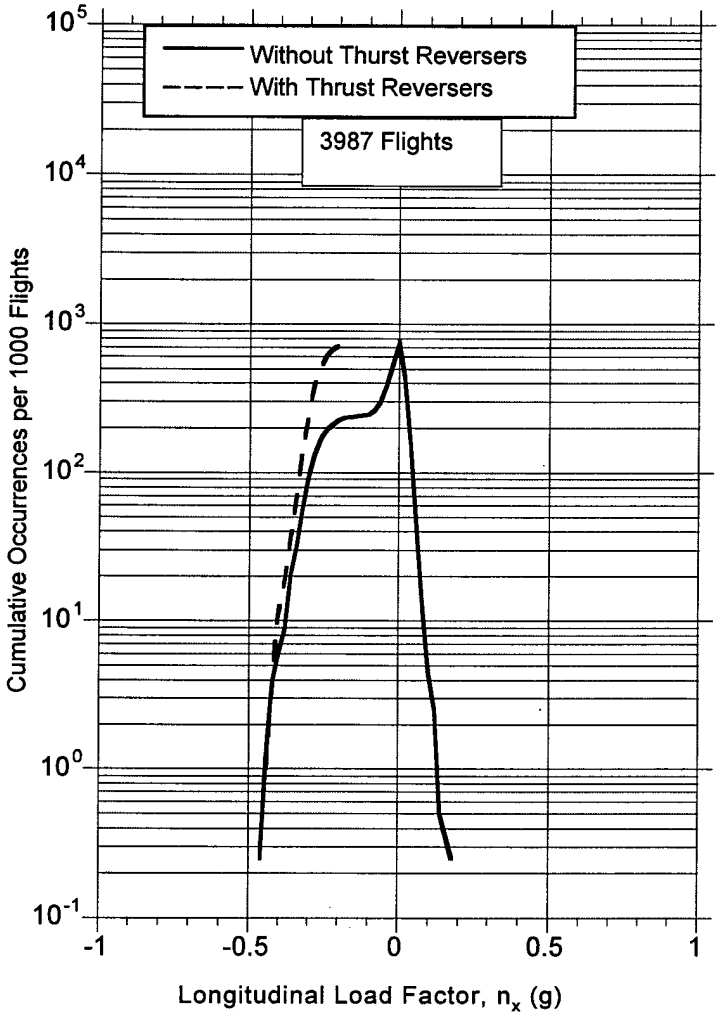

FIGURE A-13. CUMULATIVE FREQUENCY OF LONGITUDINAL LOAD FACTOR DURING LANDING ROLL

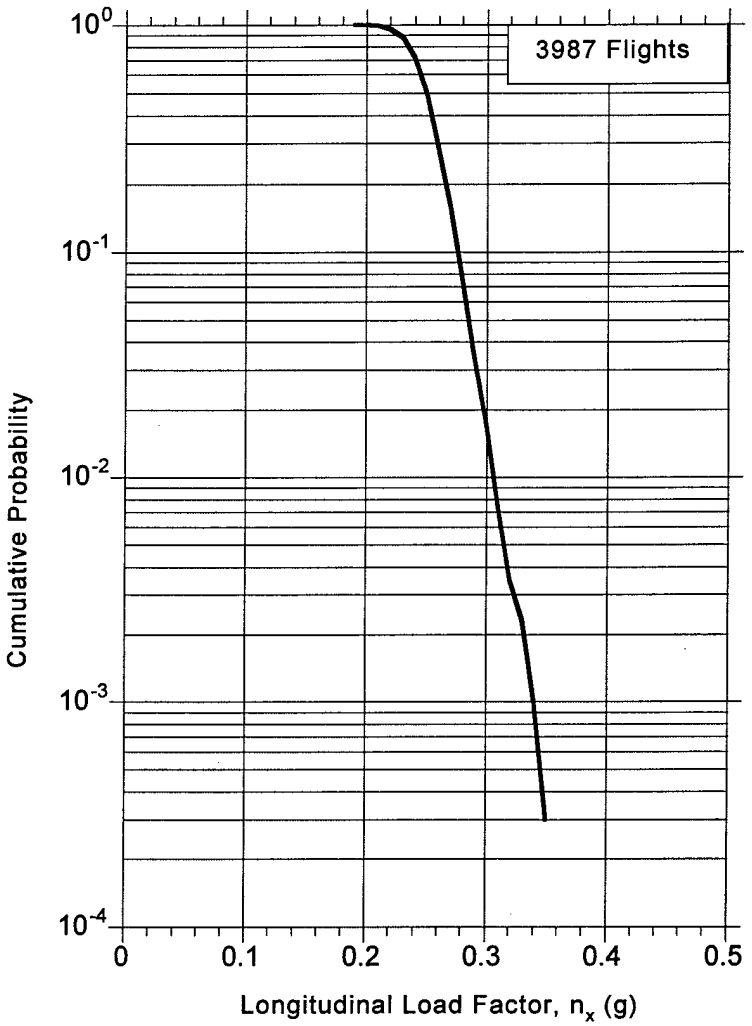

FIGURE A-14. CUMULATIVE PROBABILITY OF MAXIMUM LONGITUDINAL LOAD FACTOR DURING TAKEOFF

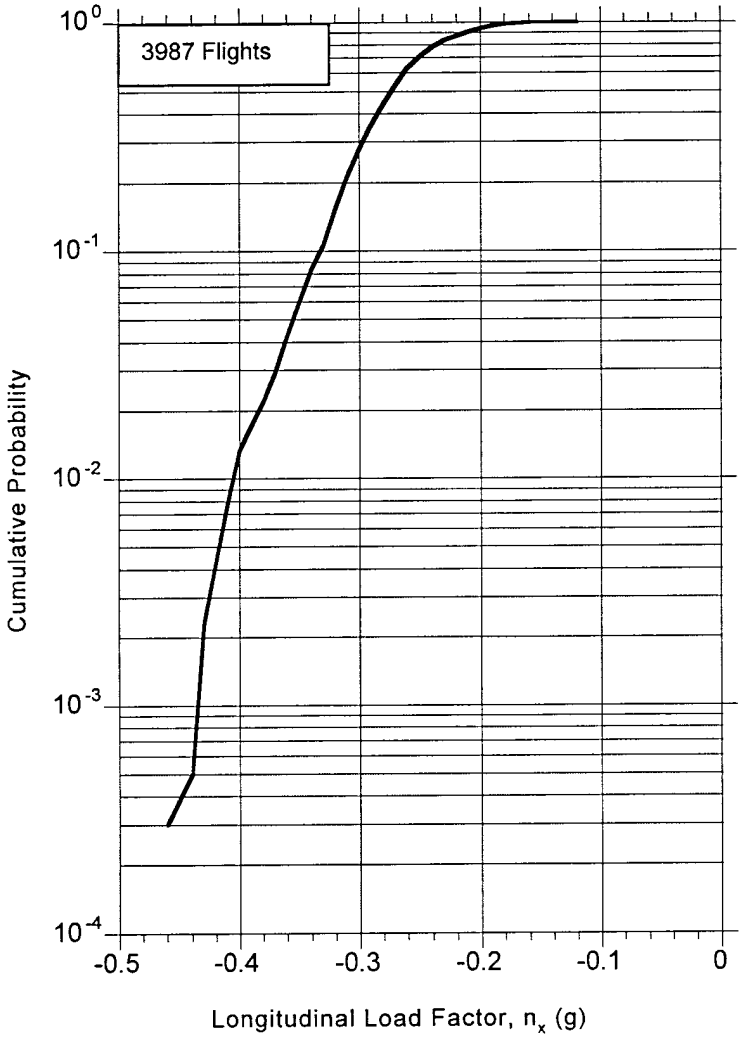

FIGURE A-15. CUMULATIVE PROBABILITY OF MINIMUM LONGITUDINAL LOAD FACTOR DURING LANDING

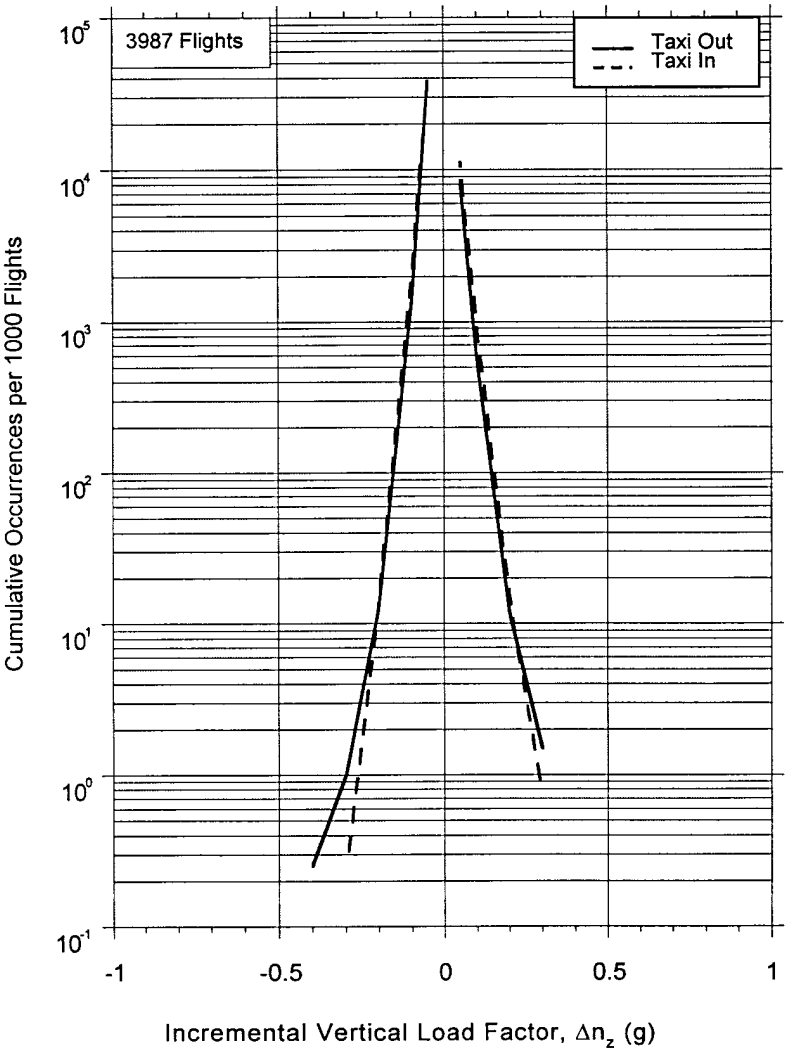

FIGURE A-16. CUMULATIVE FREQUENCY OF INCREMENTAL VERTICAL LOAD FACTOR DURING TAXI OPERATIONS

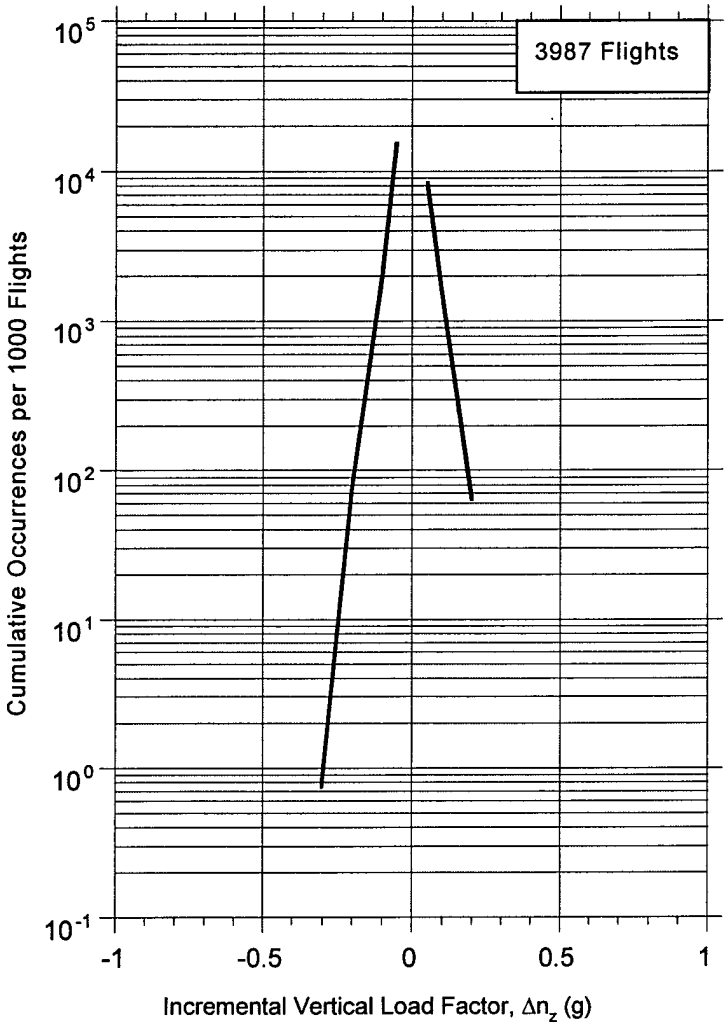

FIGURE A-17. CUMULATIVE FREQUENCY OF INCREMENTAL VERTICAL LOAD FACTOR DURING TAKEOFF ROLL

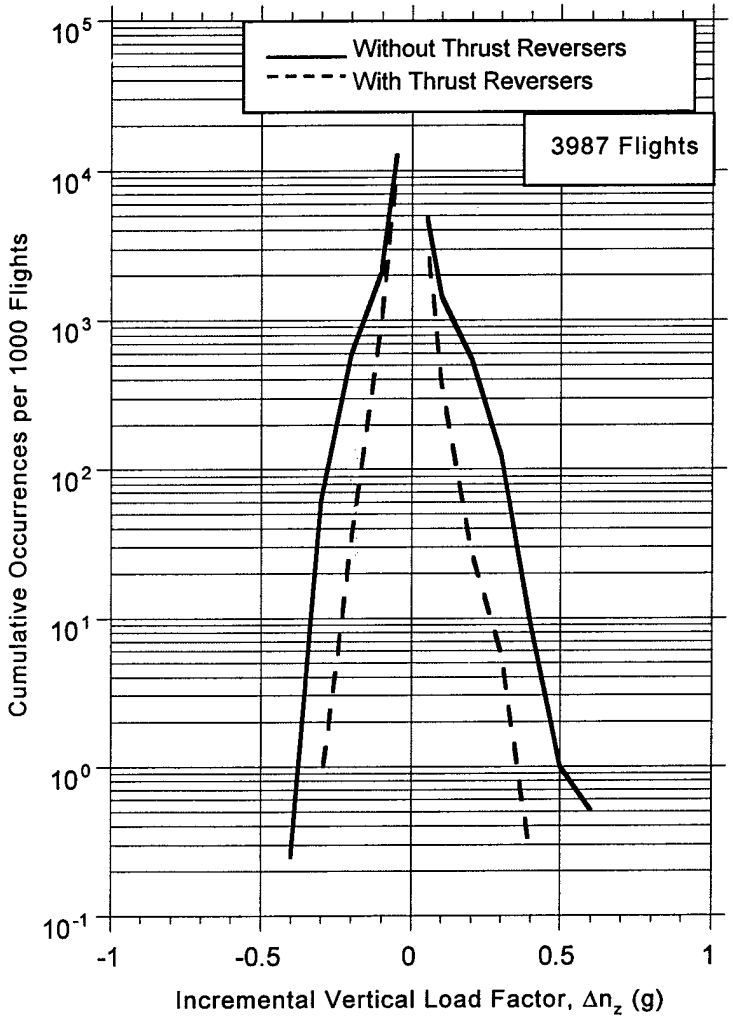

FIGURE A-18. CUMULATIVE FREQUENCY OF INCREMENTAL VERTICAL LOAD FACTOR DURING LANDING ROLL

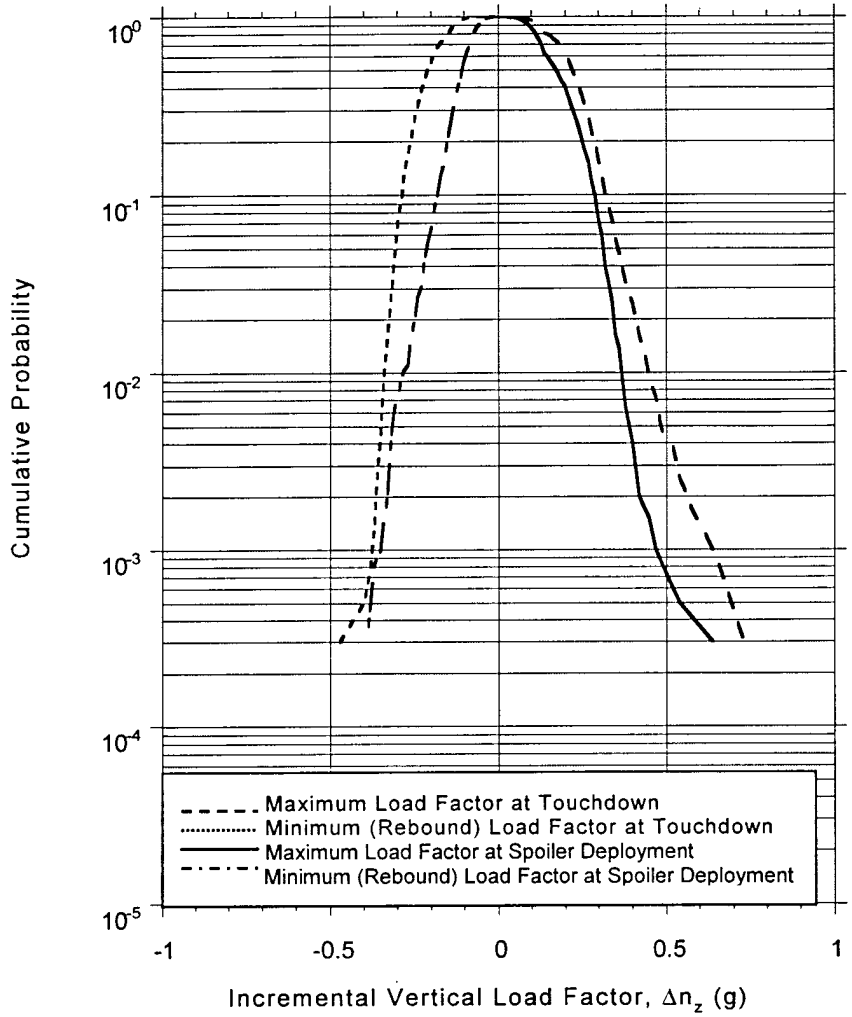

FIGURE A-19. CUMULATIVE PROBABILITY OF MINIMUM AND MAXIMUM INCREMENTAL VERTICAL LOAD FACTOR AT TOUCHDOWN AND SPOILER DEPLOYMENT

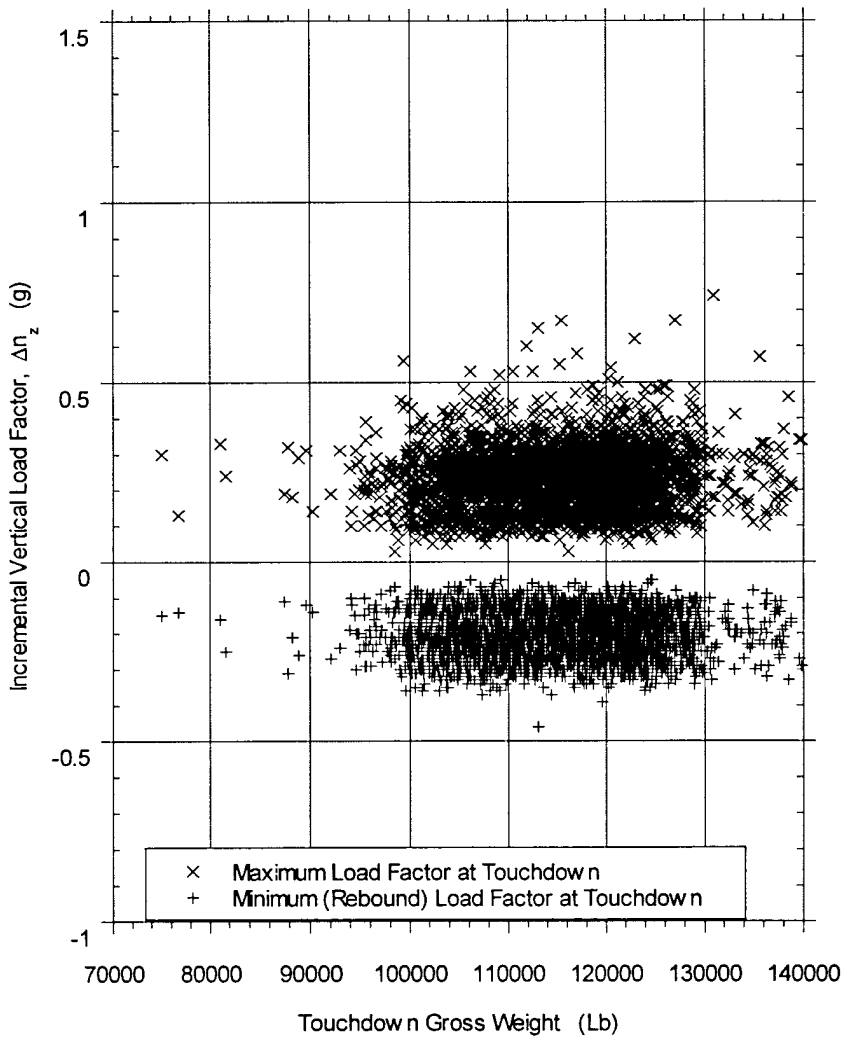

FIGURE A-20. COINCIDENT INCREMENTAL VERTICAL LOAD FACTOR AND TOUCHDOWN GROSS WEIGHT

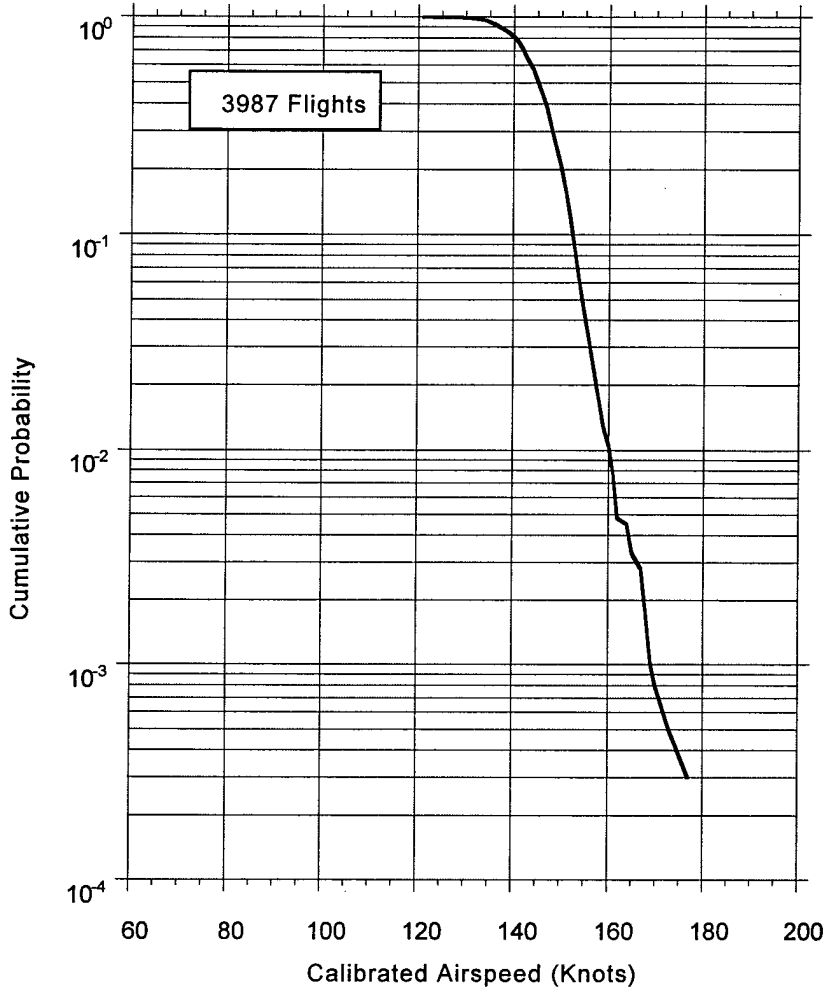

FIGURE A-21. CUMULATIVE PROBABILITY OF AIRSPEED AT LIFTOFF

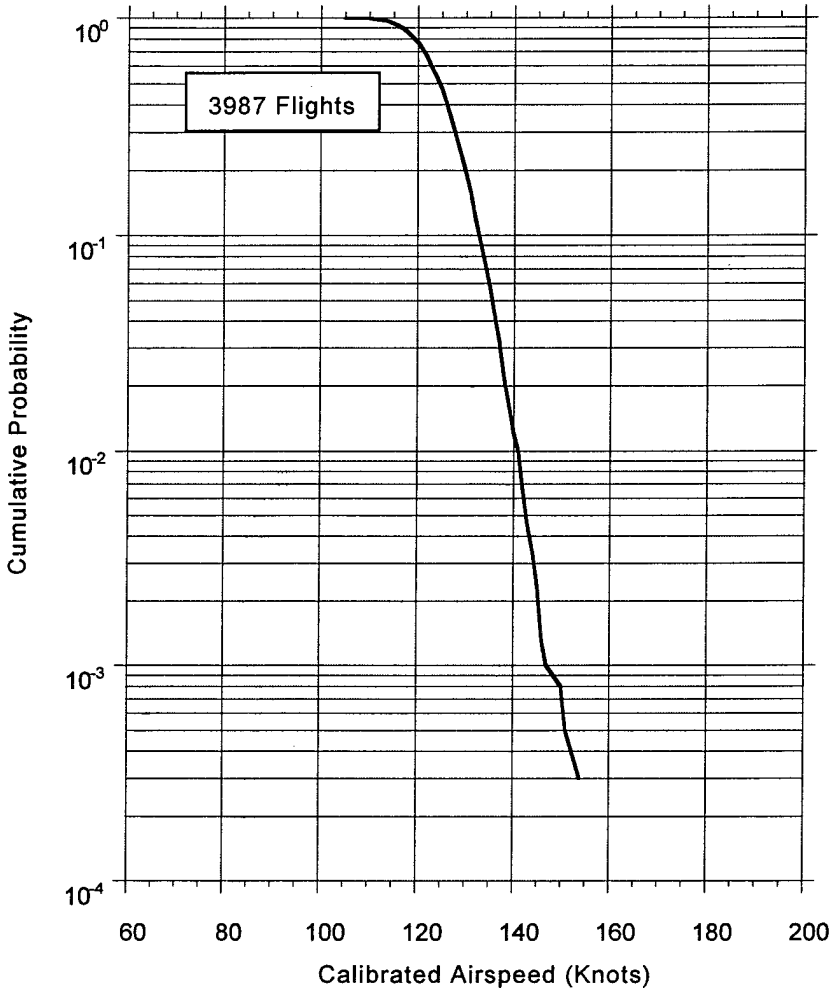

FIGURE A-22. CUMULATIVE PROBABILITY OF AIRSPEED AT TOUCHDOWN

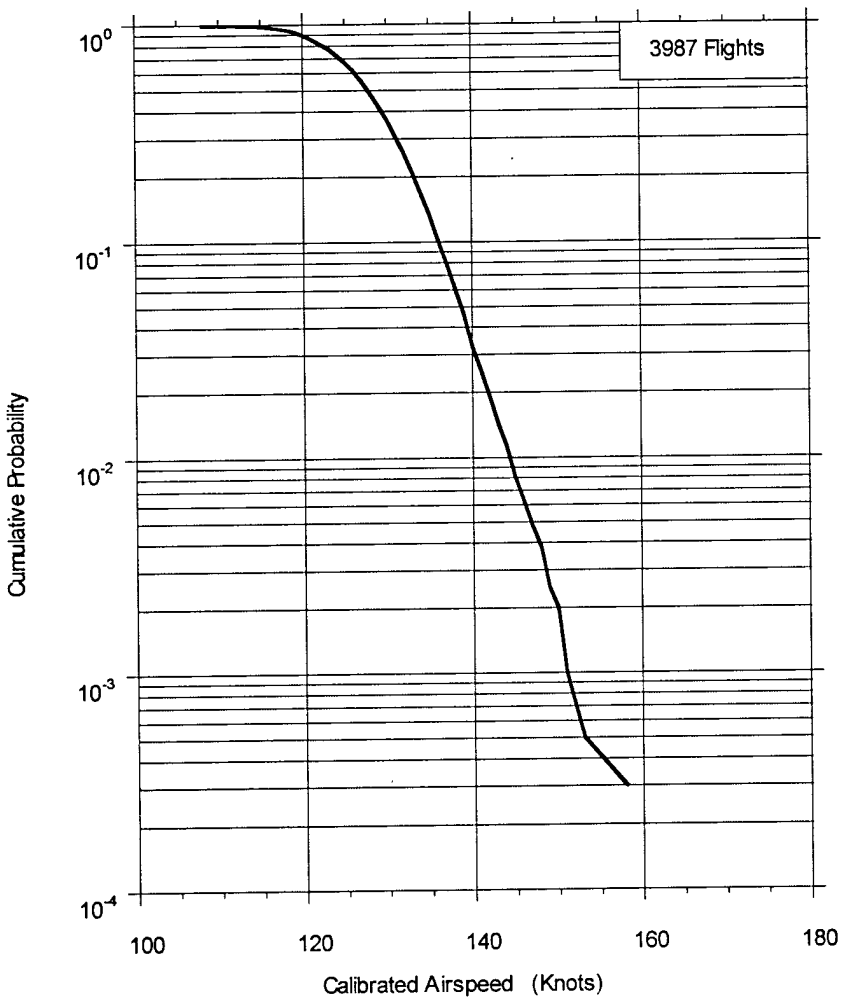

FIGURE A-23. CUMULATIVE PROBABILITY OF AIRSPEED AT FLARE

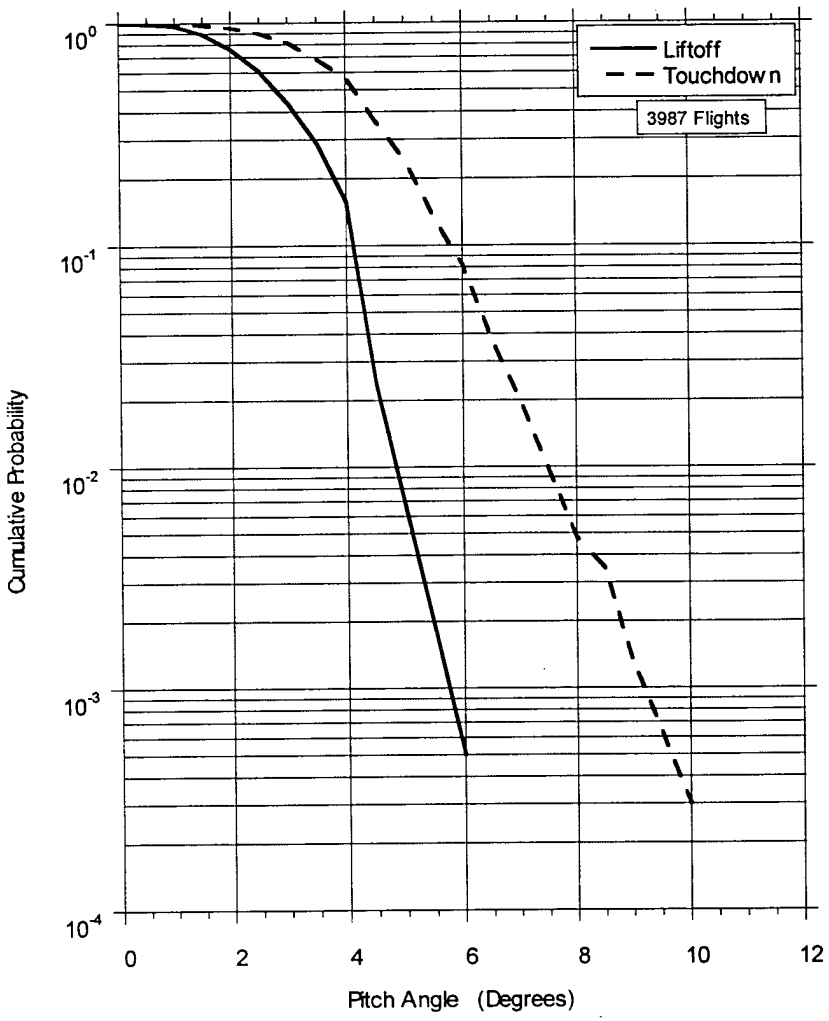

FIGURE A-24. CUMULATIVE PROBABILITY OF PITCH ANGLE AT LIFTOFF AND TOUCHDOWN

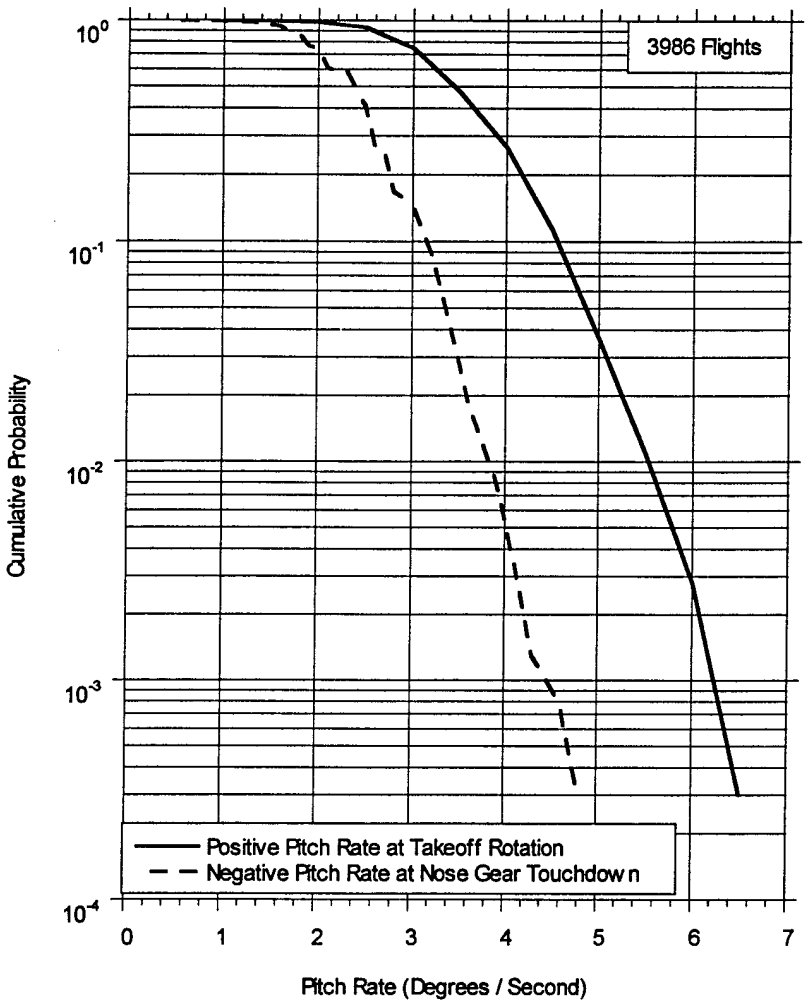

FIGURE A-25. CUMULATIVE PROBABILITY OF MAXIMUM PITCH RATE AT TAKEOFF ROTATION AND NOSE GEAR TOUCHDOWN

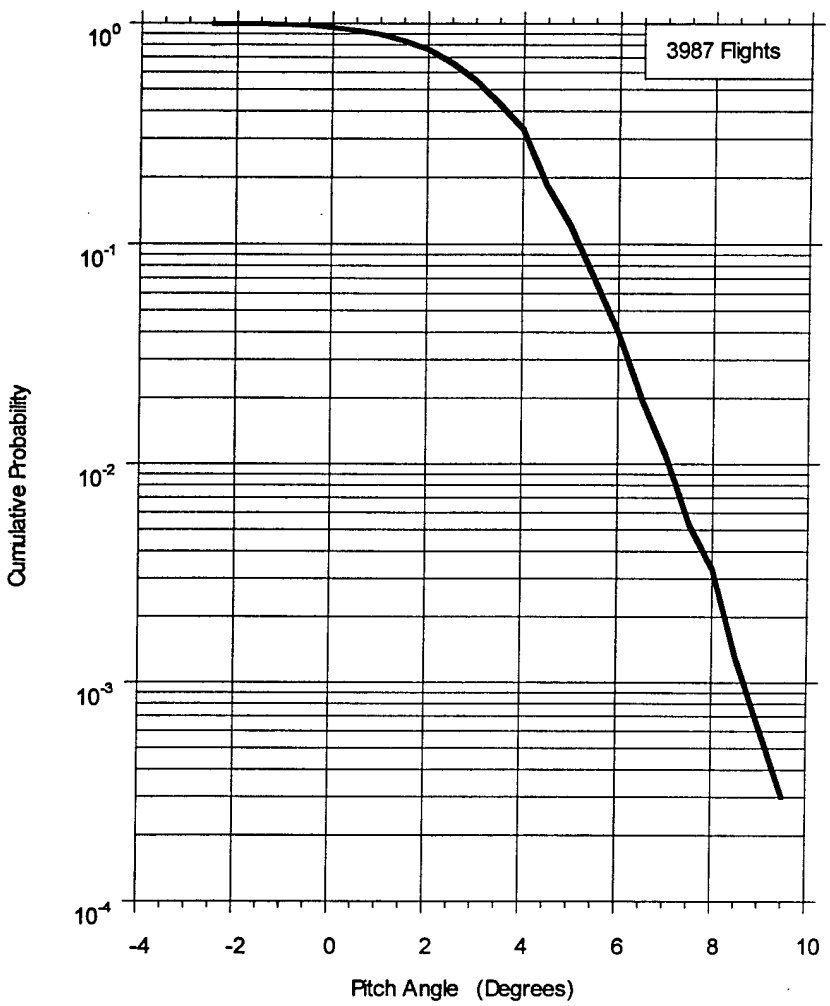

FIGURE A-26. CUMULATIVE PROBABILITY OF PITCH ANGLE AT TOUCHDOWN PEAK VERTICAL LOAD FACTOR

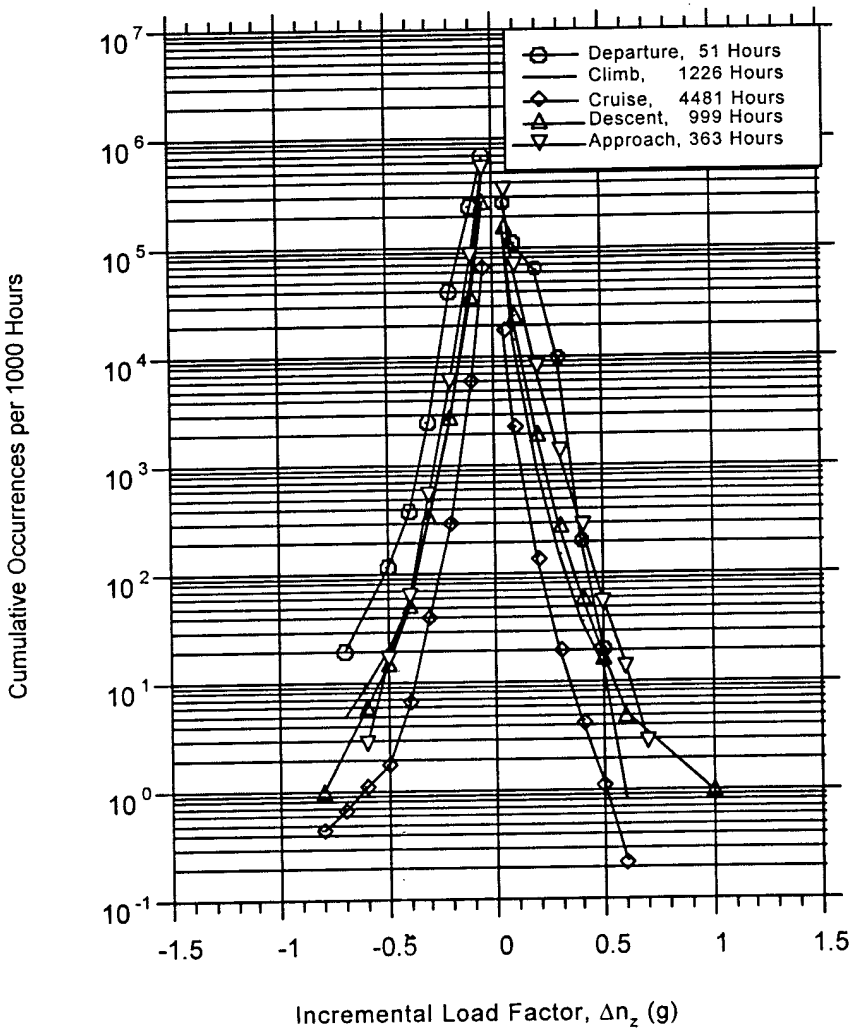

FIGURE A-27. CUMULATIVE OCCURRENCES OF VERTICAL GUST LOAD FACTOR PER 1000 HOURS BY FLIGHT PHASE

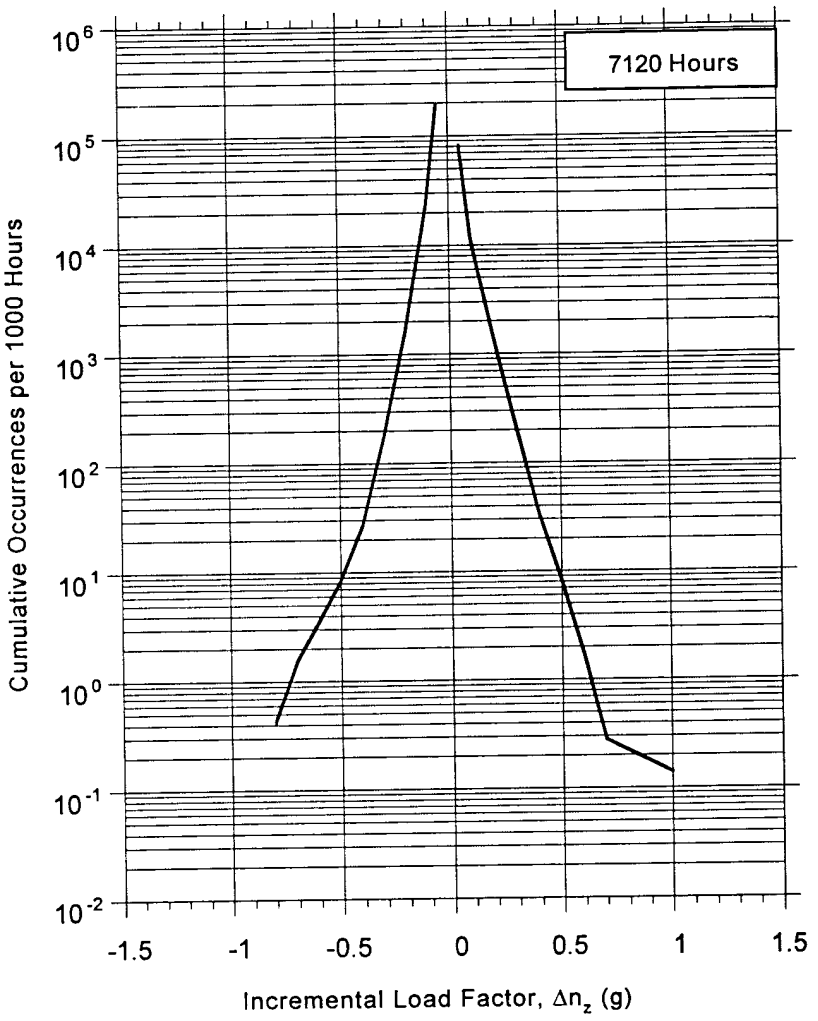

FIGURE A-28. CUMULATIVE OCCURRENCES OF INCREMENTAL VERTICAL GUST LOAD FACTOR PER 1000 HOURS, COMBINED FLIGHT PHASES

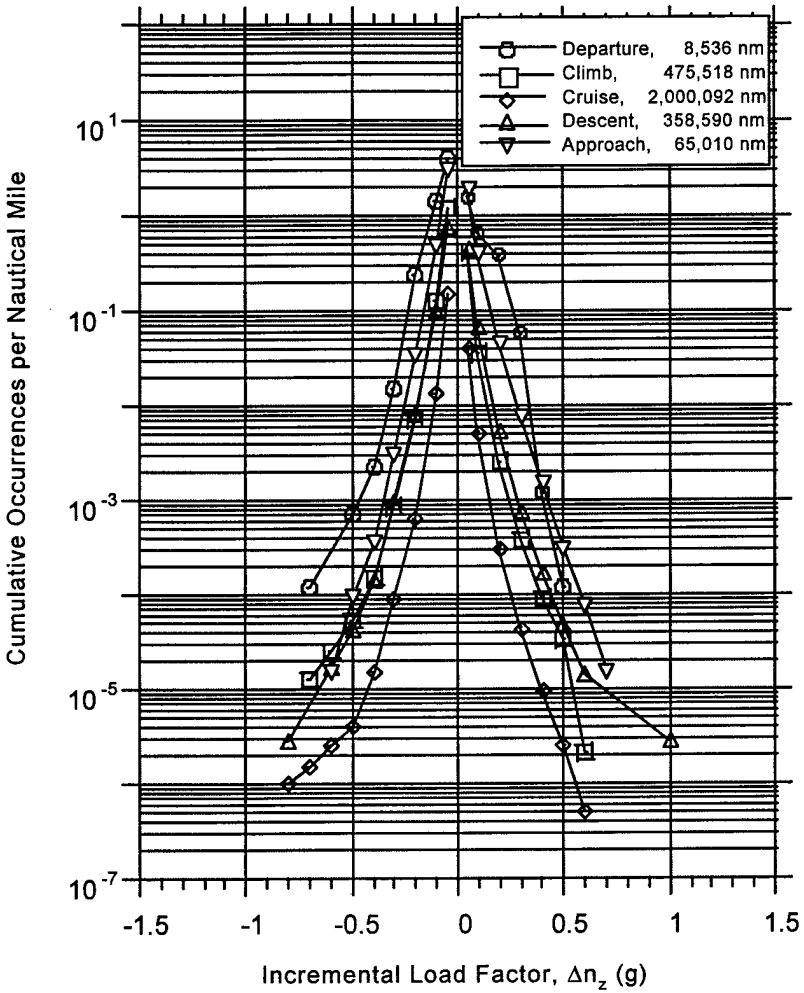

FIGURE A-29. CUMULATIVE OCCURRENCES OF VERTICAL GUST LOAD FACTOR PER NAUTICAL MILE BY FLIGHT PHASE

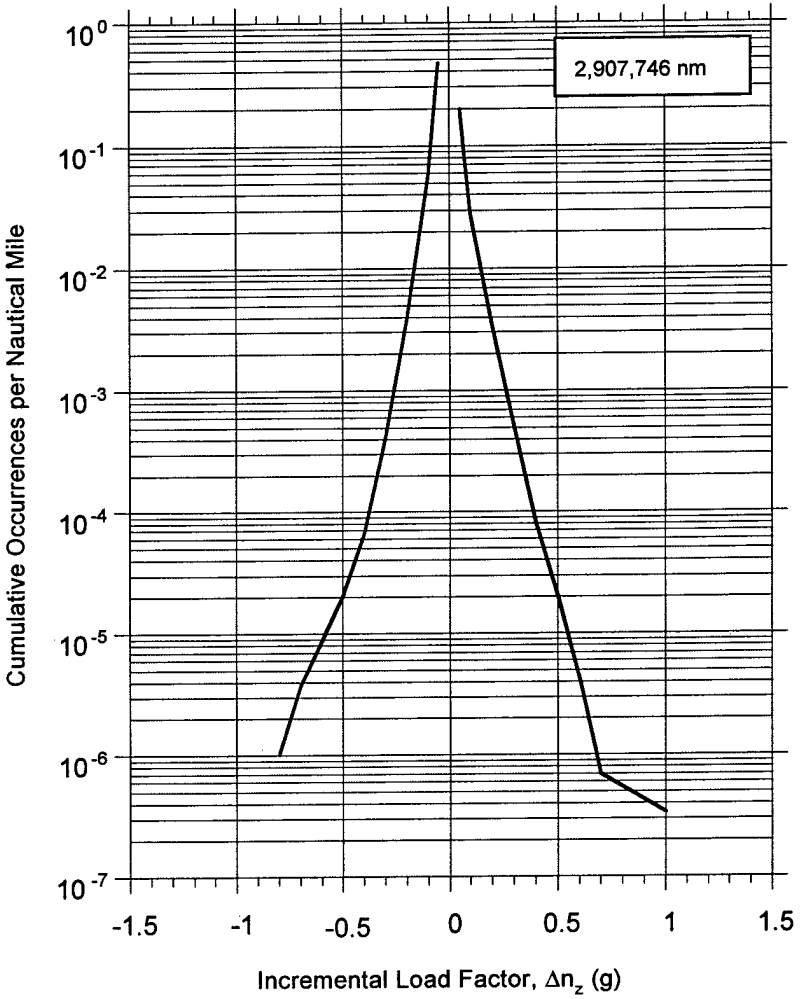

FIGURE A-30. CUMULATIVE OCCURRENCES OF INCREMENTAL VERTICAL GUST LOAD FACTOR PER NAUTICAL MILE, COMBINED FLIGHT PHASES

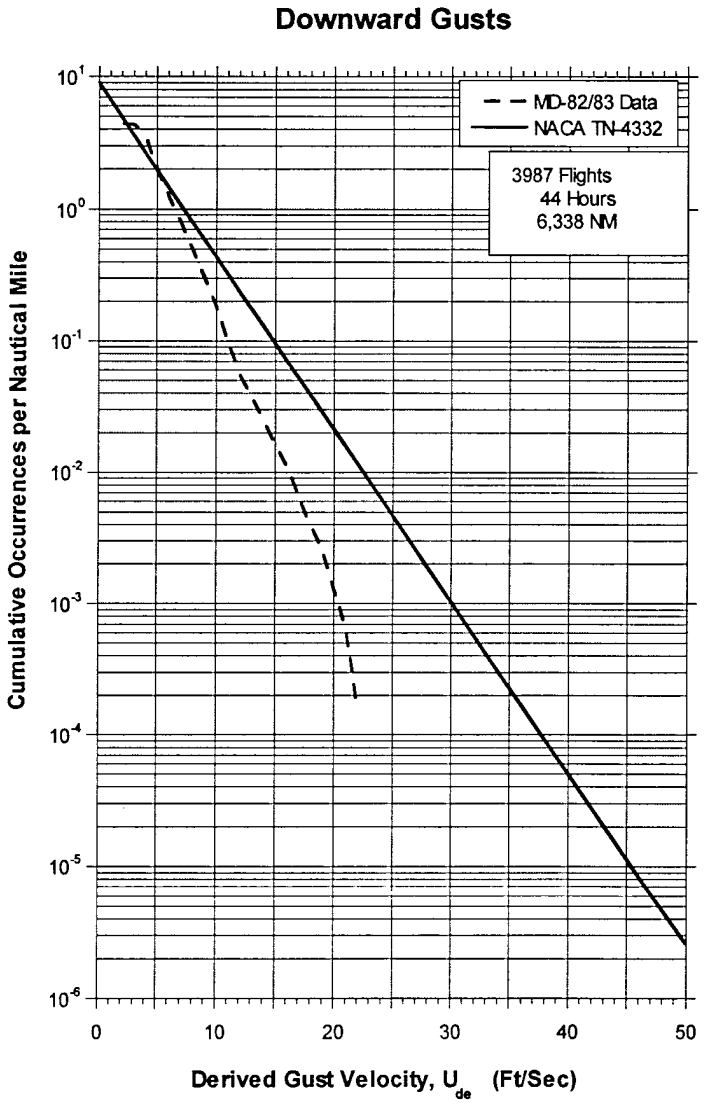

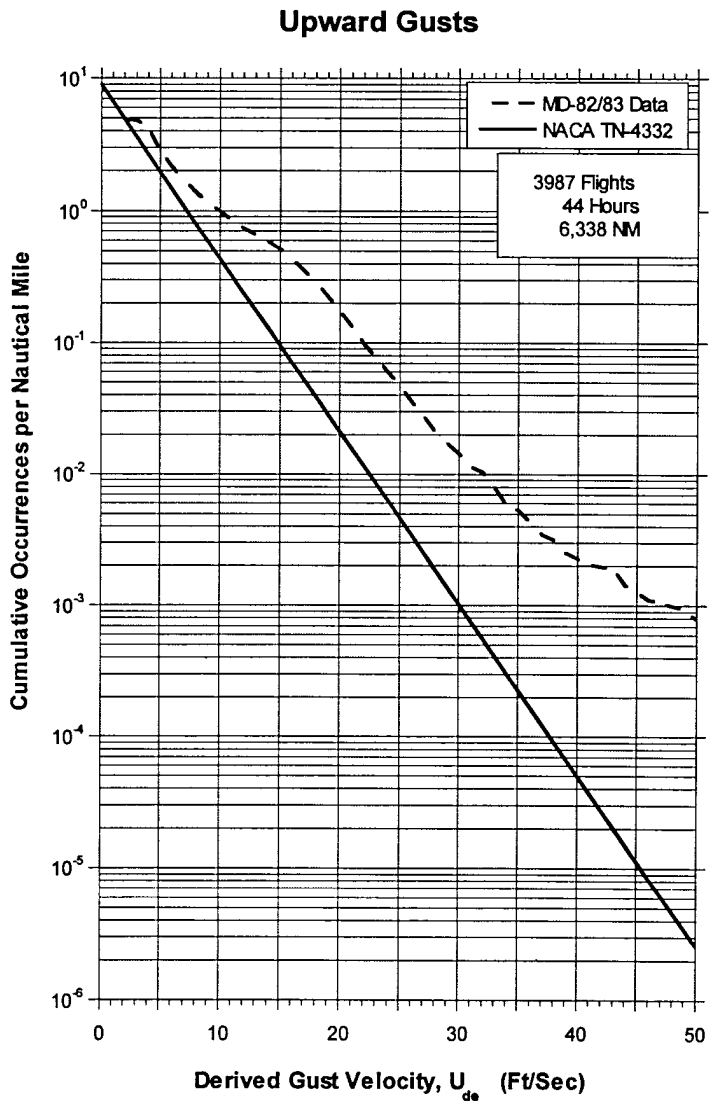

FIGURE A-31. CUMULATIVE OCCURRENCES OF DERIVED GUST VELOCITY PER NAUTICAL MILE, < 500 FEET

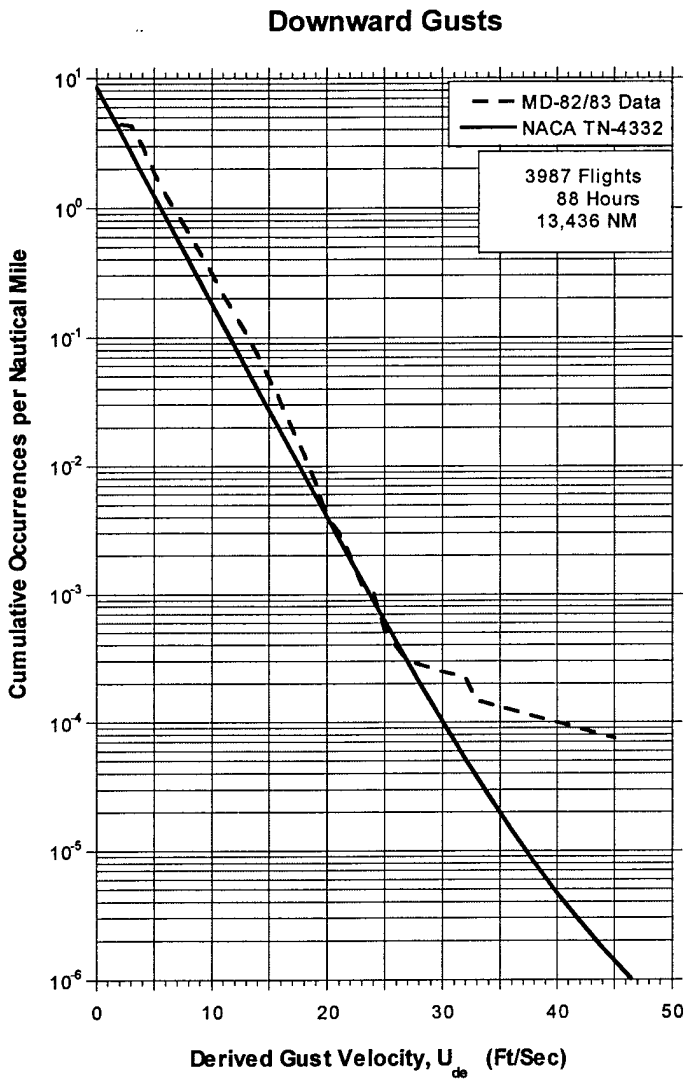

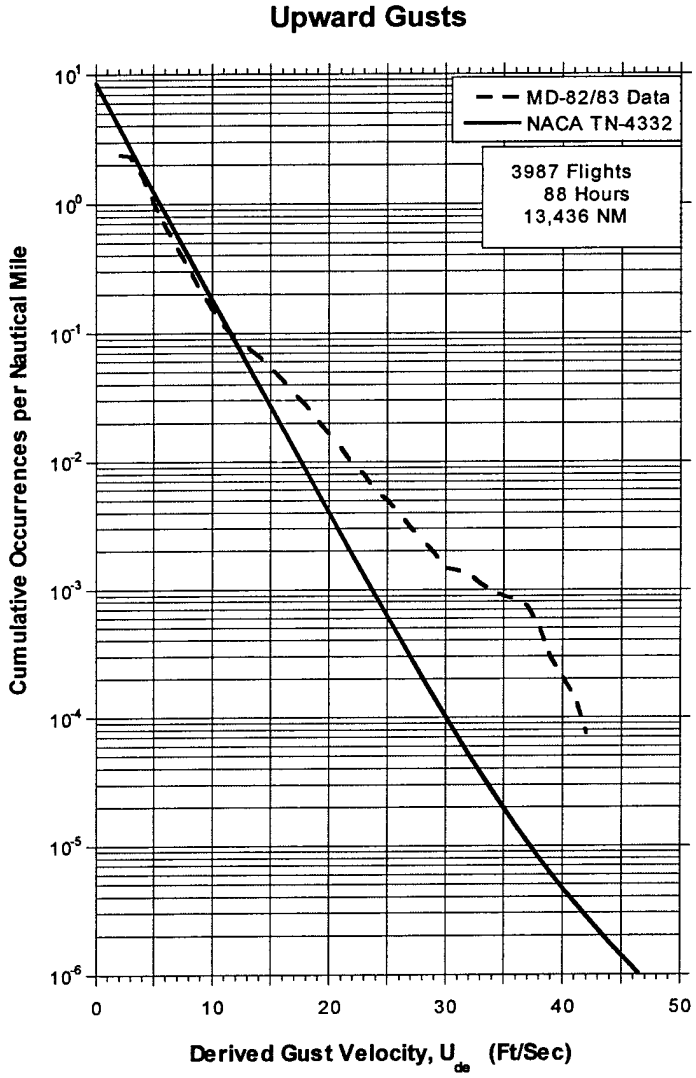

FIGURE A-32. CUMULATIVE OCCURRENCES OF DERIVED GUST VELOCITY PER NAUTICAL MILE, 500-1,500 FEET

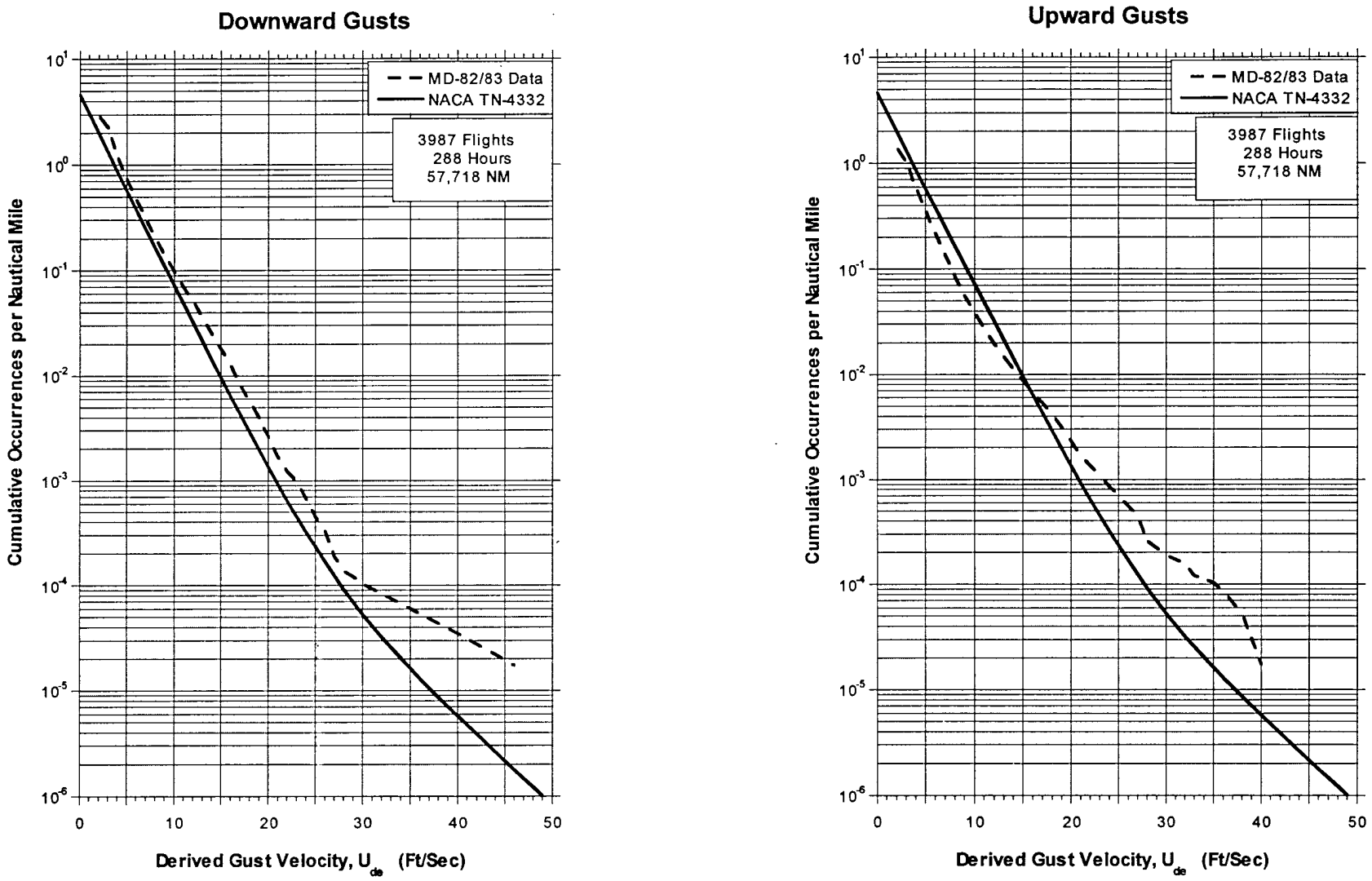

FIGURE A-33. CUMULATIVE OCCURRENCES OF DERIVED GUST VELOCITY PER NAUTICAL MILE, 1,500-4,500 FEET

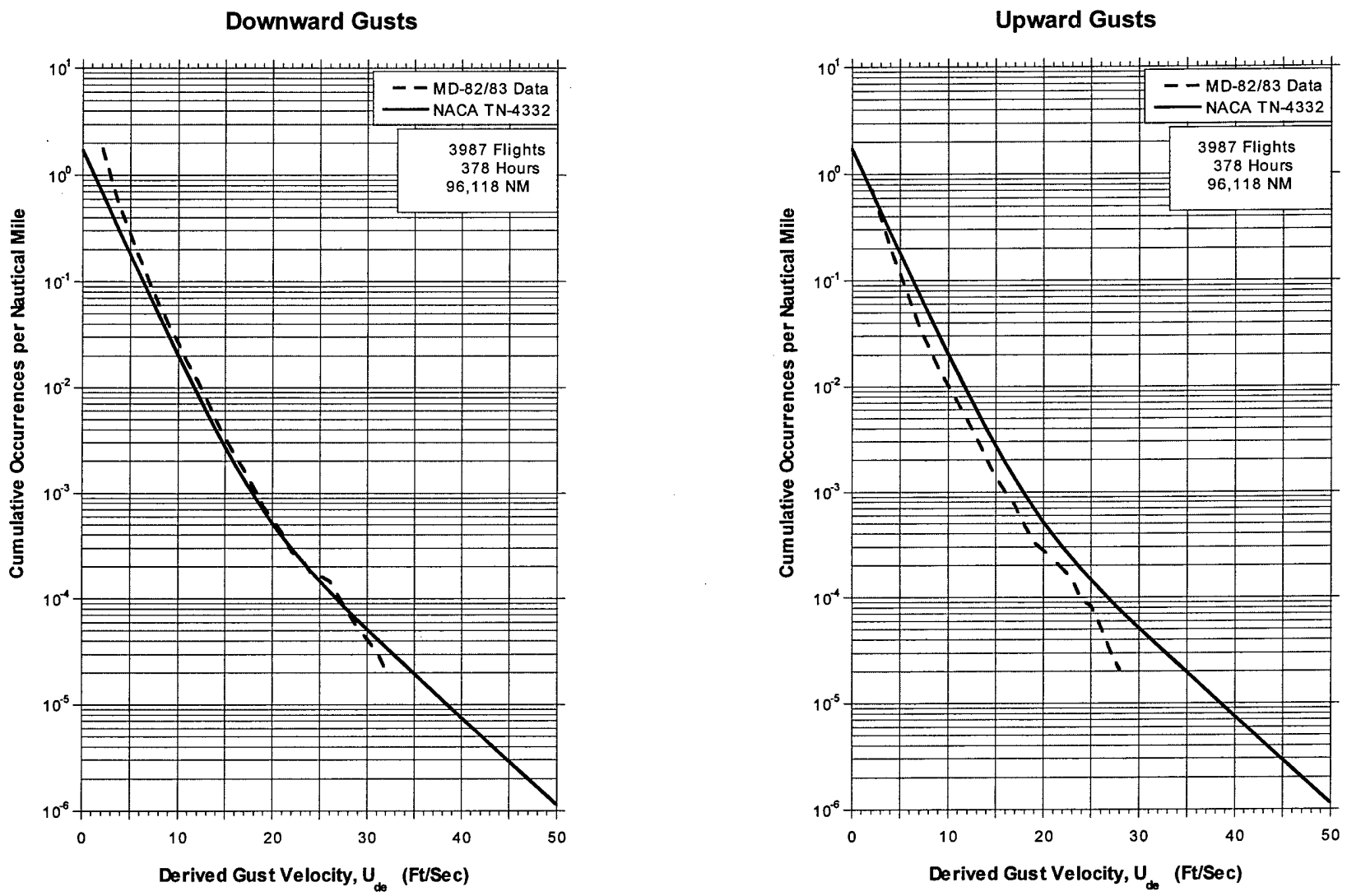

FIGURE A-34. CUMULATIVE OCCURRENCES OF DERIVED GUST VELOCITY PER NAUTICAL MILE, 4,500-9,500 FEET

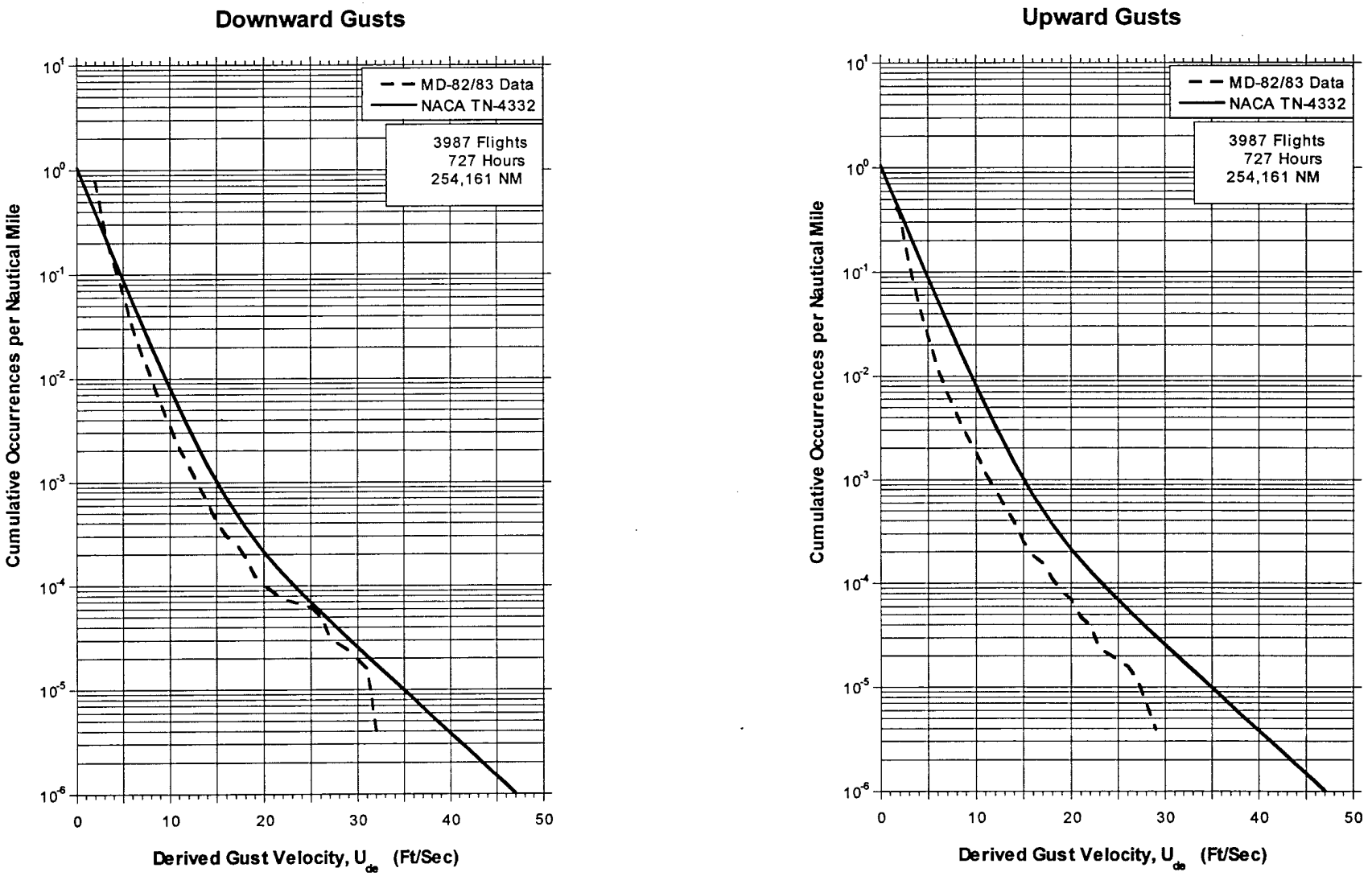

FIGURE A-35. CUMULATIVE OCCURRENCES OF DERIVED GUST VELOCITY PER NAUTICAL MILE, 9,500-19,500 FEET

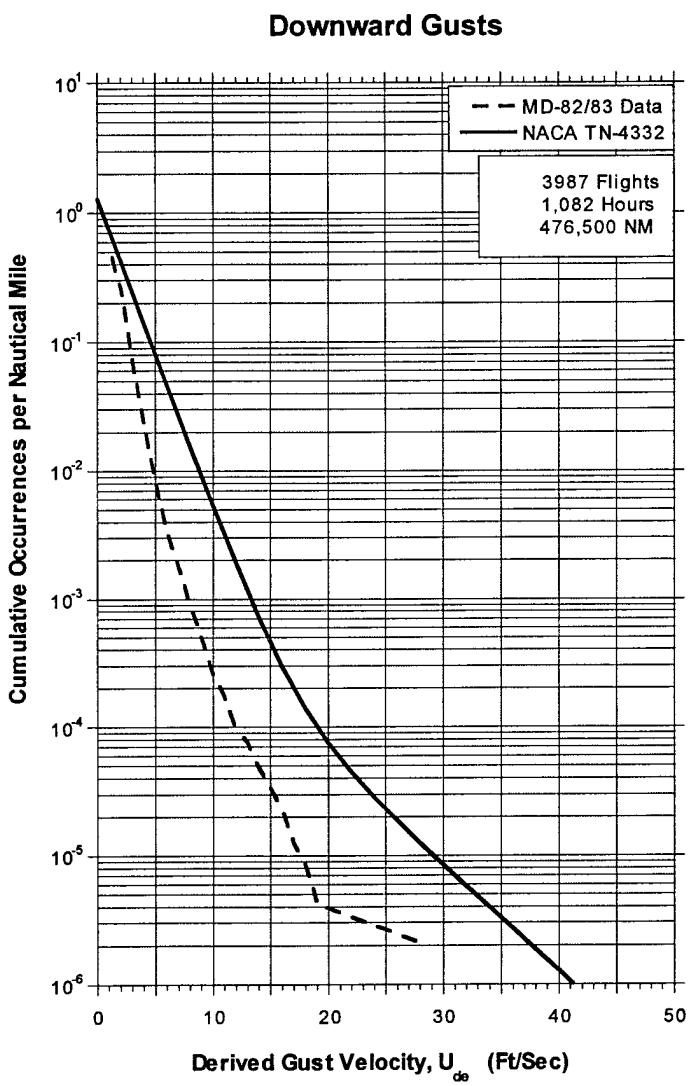

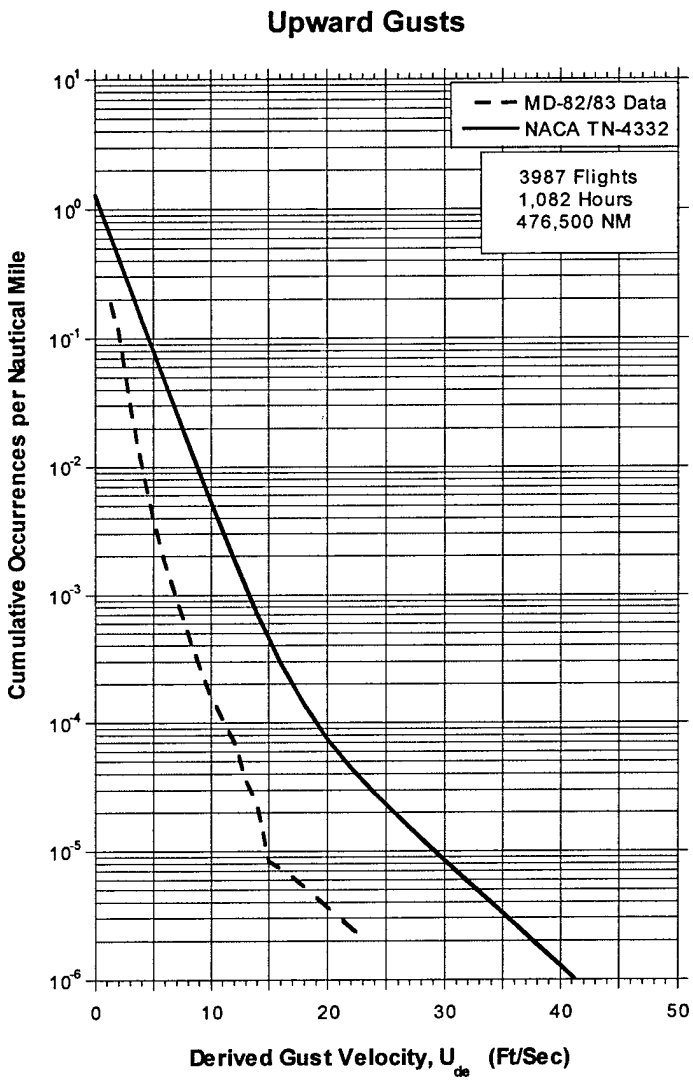

FIGURE A-36. CUMULATIVE OCCURRENCES OF DERIVED GUST VELOCITY PER NAUTICAL MILE, 19,500-29,500 FEET

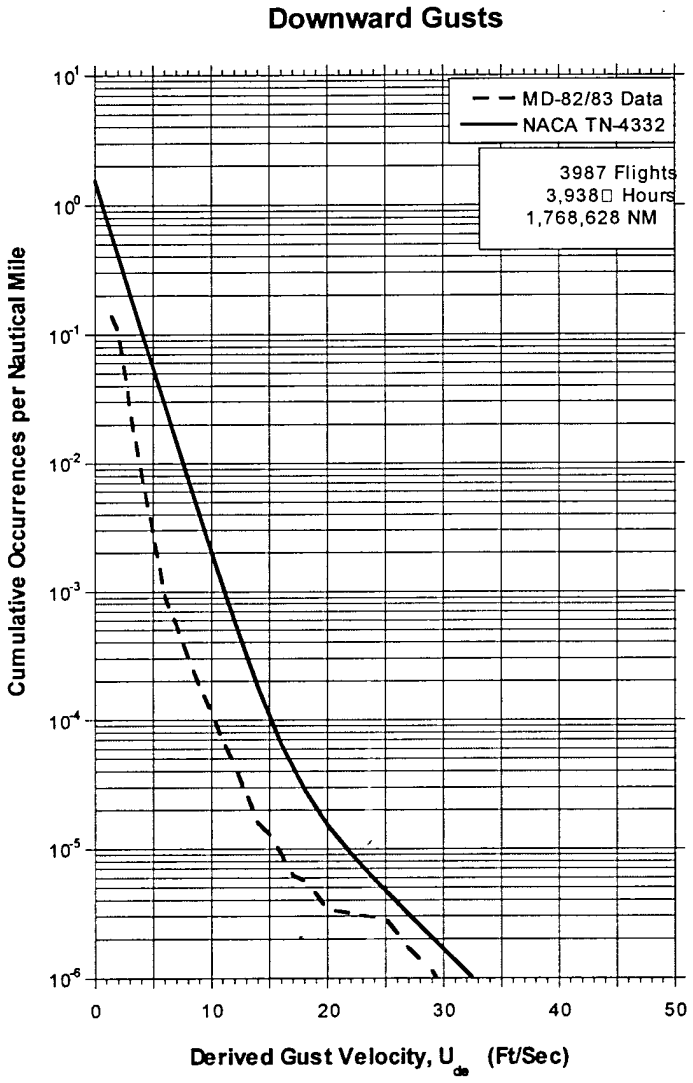

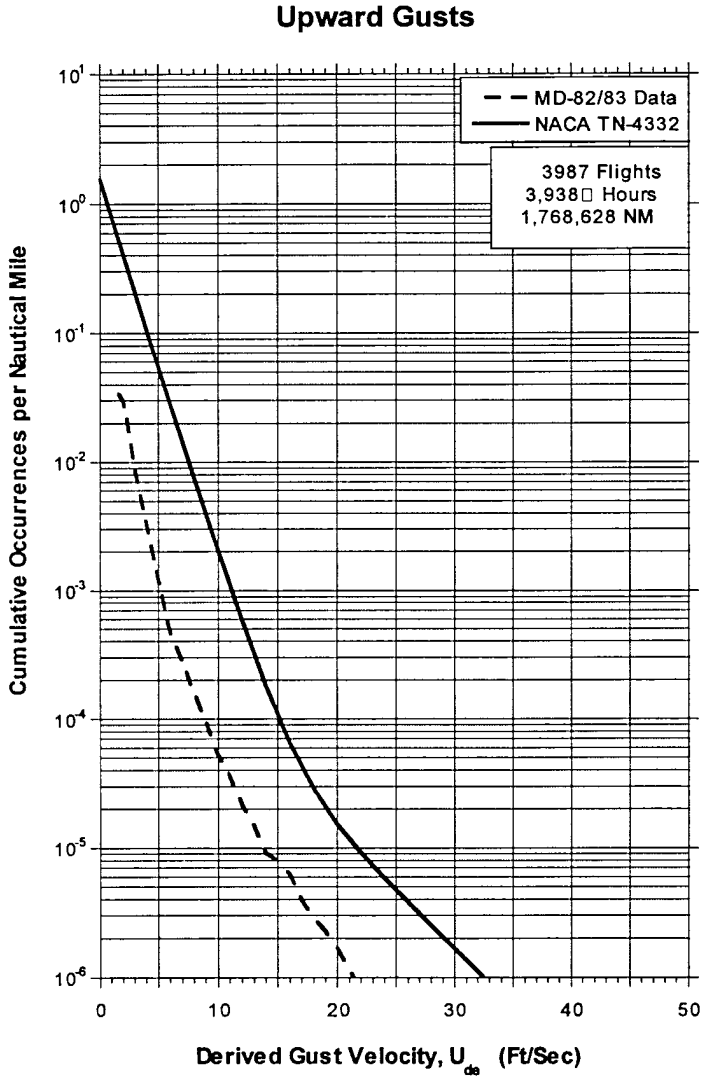

FIGURE A-37. CUMULATIVE OCCURRENCES OF DERIVED GUST VELOCITY PER NAUTICAL MILE, 29,500-39,500 FEET

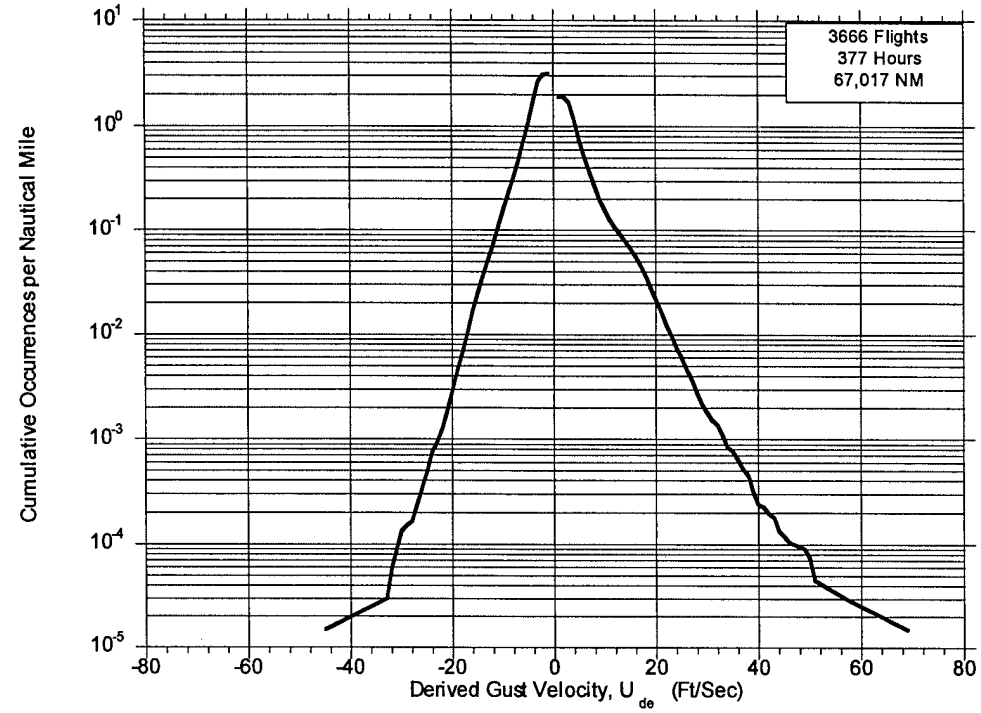

FIGURE A-38. CUMULATIVE OCCURRENCES OF DERIVED GUST VELOCITY PER NAUTICAL MILE, FLAPS EXTENDED

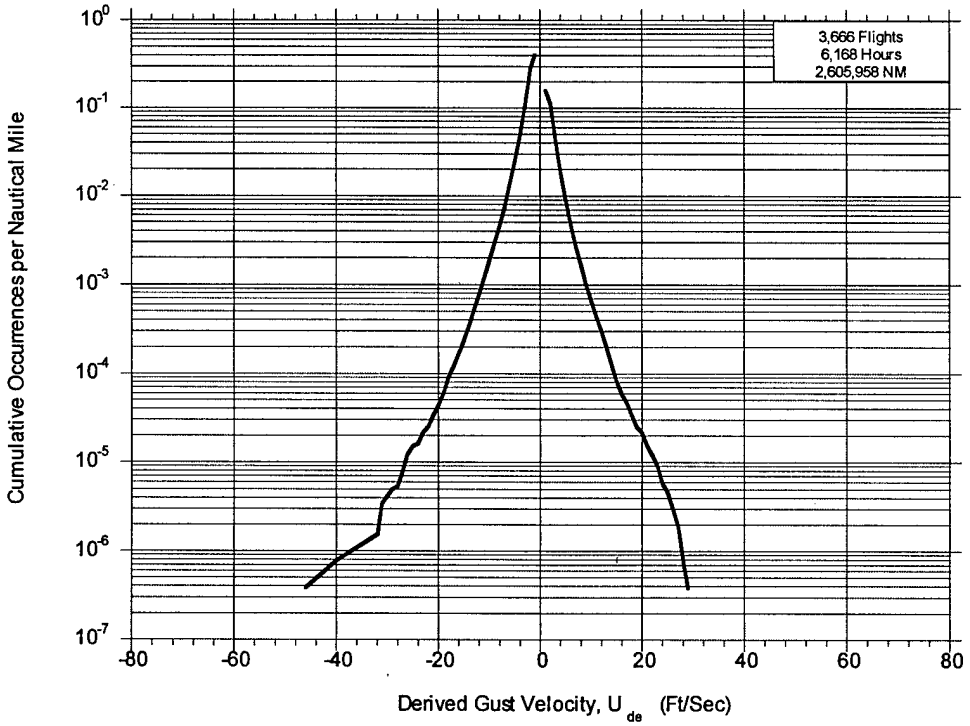

FIGURE A-39. CUMULATIVE OCCURRENCES OF DERIVED GUST VELOCITY PER NAUTICAL MILE, FLAPS RETRACTED

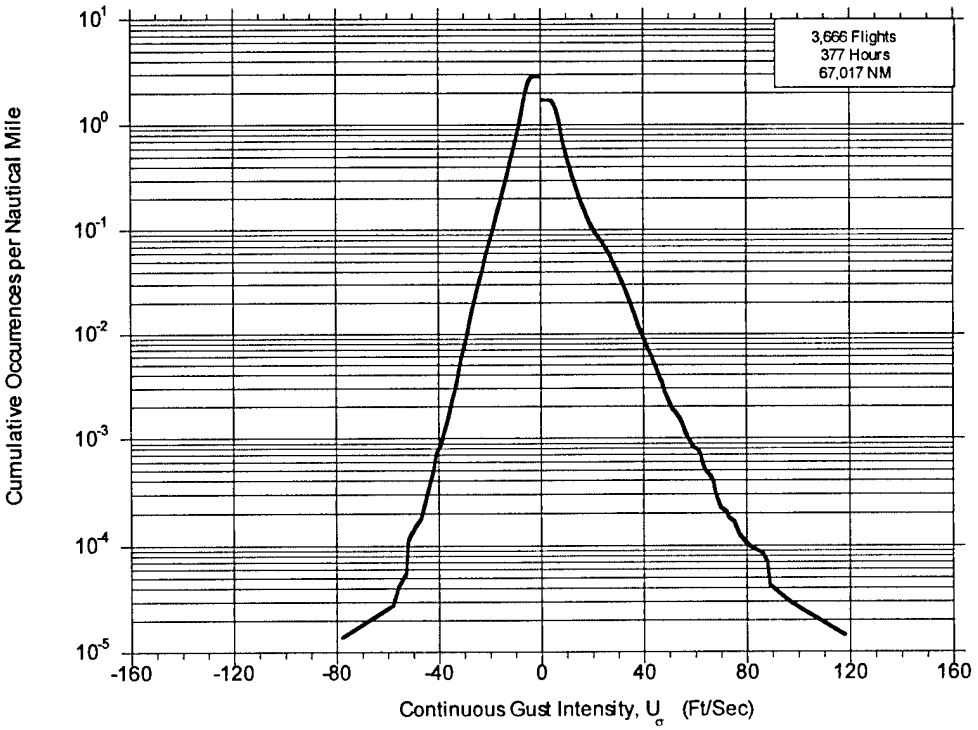

FIGURE A-40. CUMULATIVE OCCURRENCES OF CONTINUOUS GUST INTENSITY PER NAUTICAL MILE, FLAPS EXTENDED

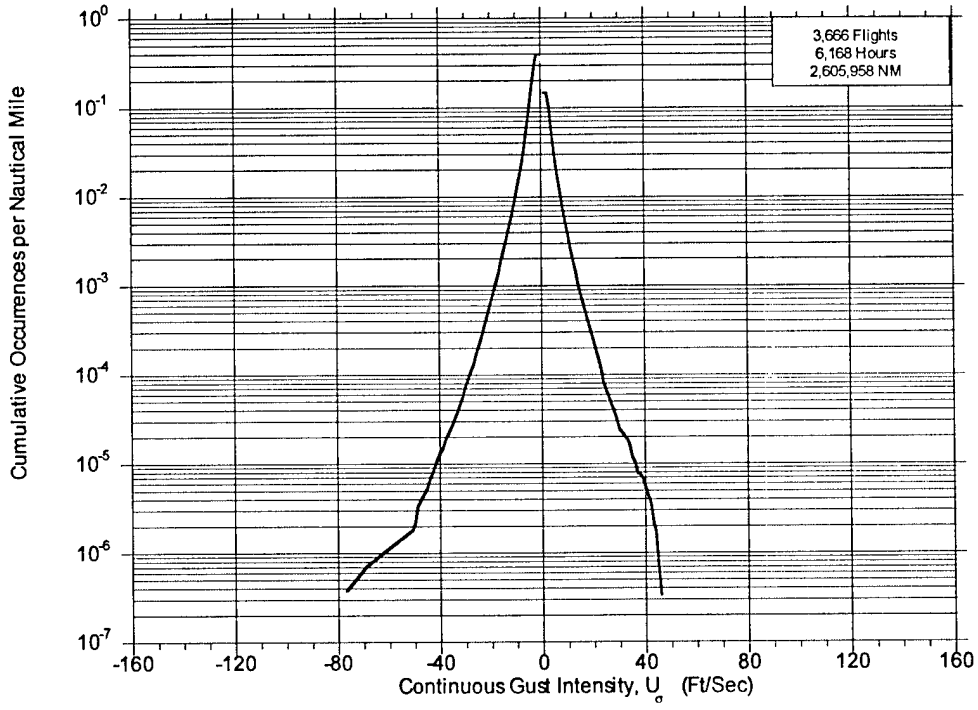

FIGURE A-41. CUMULATIVE OCCURRENCES OF CONTINUOUS GUST INTENSITY PER NAUTICAL MILE, FLAPS RETRACTED

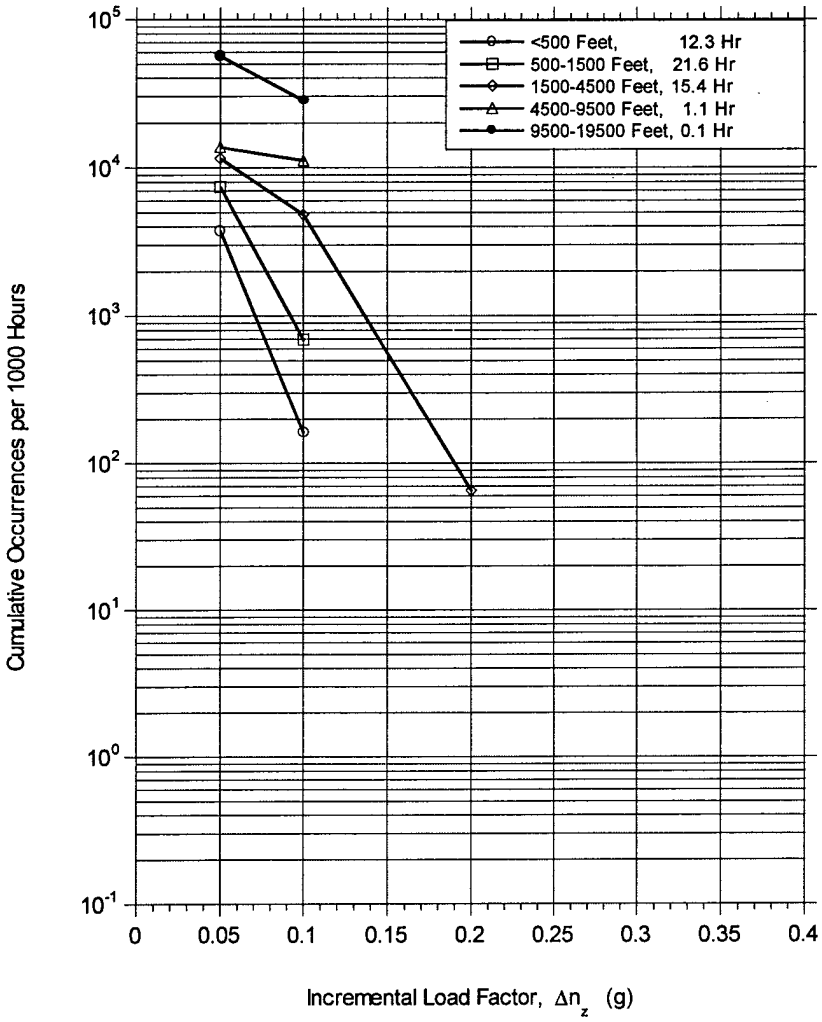

FIGURE A-42. CUMULATIVE OCCURRENCES OF INCREMENTAL MANEUVER LOAD FACTOR PER 1000 HOURS DURING DEPARTURE BY ALTITUDE

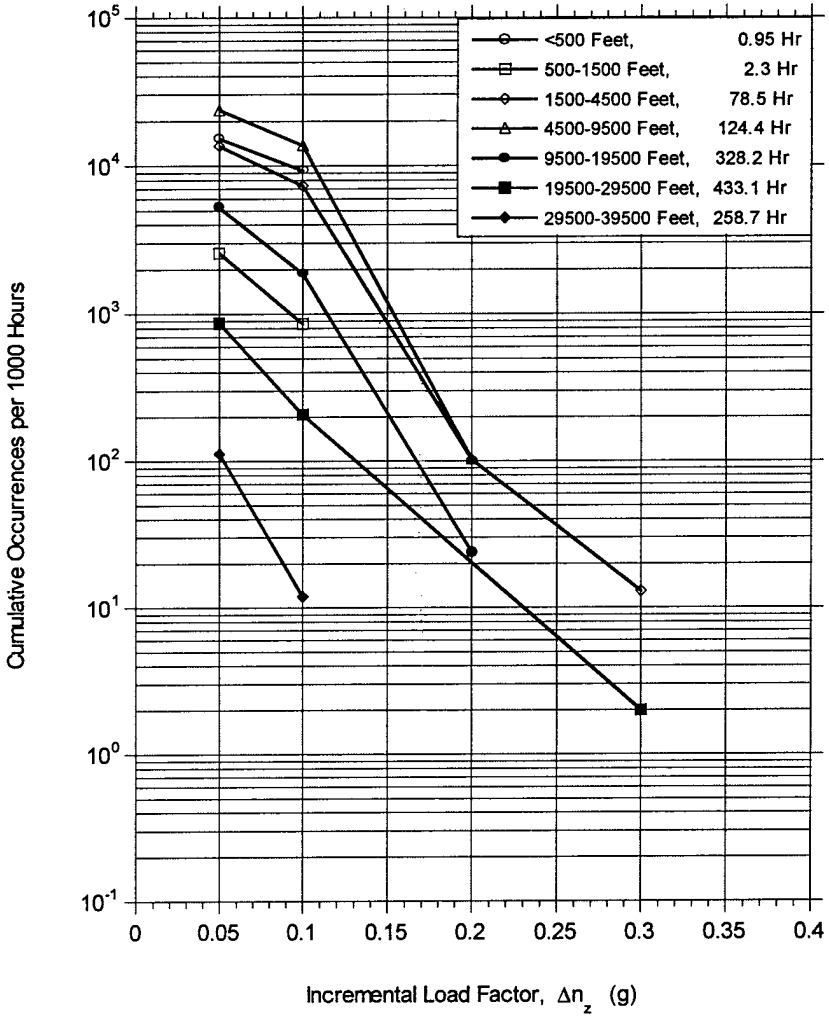

FIGURE A-43. CUMULATIVE OCCURRENCES OF INCREMENTAL MANEUVER LOAD FACTOR PER 1000 HOURS DURING CLIMB BY ALTITUDE

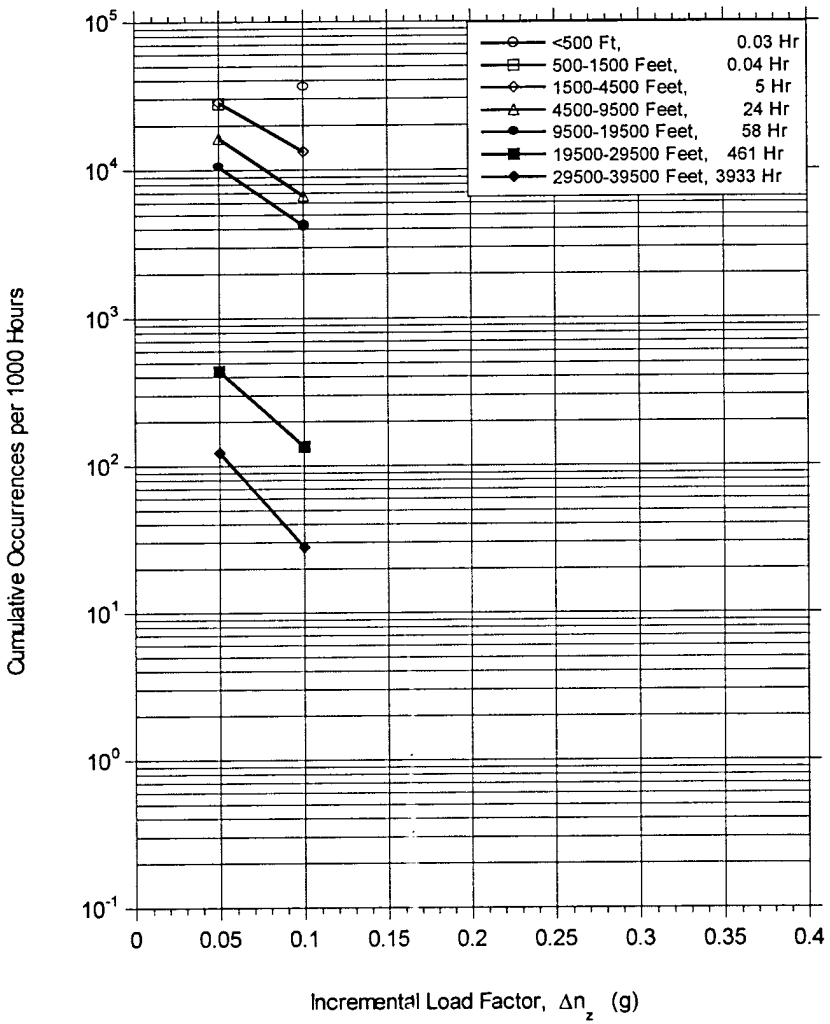

FIGURE A-44. CUMULATIVE OCCURRENCES OF INCREMENTAL MANEUVER LOAD FACTOR PER 1000 HOURS DURING CRUISE BY ALTITUDE

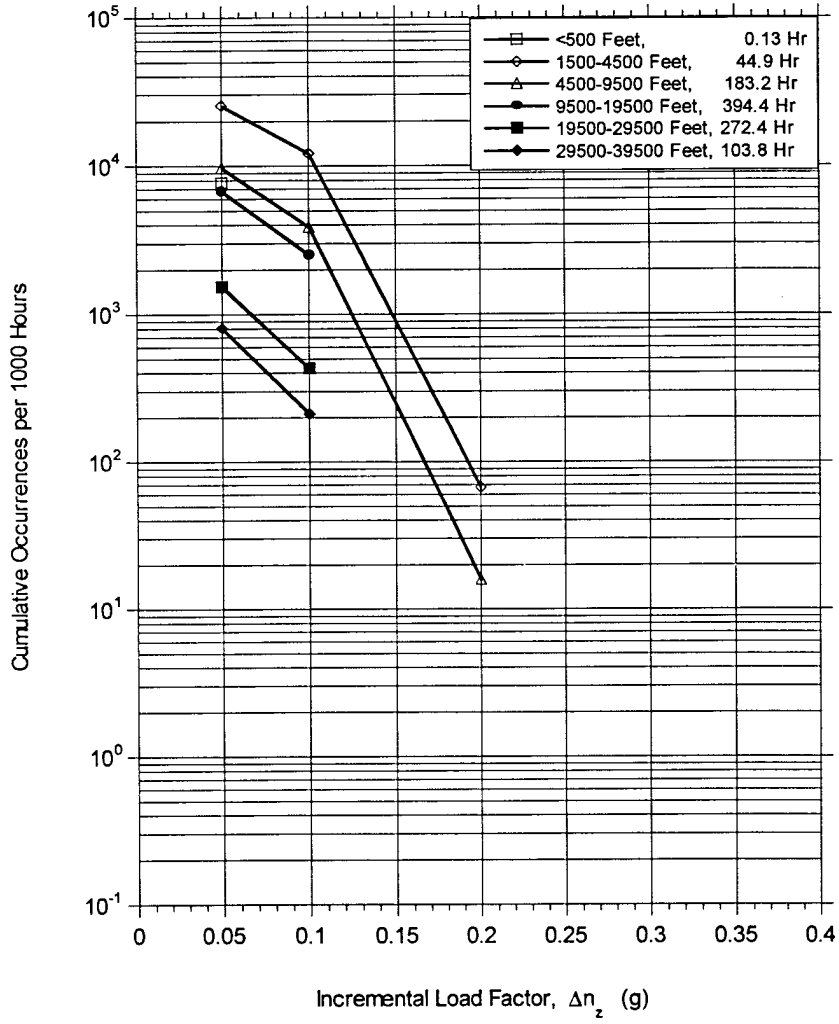

FIGURE A-45. CUMULATIVE OCCURRENCES OF MANEUVER LOAD FACTOR PER 1000 HOURS DURING DESCENT BY ALTITUDE

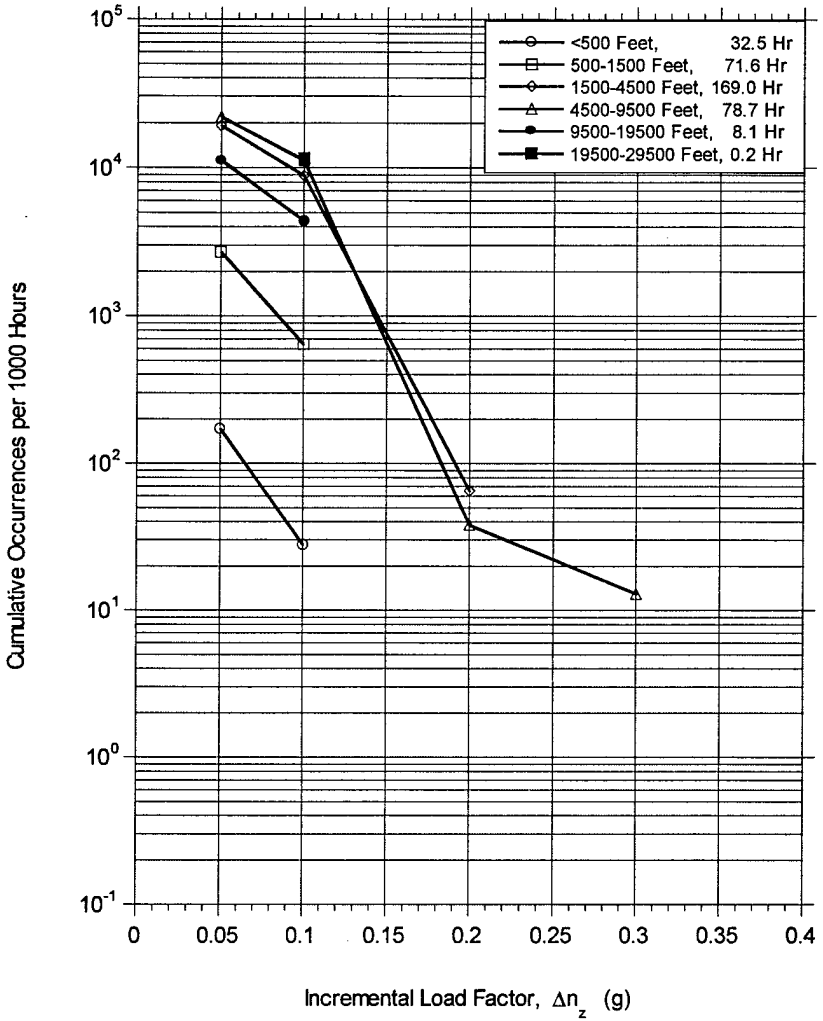

FIGURE A-46. CUMULATIVE OCCURRENCES OF MANEUVER LOAD FACTOR PER 1000 HOURS DURING APPROACH BY ALTITUDE

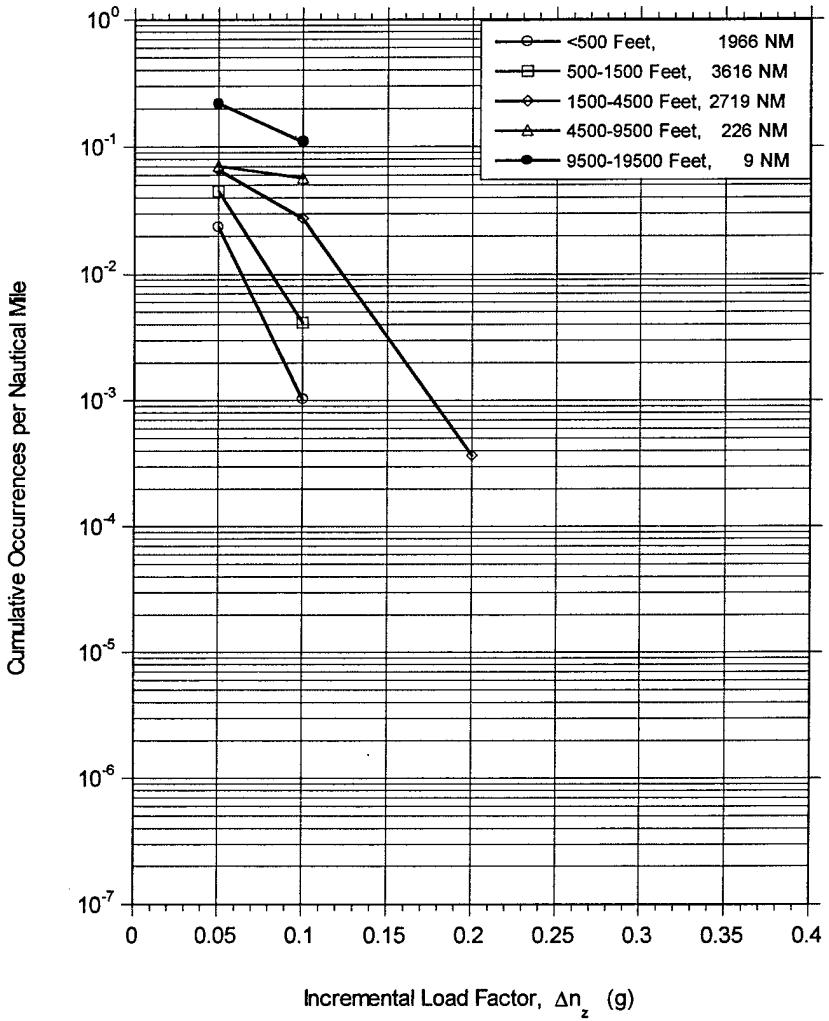

FIGURE A-47. CUMULATIVE OCCURRENCES OF MANEUVER LOAD FACTOR PER NAUTICAL MILE DURING DEPARTURE BY ALTITUDE

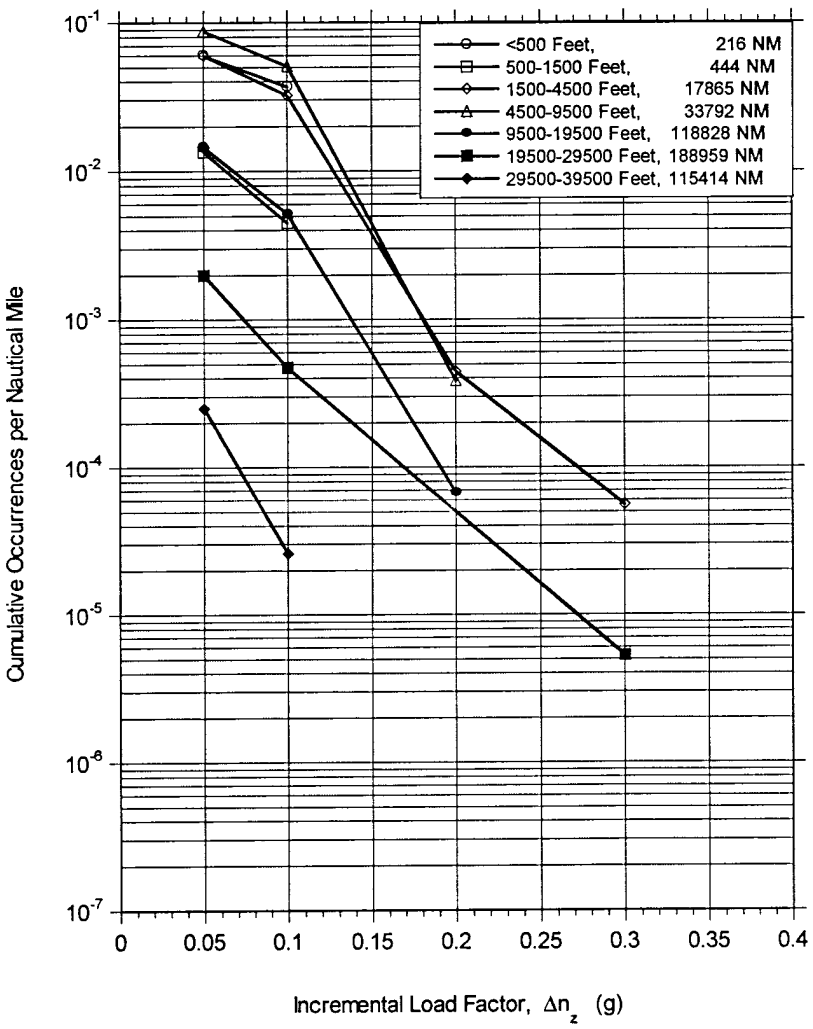

FIGURE A-48. CUMULATIVE OCCURRENCES OF MANEUVER LOAD FACTOR PER NAUTICAL MILE DURING CLIMB BY ALTITUDE

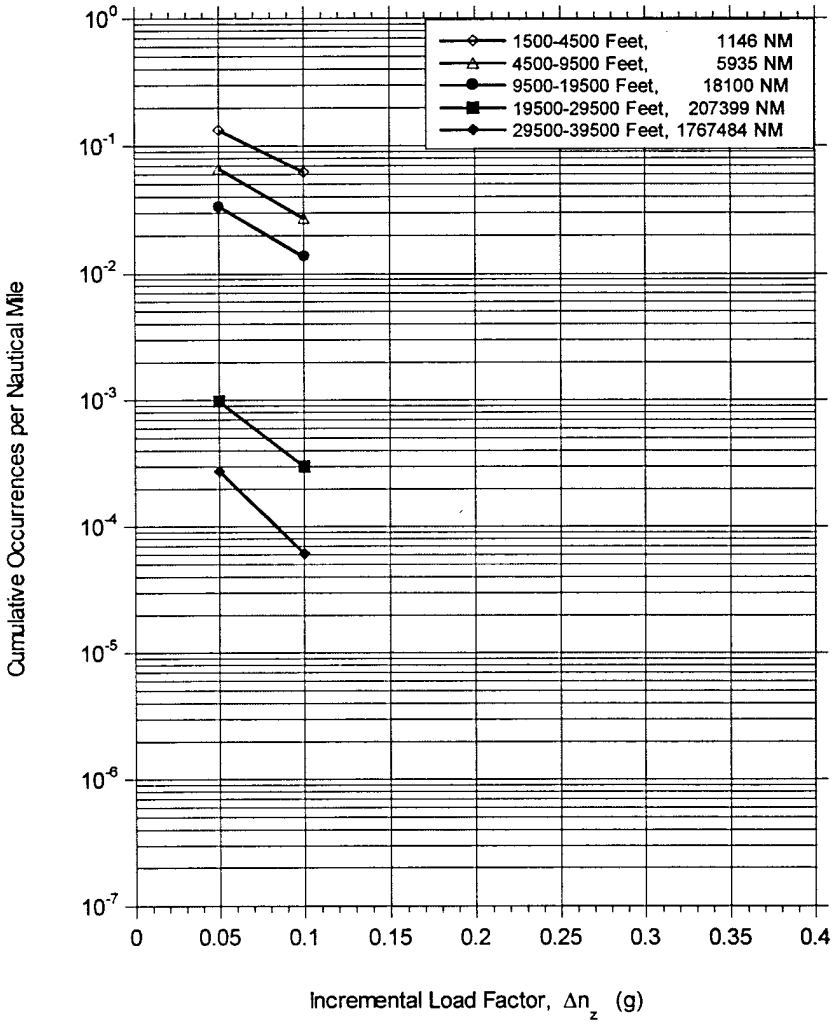

FIGURE A-49. CUMULATIVE OCCURRENCES OF MANEUVER LOAD FACTOR PER NAUTICAL MILE DURING CRUISE BY ALTITUDE

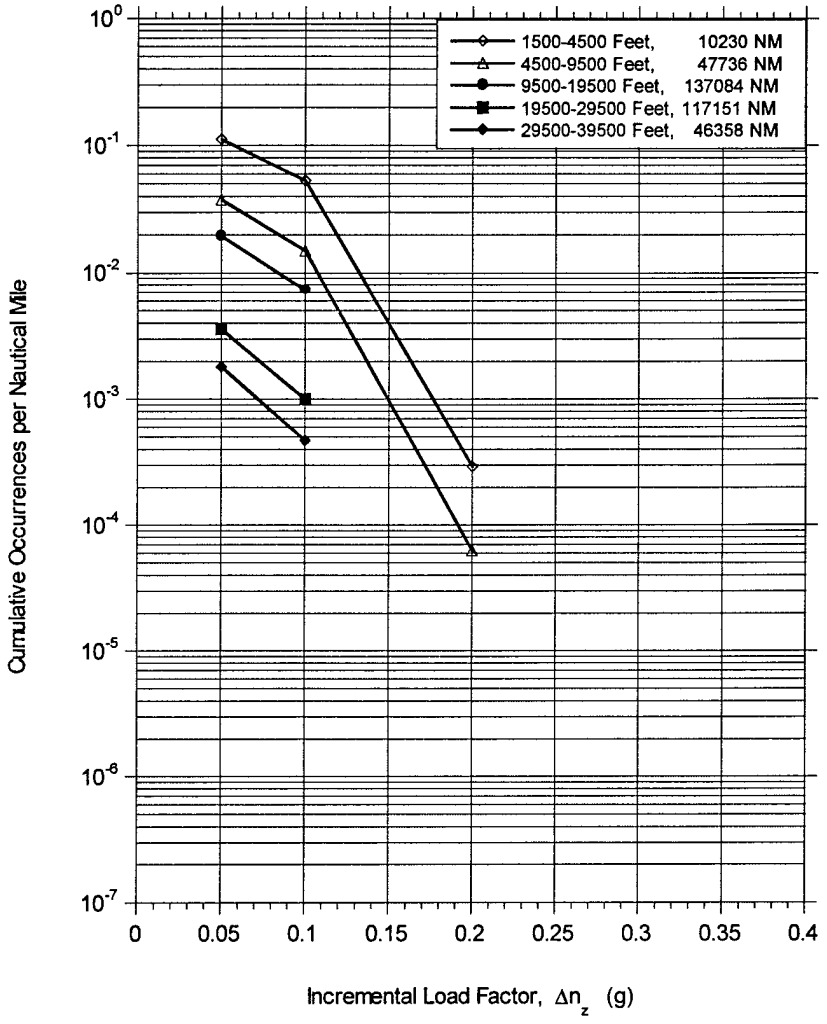

FIGURE A-50. CUMULATIVE OCCURRENCES OF MANEUVER LOAD FACTOR PER NAUTICAL MILE DURING DESCENT BY ALTITUDE

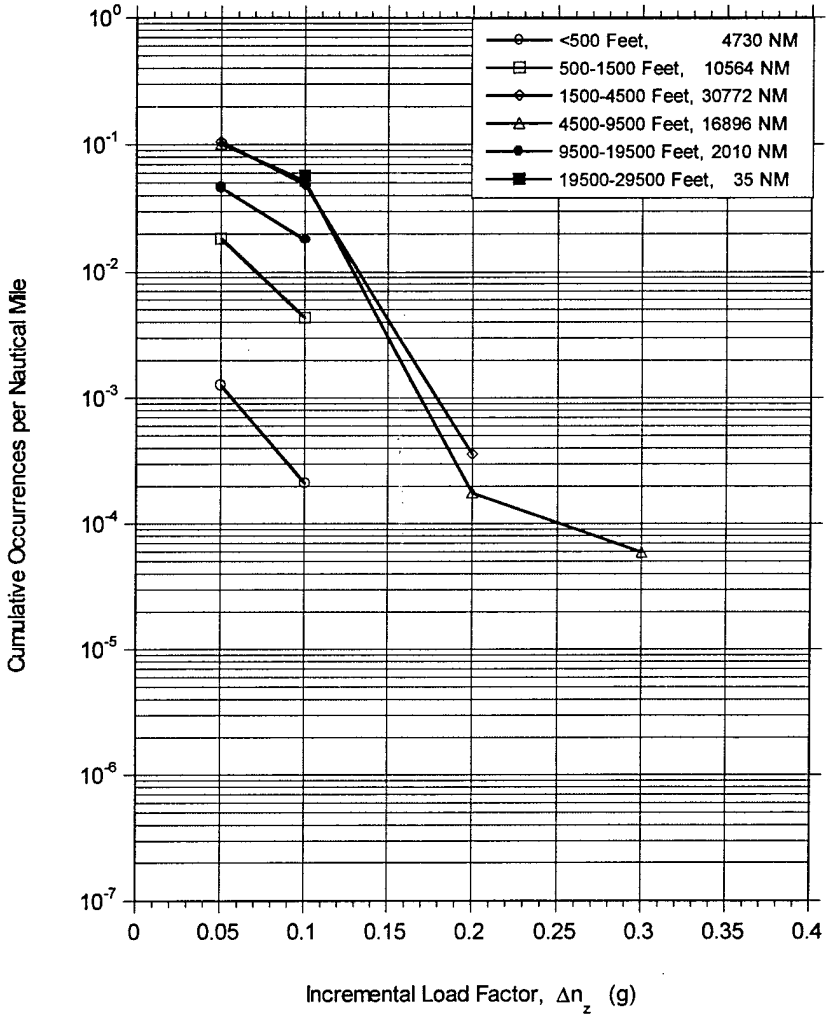

FIGURE A-51. CUMULATIVE OCCURRENCES OF MANEUVER LOAD FACTOR PER NAUTICAL MILE DURING APPROACH BY ALTITUDE

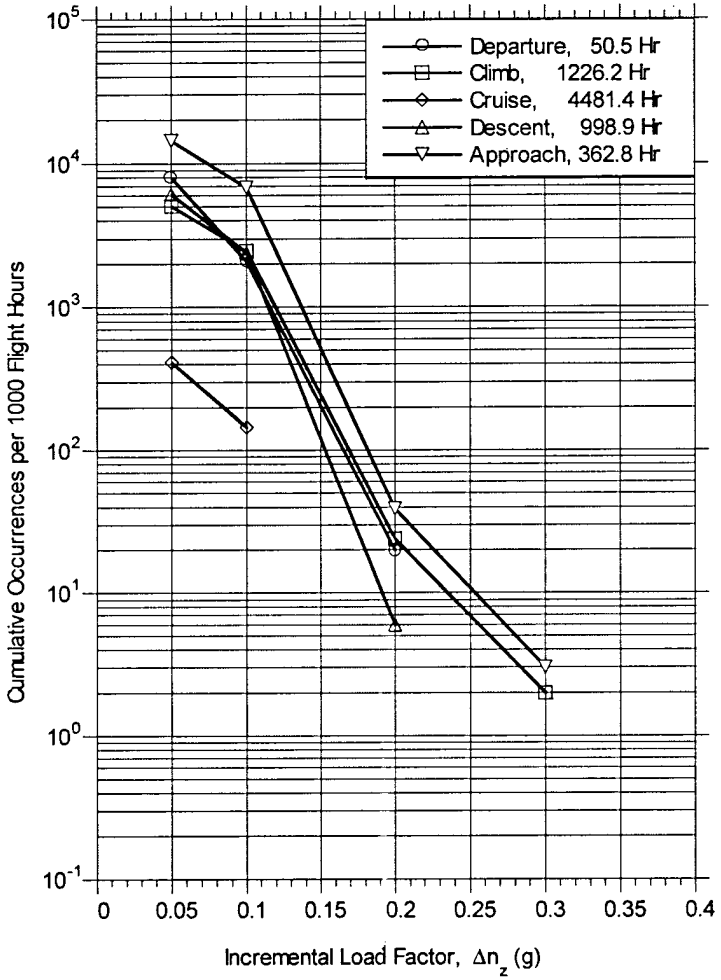

FIGURE A-52. CUMULATIVE OCCURRENCES OF MANEUVER LOAD FACTOR PER 1000 HOURS BY FLIGHT PHASE

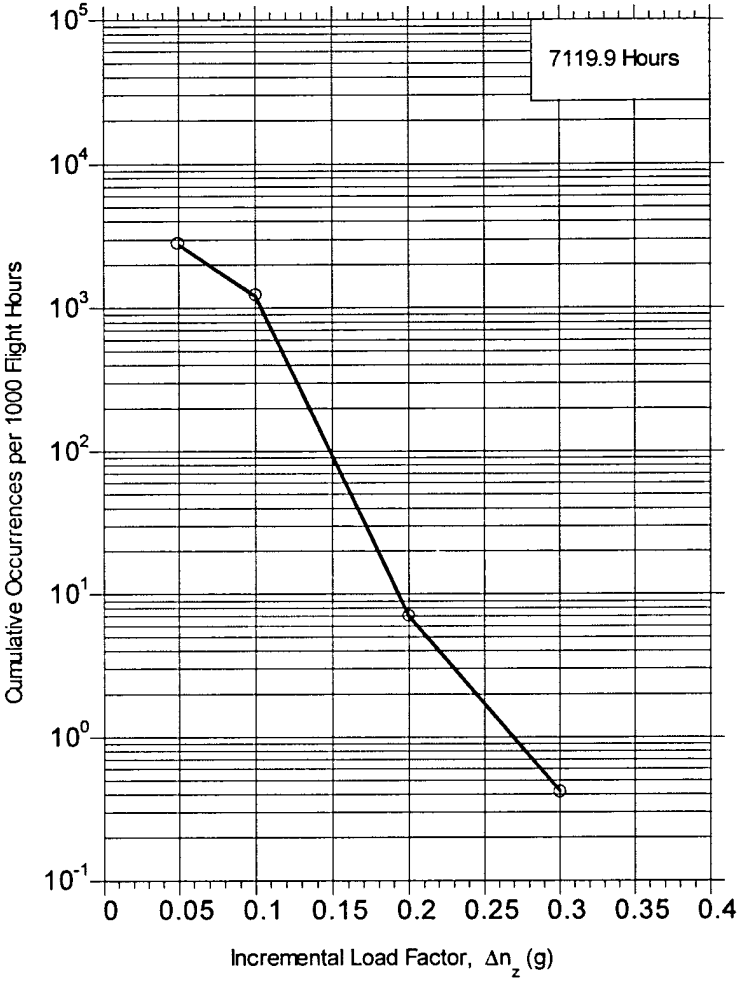

FIGURE A-53. CUMULATIVE OCCURRENCES OF MANEUVER LOAD FACTOR PER 1000 HOURS, COMBINED FLIGHT PHASES

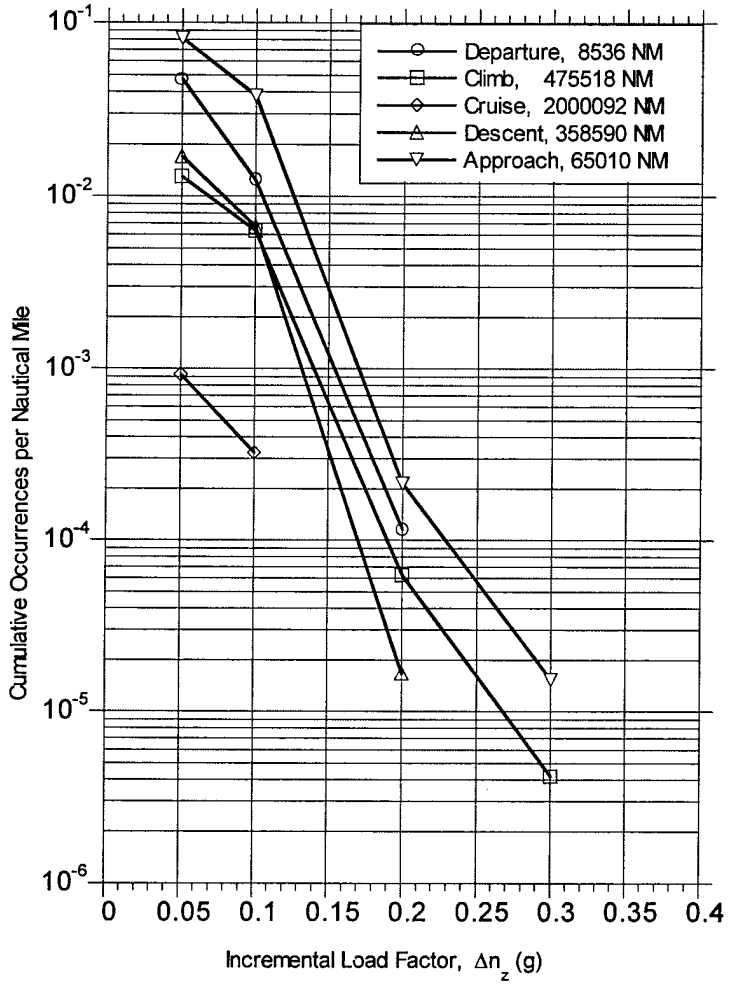

FIGURE A-54. CUMULATIVE OCCURRENCES OF MANEUVER LOAD FACTOR PER NAUTICAL MILE BY FLIGHT PHASE

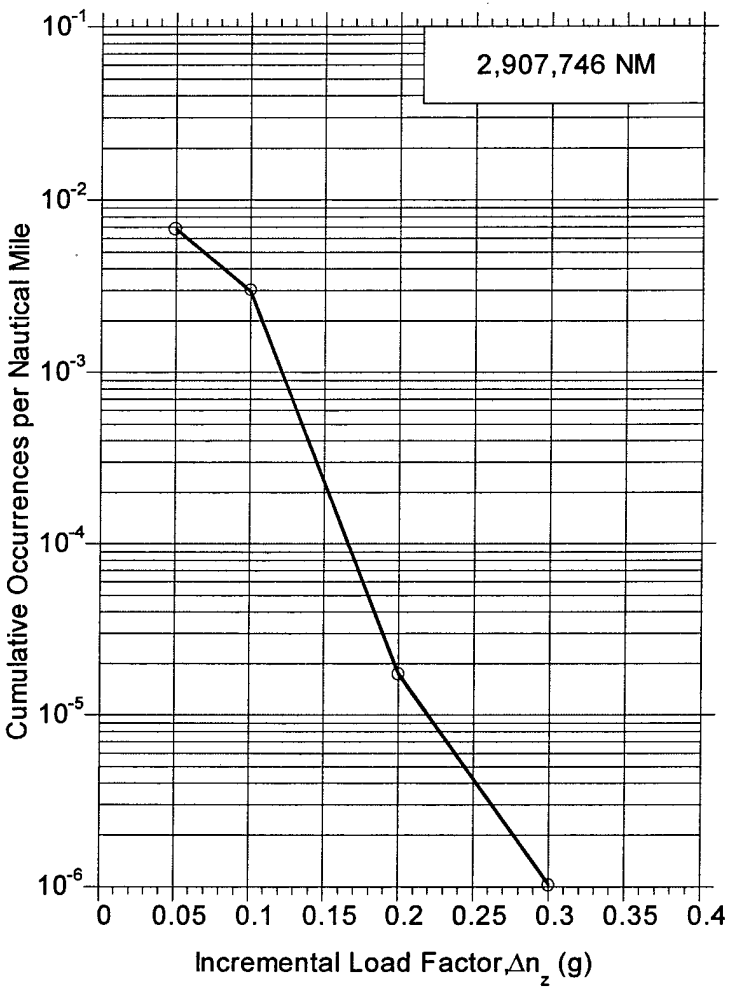

FIGURE A-55. CUMULATIVE OCCURRENCES OF MANEUVER LOAD FACTOR PER NAUTICAL MILE, COMBINED FLIGHT PHASES

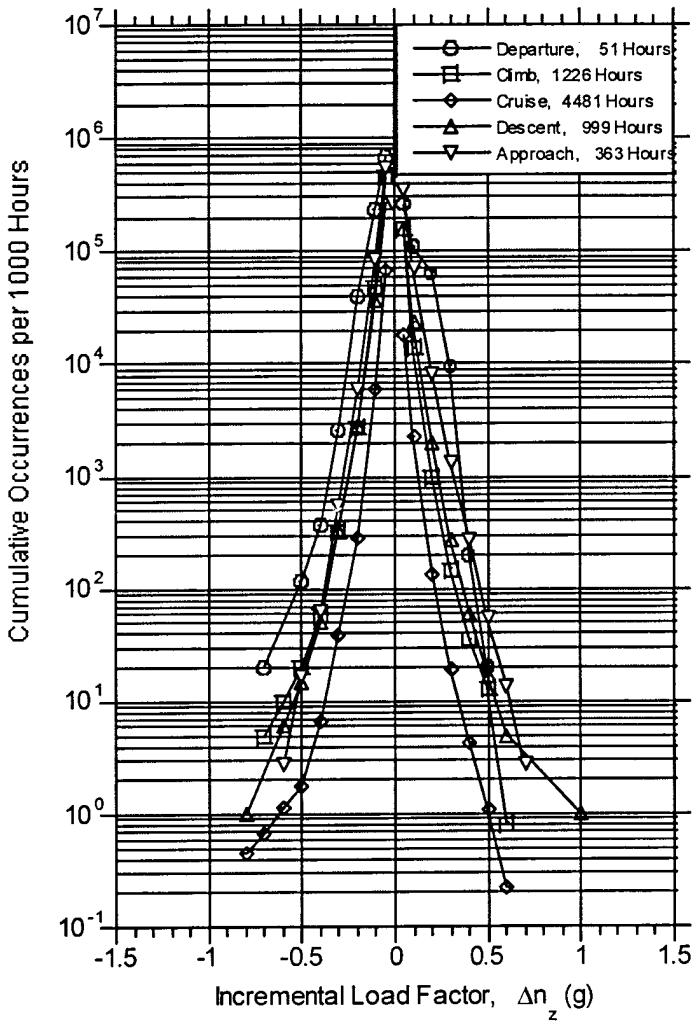

FIGURE A-56. CUMULATIVE OCCURRENCES OF COMBINED MANEUVER AND GUST VERTICAL LOAD FACTOR PER 1000 HOURS BY FLIGHT PHASE

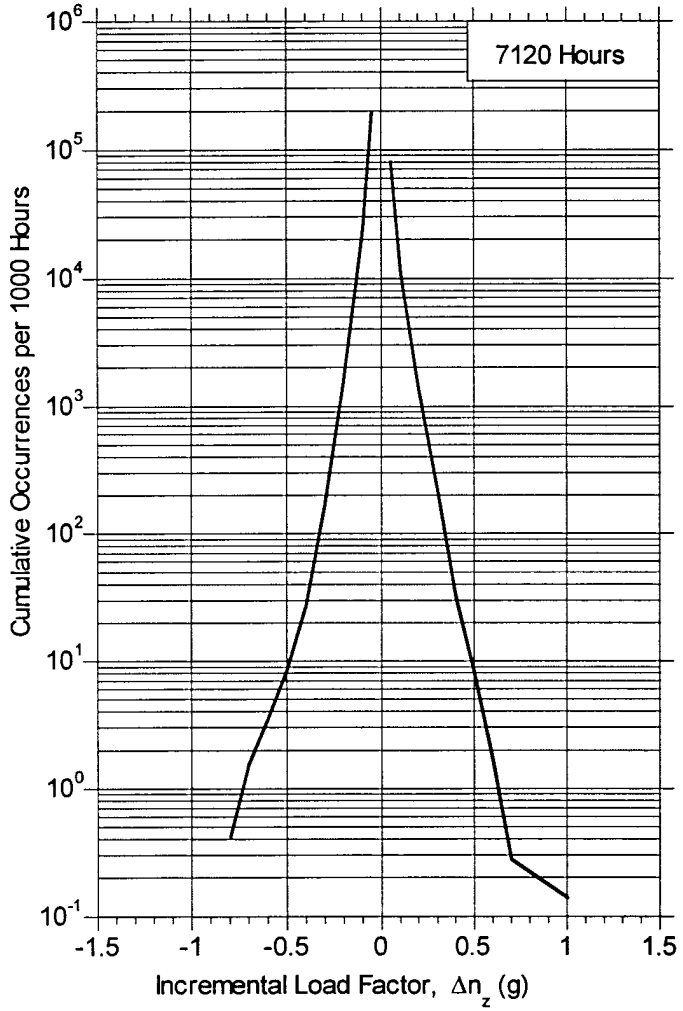

FIGURE A-57. CUMULATIVE OCCURRENCES OF VERTICAL LOAD FACTOR PER 1000 HOURS, COMBINED FLIGHT PHASES

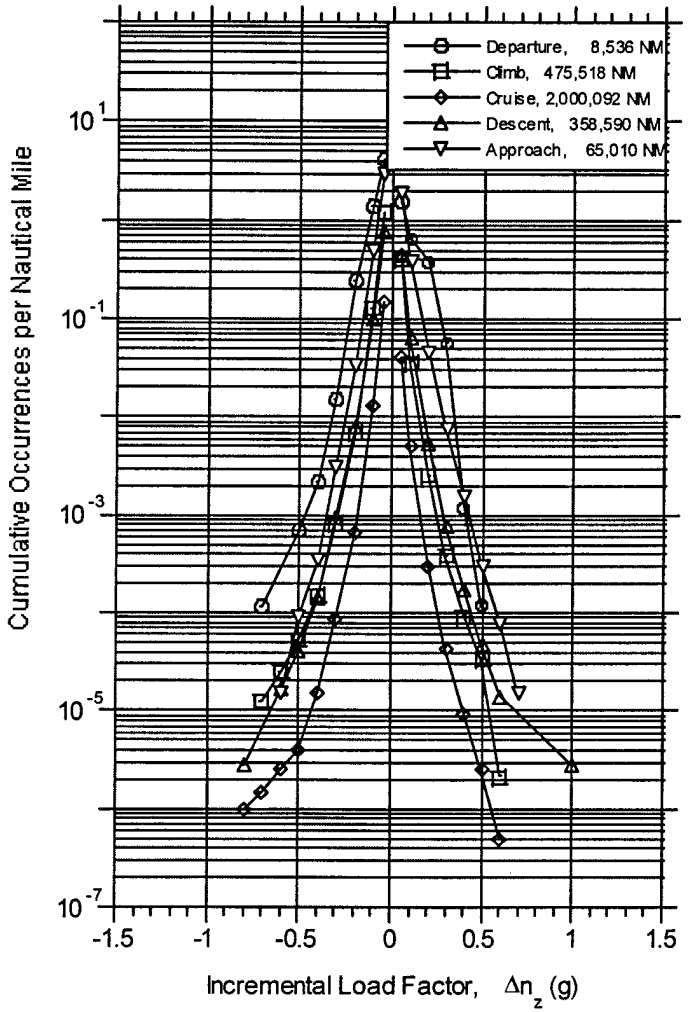

FIGURE A-58. CUMULATIVE OCCURRENCES OF VERTICAL LOAD FACTOR PER NAUTICAL MILE BY FLIGHT PHASE

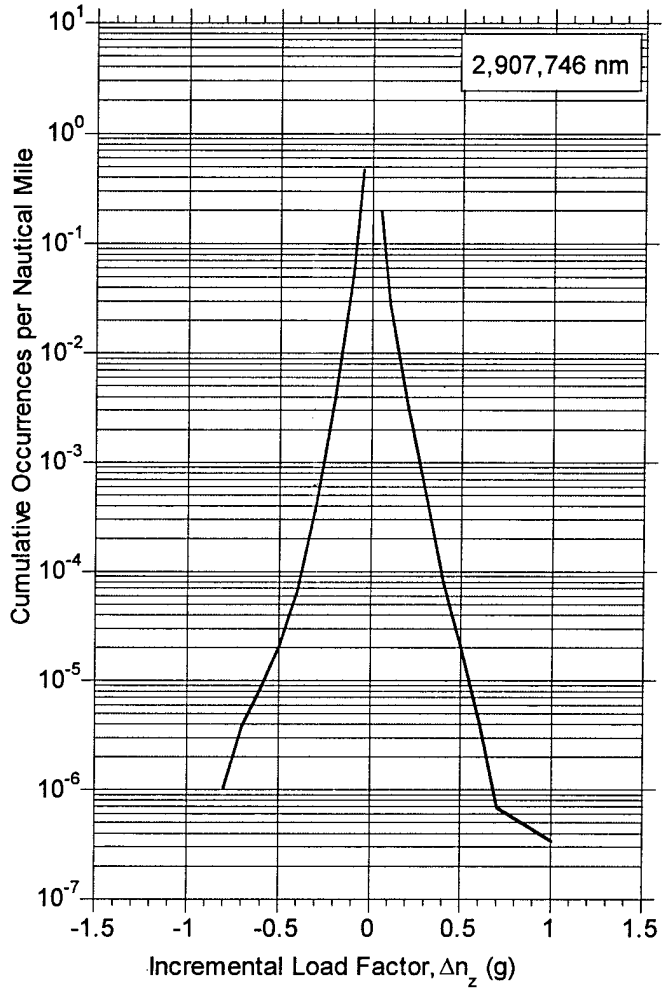

FIGURE A-59. CUMULATIVE OCCURRENCES OF VERTICAL LOAD FACTOR PER NAUTICAL MILE, COMBINED FLIGHT PHASES

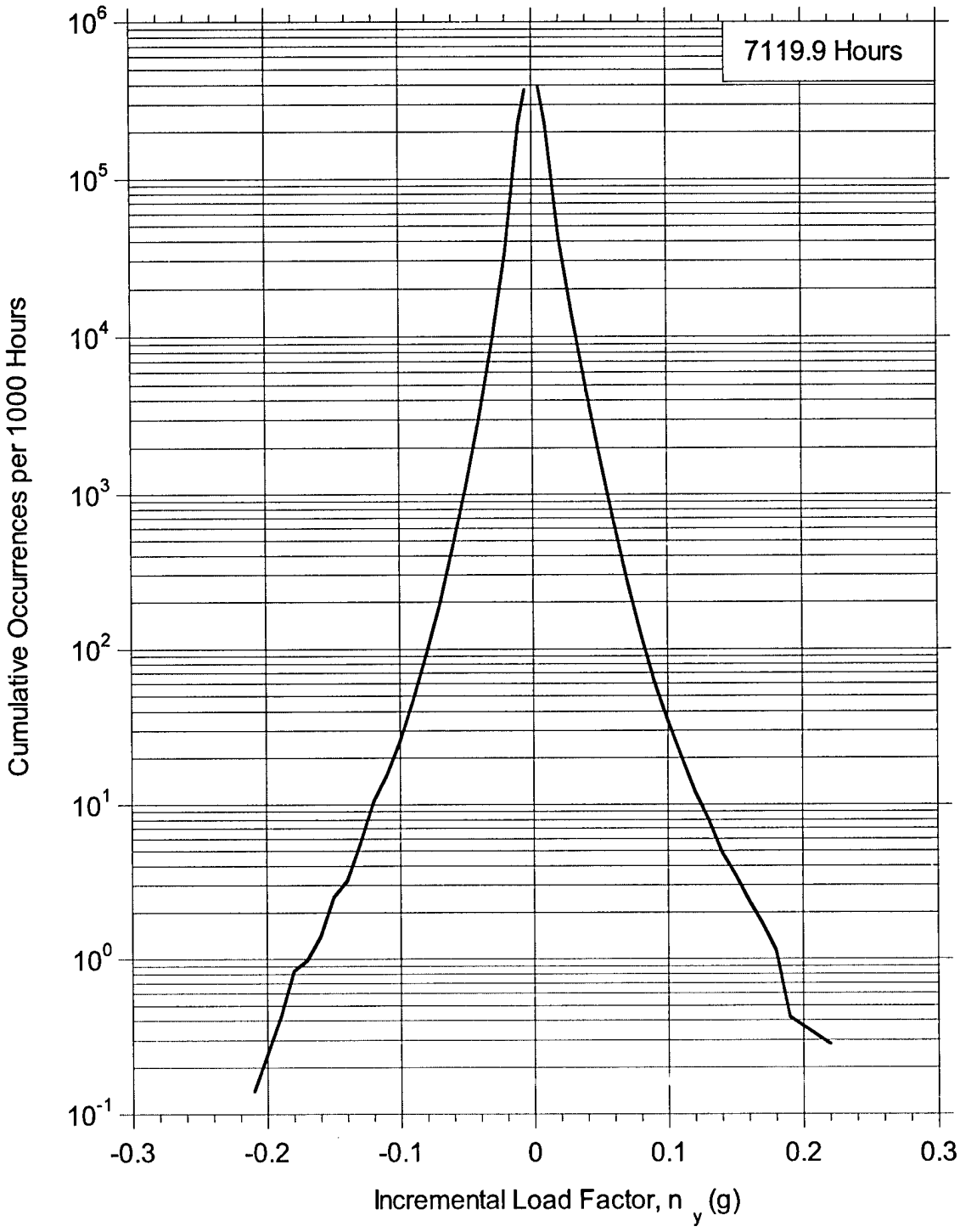

FIGURE A-60. CUMULATIVE OCCURRENCES OF LATERAL LOAD FACTOR PER 1000 HOURS, COMBINED FLIGHT PHASES

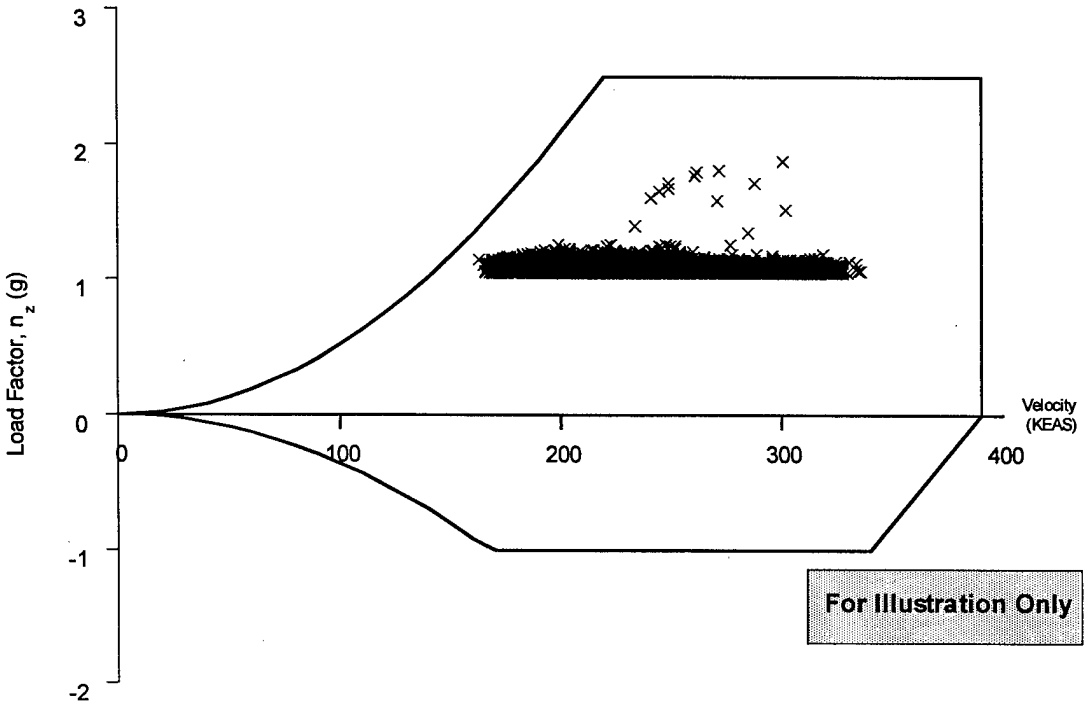

FIGURE A-61. COINCIDENT MANEUVER LOAD FACTOR AND SPEED VERSUS V-n DIAGRAM FOR FLAPS RETRACTED

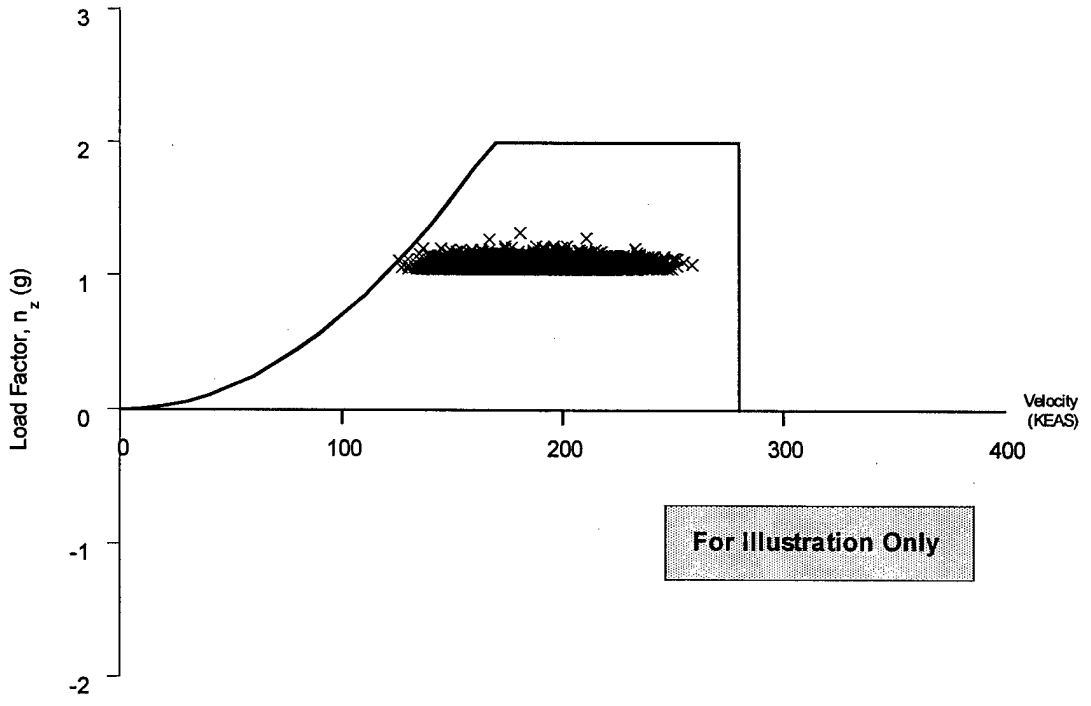

FIGURE A-62. COINCIDENT MANEUVER LOAD FACTOR AND SPEED VERSUS V-n DIAGRAM FOR FLAPS EXTENDED

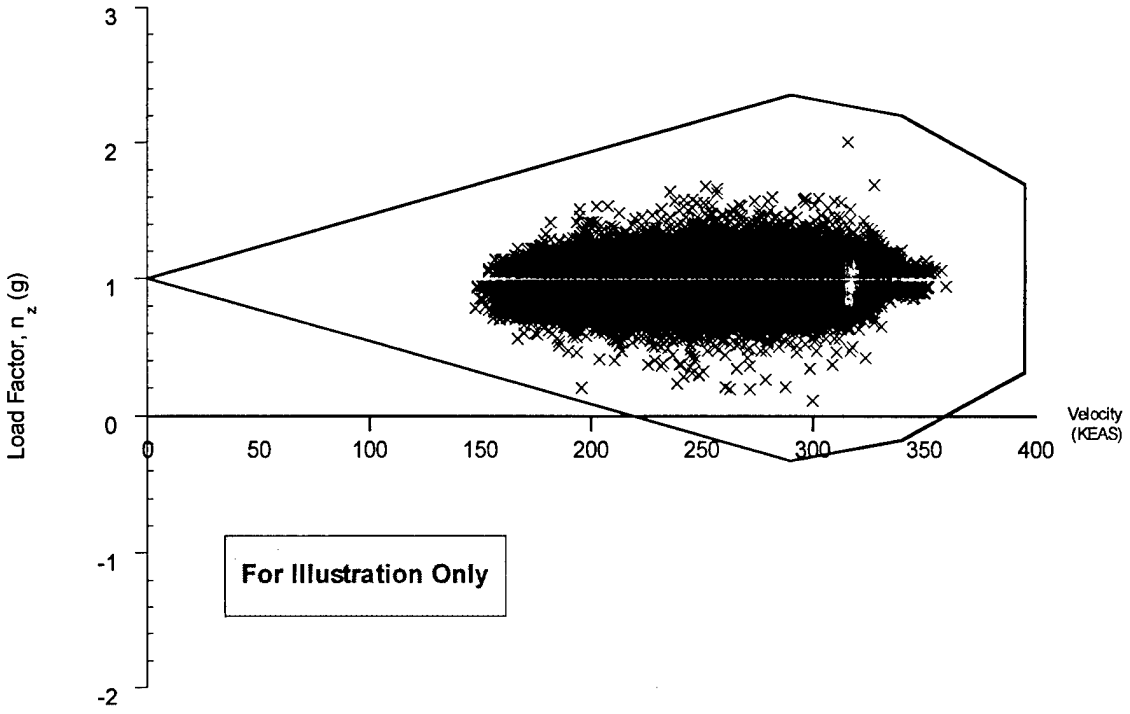

FIGURE A-63. COINCIDENT GUST LOAD FACTOR AND SPEED VERSUS V-n DIAGRAM FOR FLAPS RETRACTED

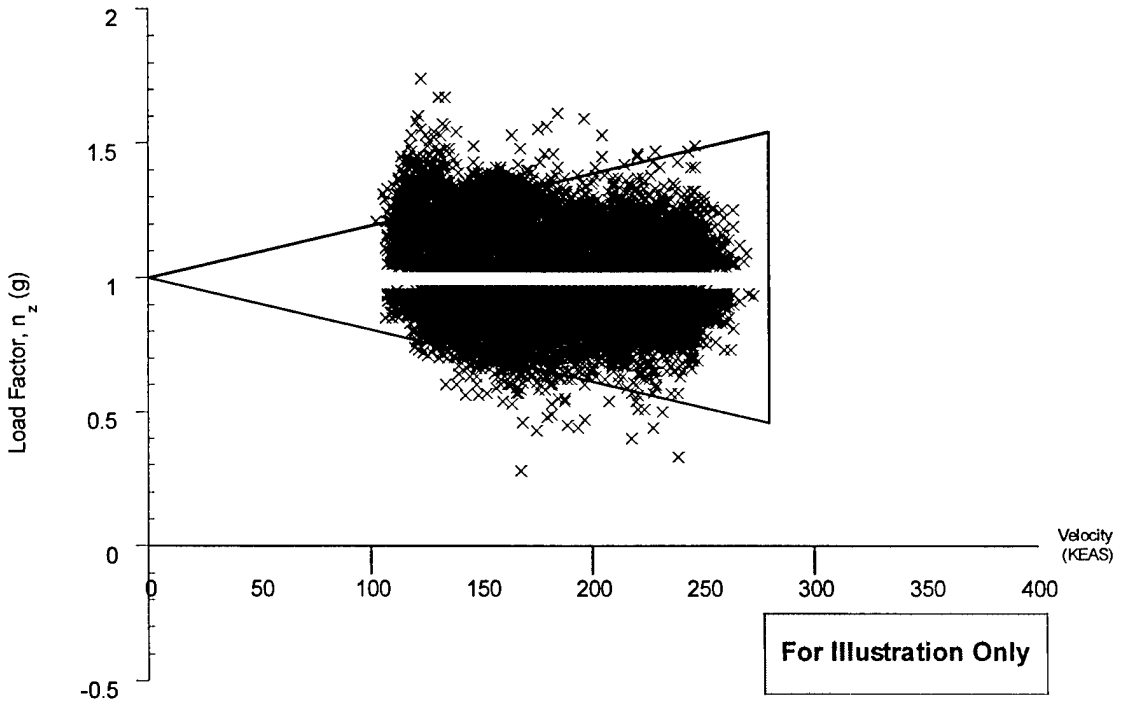

FIGURE A-64. COINCIDENT GUST LOAD FACTOR AND SPEED VERSUS V-n DIAGRAM FOR FLAPS EXTENDED

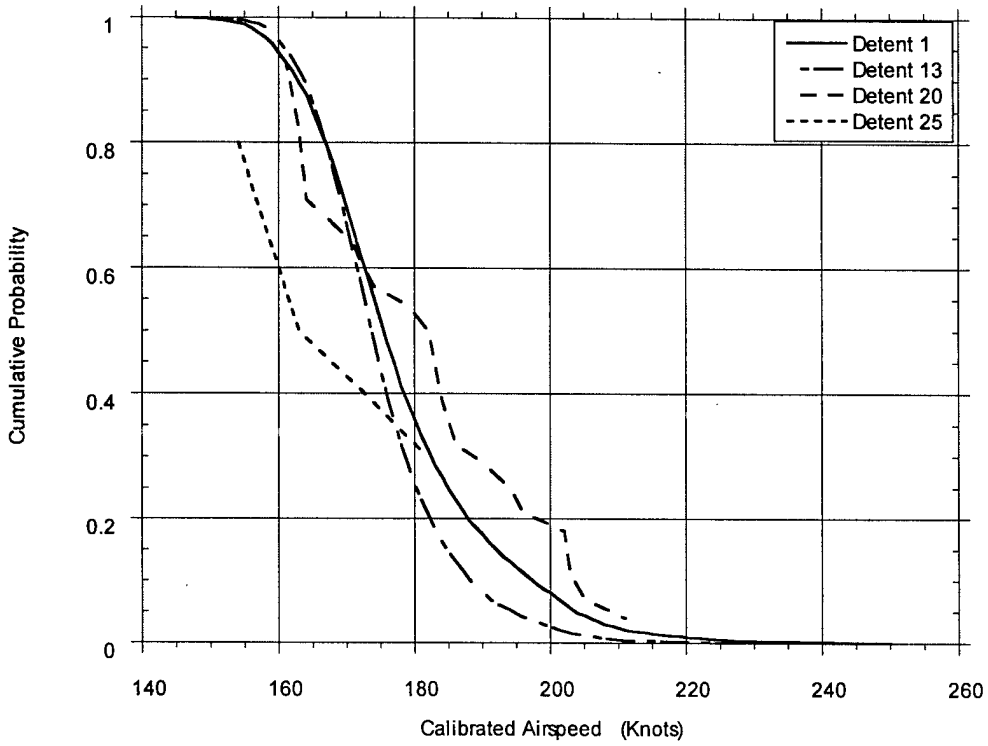

FIGURE A-65. CUMULATIVE PROBABILITY OF MAXIMUM AIRSPEED IN FLAP DETENT DURING DEPARTURE

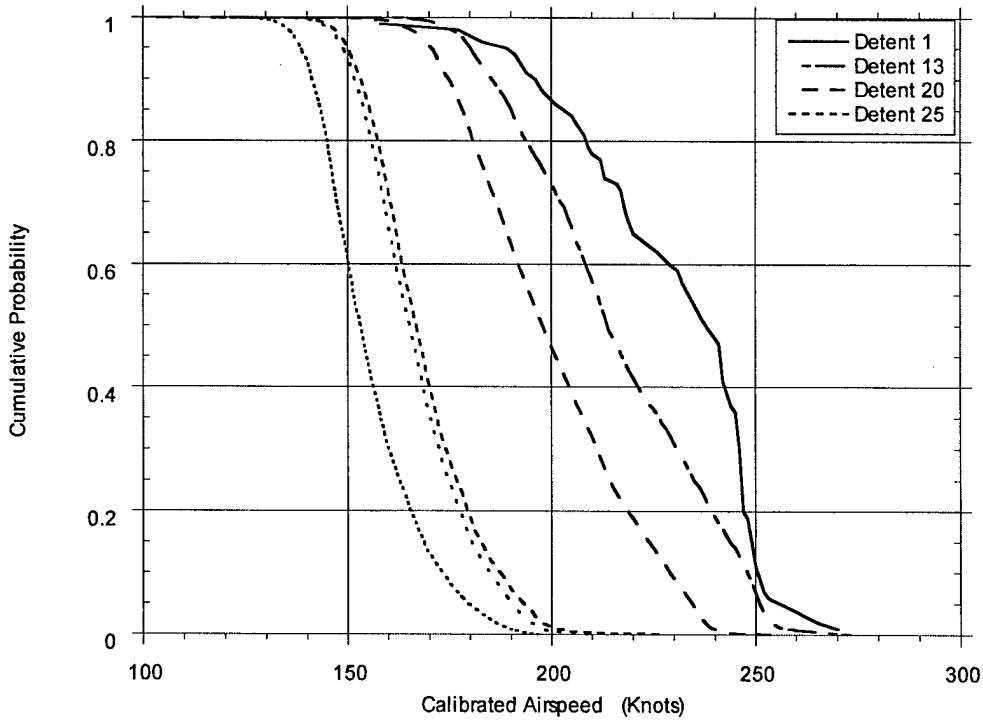

FIGURE A-66. CUMULATIVE PROBABILITY OF MAXIMUM AIRSPEED IN FLAP DETENT DURING APPROACH

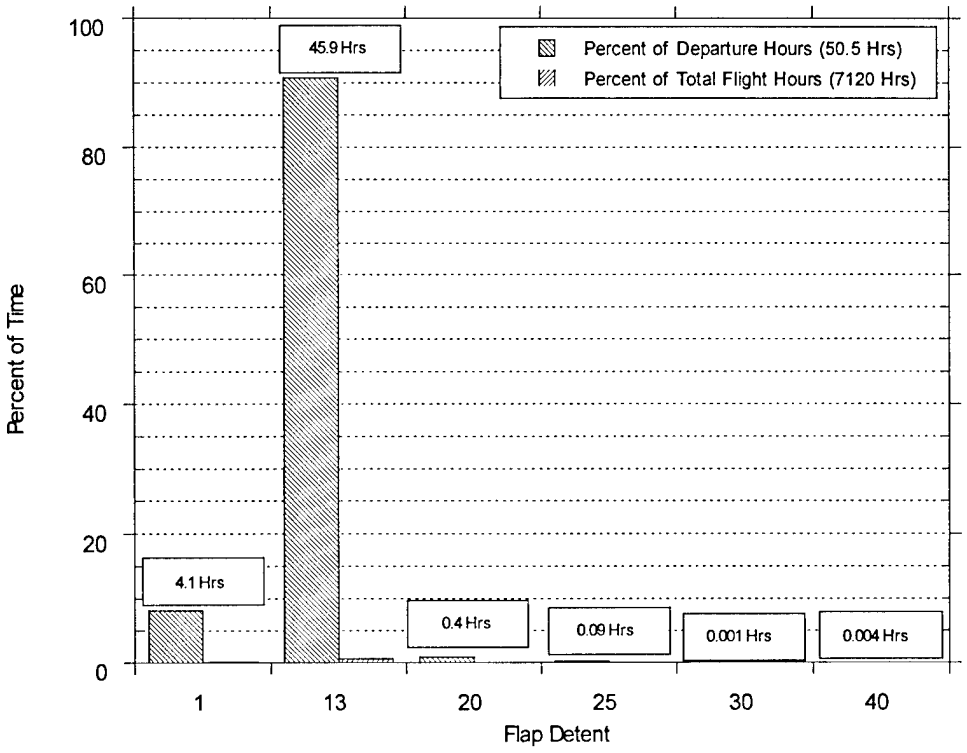

FIGURE A-67. PERCENT OF TIME IN FLAP DETENT DURING DEPARTURE

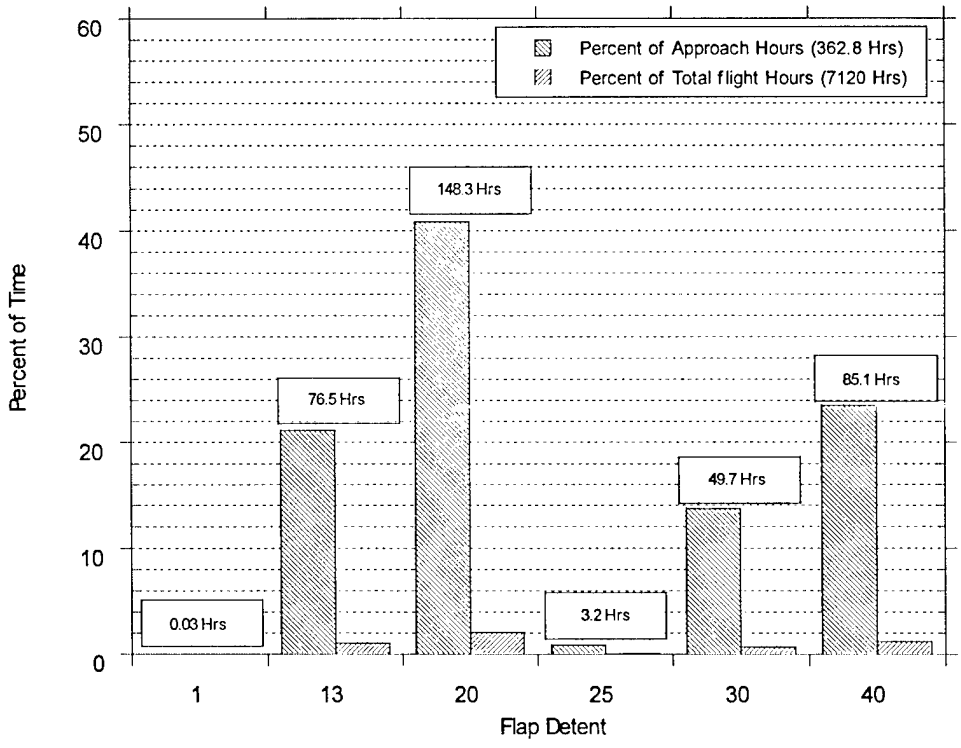

FIGURE A-68. PERCENT OF TIME IN FLAP DETENT DURING APPROACH

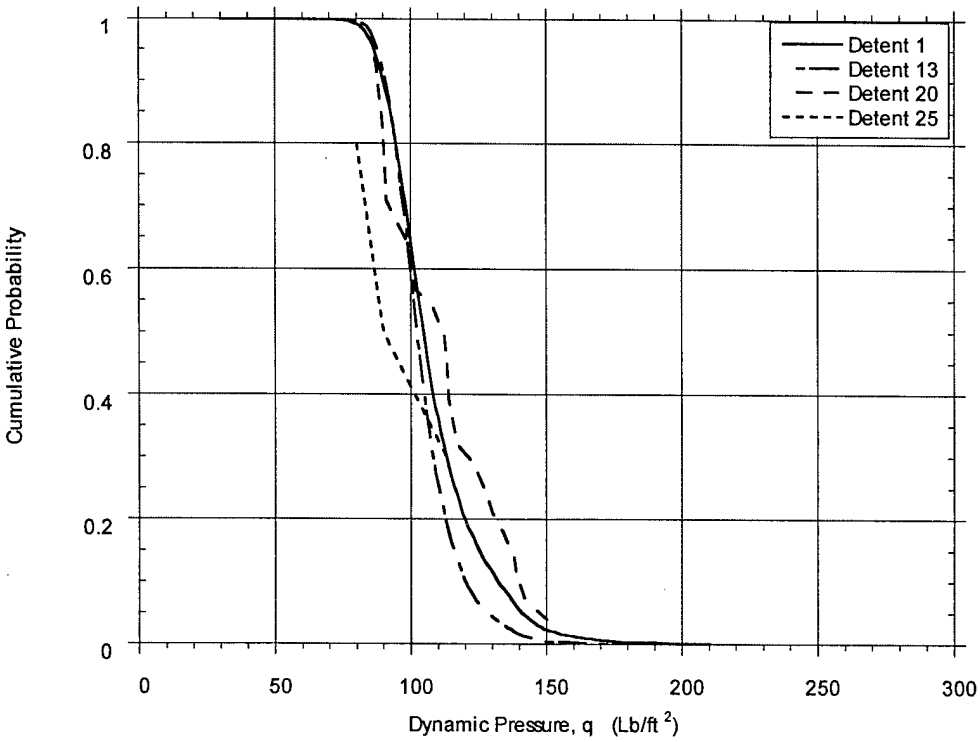

FIGURE A-69. CUMULATIVE PROBABILITY OF MAXIMUM DYNAMIC PRESSURE IN FLAP DETENT DURING DEPARTURE

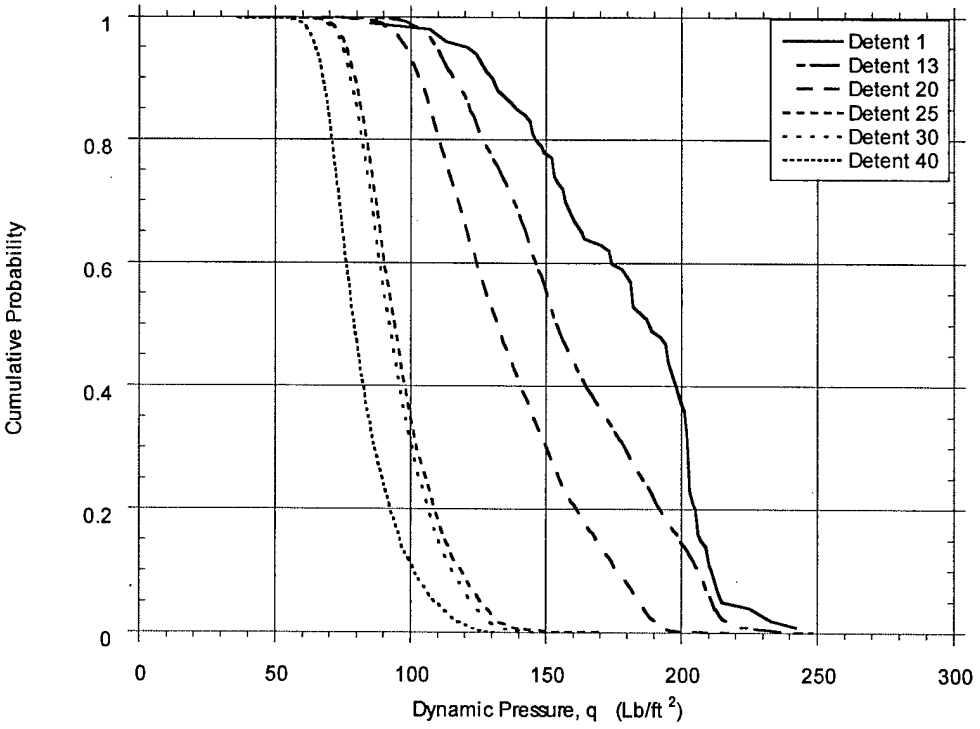

FIGURE A-70. CUMULATIVE PROBABILITY OF MAXIMUM DYNAMIC PRESSURE IN FLAP DETENT DURING APPROACH

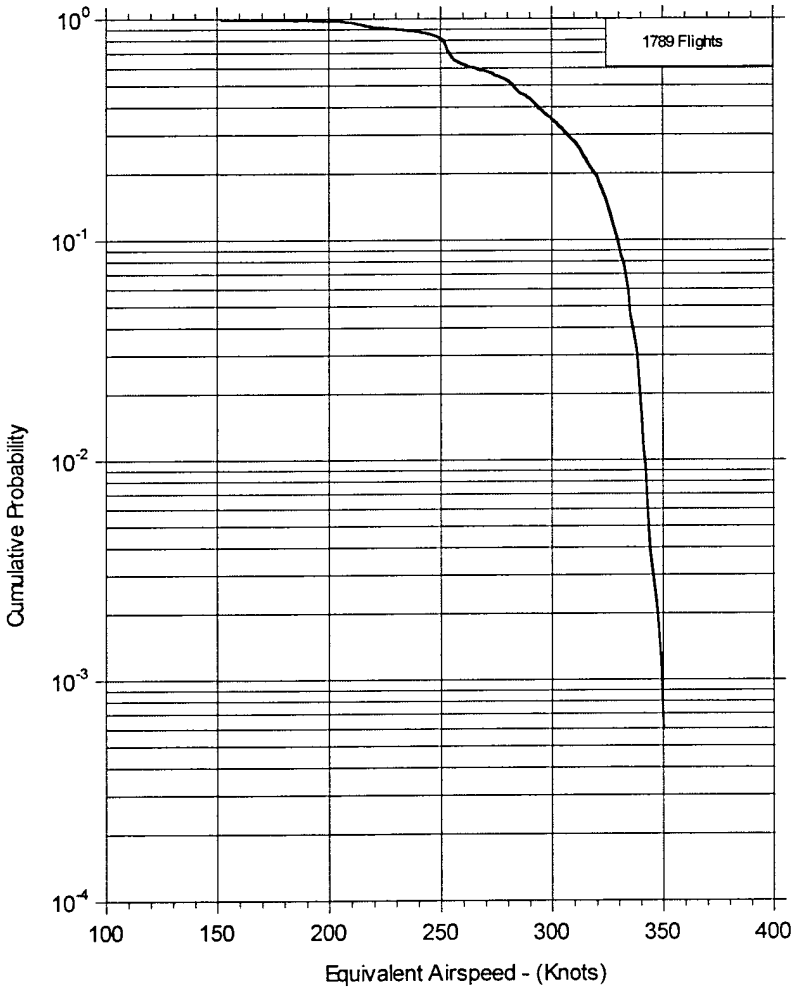

FIGURE A-71. CUMULATIVE PROBABILITY OF MAXIMUM SPEED DURING SPEED BRAKE DEPLOYMENT

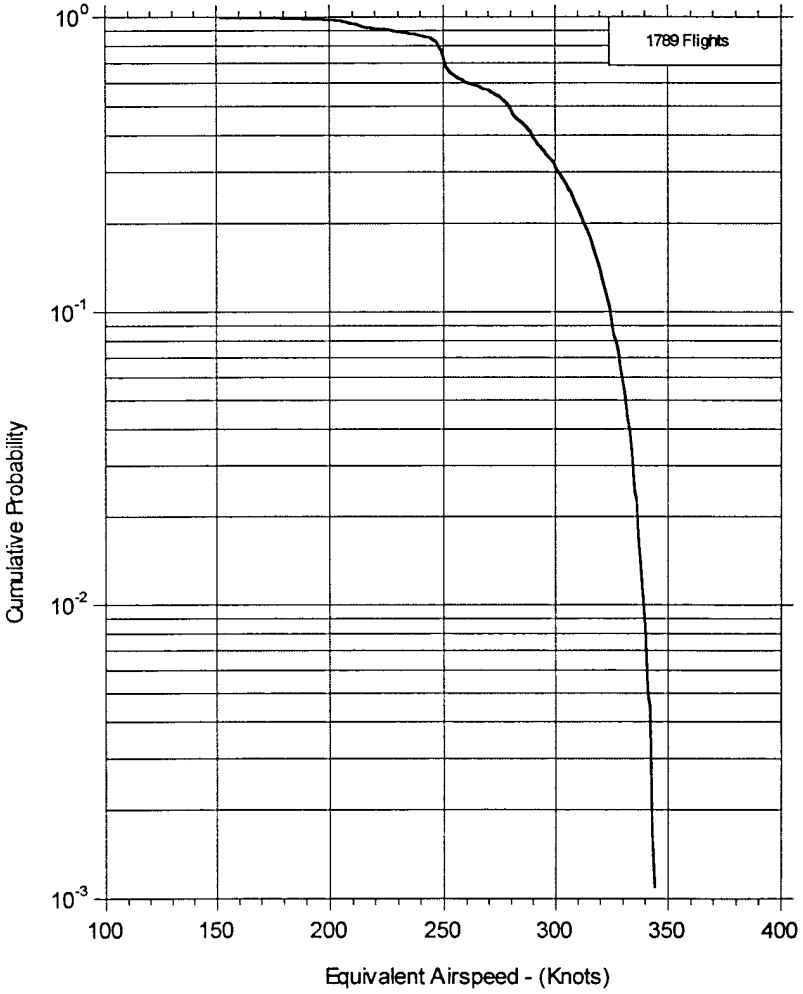

FIGURE A-72. CUMULATIVE FREQUENCY OF SPEED AT SPEED BRAKE DEPLOYMENT

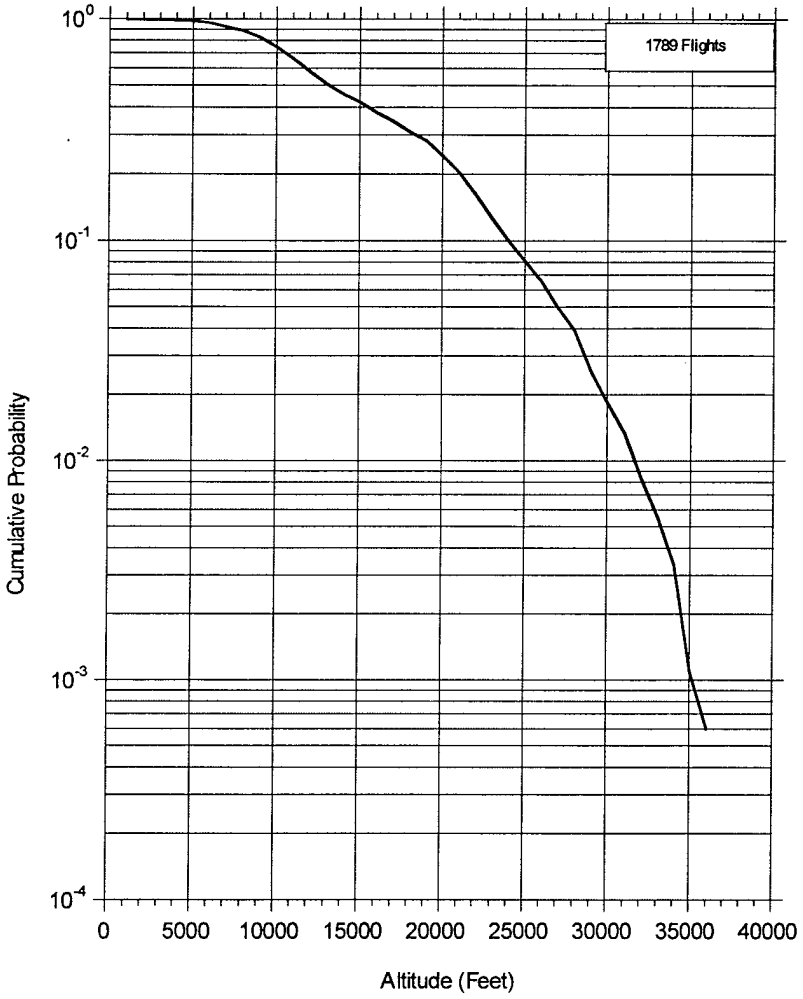

FIGURE A-73. CUMULATIVE FREQUENCY OF ALTITUDE AT SPEED BRAKE DEPLOYMENT

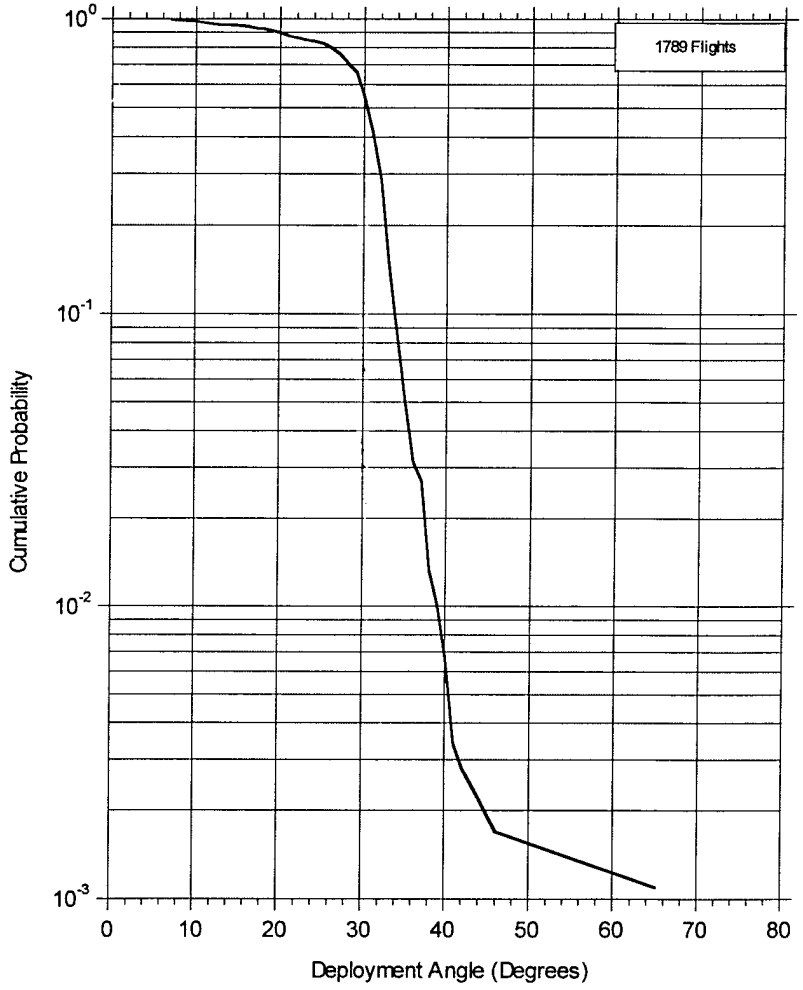

FIGURE A-74. CUMULATIVE PROBABILITY OF MAXIMUM DEPLOYMENT ANGLE DURING SPEED BRAKE DEPLOYMENT, FLAPS RETRACTED

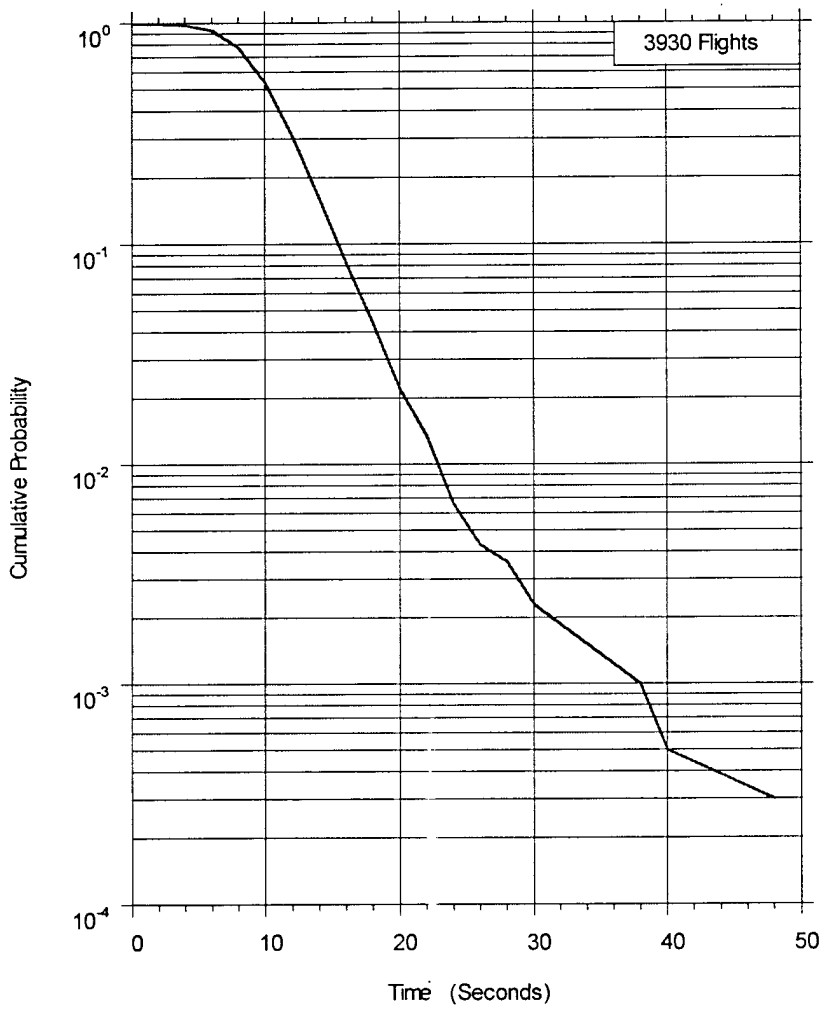

FIGURE A-75. CUMULATIVE PROBABILITY OF TIME WITH THRUST REVERSERS DEPLOYED

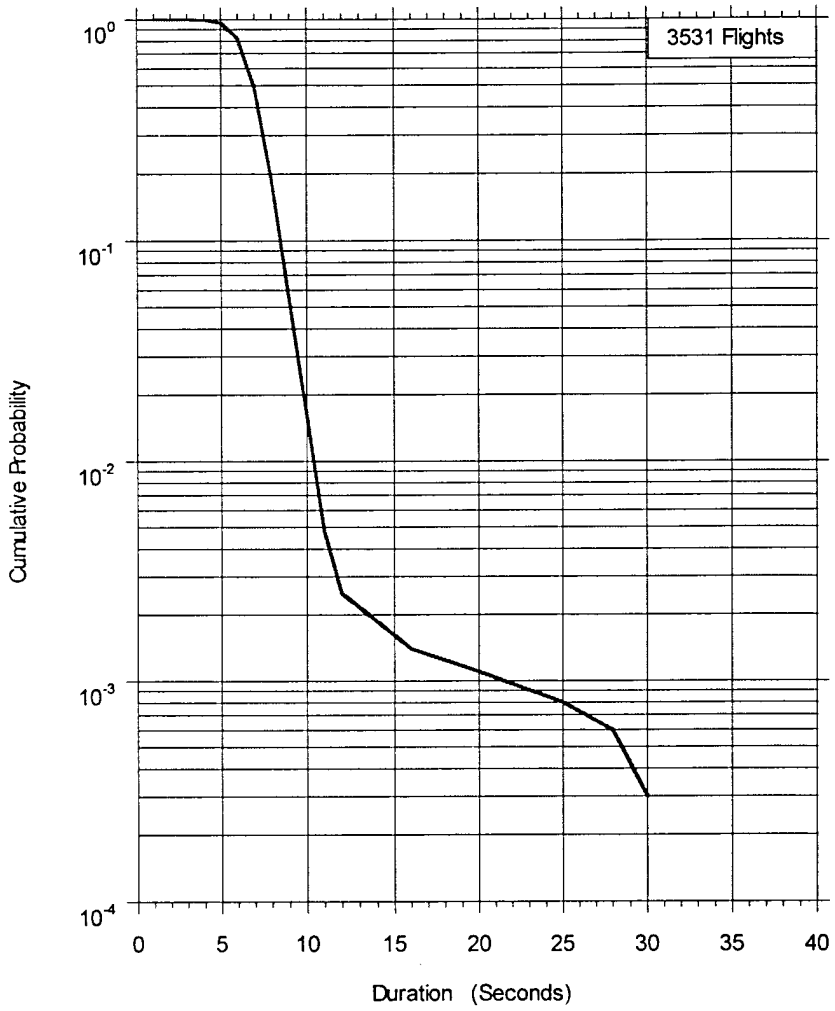

FIGURE A-76. CUMULATIVE PROBABILITY OF TIME WITH LANDING GEAR EXTENDED AFTER LIFTOFF

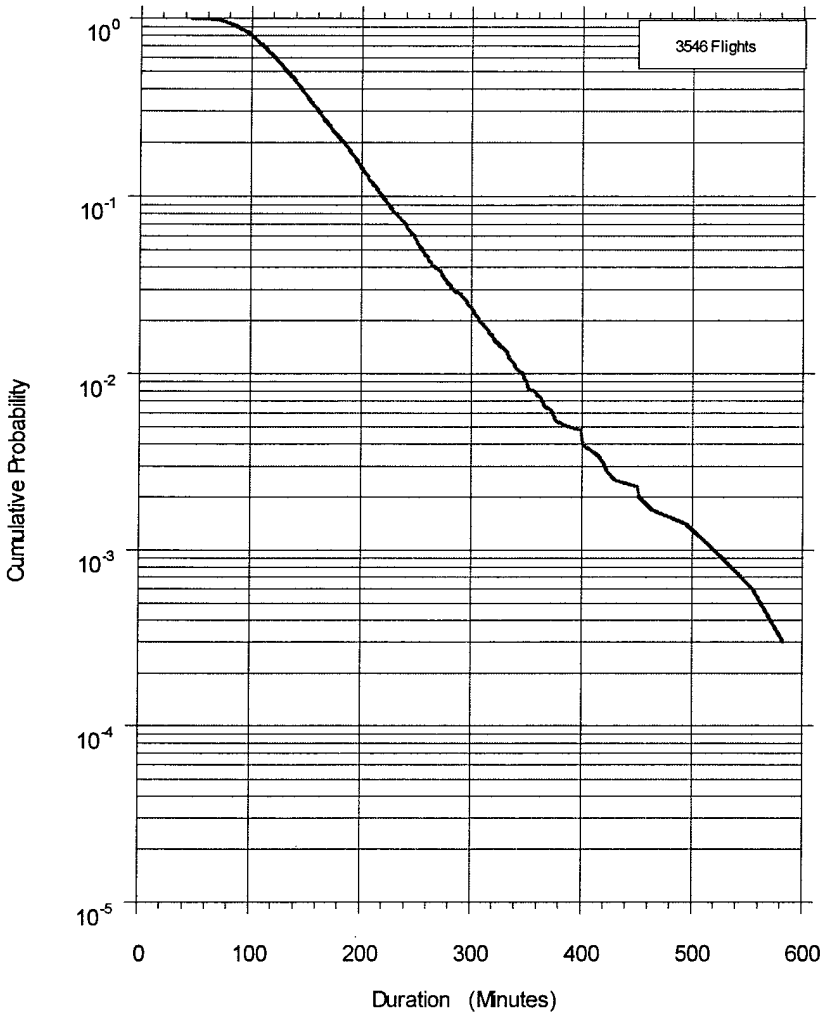

FIGURE A-77. CUMULATIVE PROBABILITY OF TIME WITH LANDING GEAR EXTENDED PRIOR TO TOUCHDOWN

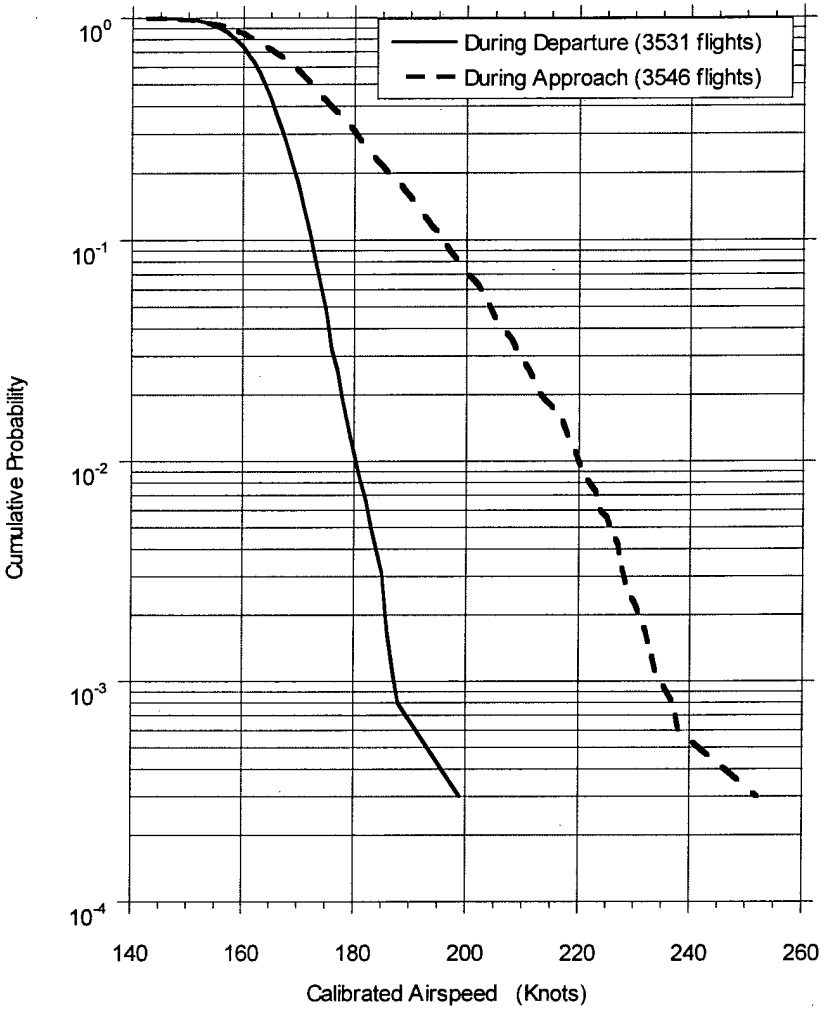

FIGURE A-78. CUMULATIVE PROBABILITY OF MAXIMUM AIRSPEED WITH GEAR EXTENDED

APPENDIX B—GREAT CIRCLE DISTANCE CALCULATION

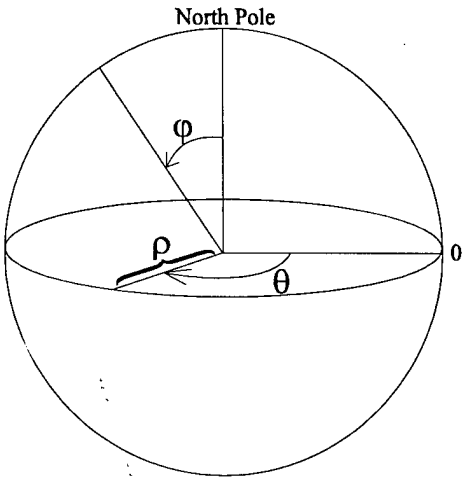

Given:

Latitude and Longitude of Departure and Destination Airports	ρ = distance from center φ = angle from North Pole θ = angle E/W of prime meridian

Procedure: (see sketch)

The standard mathematical system for spherical coordinates is shown, where three variables specify location: ρ, φ, and θ.

Let a = Great Circle Distance in angular measure.

Latitude is measured away from the Equator (0°) to the North Pole (+90°) and the South Pole (-90°); whereas in the standard spherical coordinate system, the North Pole, Equator, and South Pole lie at 0°, 90°, and 180°, respectively. Therefore,

$$\varphi = 90° - \text{latitude}$$

transforms latitude readings into equivalent angles (φ) in the standard spherical coordinate system.

Then

$$b = 90° - \text{Latitude}_{Dep}$$
$$c = 90° - \text{Latitude}_{Des}$$

where b and c are values of φ for the departure and destination locations, respectively.

Longitude is measured away from the prime meridian (0°). Longitudes to the east are positive and to the west negative. However, the standard spherical coordinate system measures its angles in the opposite direction. Therefore,

$$\theta = - \text{ longitude}$$

transforms longitude readings into equivalent angles (θ) in the standard spherical coordinate system.

Then

$$\begin{aligned} A &= (- \text{Longitude}_{Des}) - (- \text{Longitude}_{Dep}) \\ &= \text{Longitude}_{Dep} - \text{Longitude}_{Des} \end{aligned}$$

where A is the value of θ between the departure and destination locations.

The following equation, based on the spherical coordinate system, allows the computation of the Great Circle Distance, a. (Law of cosines for oblique spherical triangles)

$$\cos a = \cos b \cos c + \sin b \sin c \cos A$$

Substituting for b, c, and A from the above equalities,

$$\begin{aligned} \cos a = &\cos (90° - \text{Lat}_{Dep}) \cos (90° - \text{Lat}_{Des}) \\ &+ \sin (90° - \text{Lat}_{Dep}) \sin (90° - \text{Lat}_{Des}) \cos (\text{Lon}_{Dep} - \text{Lon}_{Des}) \end{aligned}$$

Since

$$\begin{aligned} \cos (90° - \text{Lat}_{Dep}) &= \sin \text{Lat}_{Dep} \\ \cos (90° - \text{Lat}_{Des}) &= \sin \text{Lat}_{Des} \\ \sin (90° - \text{Lat}_{Dep}) &= \cos \text{Lat}_{Dep} \\ \sin (90° - \text{Lat}_{Des}) &= \cos \text{Lat}_{Des} \end{aligned}$$

by replacement one obtains

$$\cos a = \sin (\text{Lat}_{Dep}) \sin (\text{Lat}_{Des}) + \cos (\text{Lat}_{Dep}) \cos (\text{Lat}_{Des}) \cos (\text{Lon}_{Des} - \text{Lon}_{Dep})$$

Thus a, the angular measure of the great circle arc connecting the departure and destination locations, is obtained as

$$a = \cos^{-1} [\sin (\text{Lat}_{Dep}) \sin (\text{Lat}_{Des}) + \cos (\text{Lat}_{Dep}) \cos (\text{Lat}_{Des}) \cos (\text{Lon}_{Des} - \text{Lon}_{Dep})]$$

So, for a expressed in radians

$$GCD = a \text{ radians} \left(\frac{180 \text{ deg.}}{\pi \text{ radians}} \right) \left(\frac{60 \text{ min.}}{1 \text{ deg.}} \right) \left(\frac{1 \text{nm}}{1 \text{ min.}} \right) = \left(\frac{10800a}{\pi} \right) \text{ nm}$$

and for a expressed in degrees,

$$GCD = a \text{ degrees} \left(\frac{60 \text{ min.}}{1 \text{ deg.}} \right) \left(\frac{1 \text{ nm}}{1 \text{ min.}} \right) = 60a \text{ nm}$$